INSIGHTS INTO HUMAN CARBONIC ANHYDRASE INHIBITOR DESIGN

By

MAYANK AGGARWAL

A DISSERTATION PRESENTED TO THE GRADUATE SCHOOL
OF THE UNIVERSITY OF FLORIDA IN PARTIAL FULFILLMENT
OF THE REQUIREMENTS FOR THE DEGREE OF
DOCTOR OF PHILOSOPHY

UNIVERSITY OF FLORIDA

2013

To my Parents

ACKNOWLEDGMENTS

It has taken a perfect assortment of incredibly supportive and sacrificing parents, a thoughtful committee, and needless to mention, an extremely helpful and skilled-in-teaching mentor for this dissertation to reach its culmination.

Benjamin Franklin once said, "Tell me and I forget, teach me and I may remember, involve me and I will learn". I consider myself very lucky to have the good fortune of learning under the likes of Dr. Robert McKenna and Dr. Mavis Agbandje-McKenna who taught me how, rather than what, to think. I thank, with all my heart, the two people behind the curtain who left no stone unturned in shaping my career. They provided me with regular opportunities to attend scientific conferences (national and international) that not only boosted my confidence, but also inculcated in me a great sense of presenting data in a scientific community. Leading by example, Rob and Mavis are, without a doubt, professors that "inspire". Apart from science, I have learnt many life lessons including, but not limited to, work ethics and principles that I will cherish for the rest of my life.

It was the insightful and constructive criticism of my committee which remolded and gave a new design to my proposal early on during my research. That initial ostensible failure turned out to be a salutary experience and helped me mature as a thinker, a critic, a scientist. I thank my committee members Dr. David Silverman, Dr. Arthur Edison, Dr. Linda Bloom, and Dr. Steven Bruner for providing me with their crucial time, guidance and critique.

A special word of thanks must be dedicated to the former members of the McKenna lab: Dr. Arthur Robbins for training me in X-ray crystallography; Dr. Zoë Fisher who taught me the basics of neutron crystallography; Dr. Balendu Avvaru and Dr.

Robert Ng for helping me with various structural biology softwares; Dr. Katherine Sippel, Dr. Dayne West and Dr. John Domsic for training me in protein expression and purification. I also thank Dr. Sujata Halder, Dr. Antonette Bennet, and my dear friend Shweta Kailasan for providing their guidance and time during my stint as a virologist. This dissertation is a combined effort of many hands including those of Christopher Boone and Bhargav Kondeti who have helped me in giving words to my research and get quick publications in various peer-reviewed journals.

My parents have provided me with a constant motivation and "kick" (when required) throughout my academic career. If it were not for their belief in me, I would have never made thus far. I dedicate this research and dissertation of mine to my family who stood by me at all times. I may not have said this ever before, but I hereby let my hair down and acknowledge the sacrifices of my mother Mrs. Archna Aggarwal, efforts of my father Dr. Madhusudan Aggarwal, teachings and blessings of my grandfather Mr. Yashpal Shastri, and the love of my sister Sugandha Aggarwal. Additionally, I would like to recognize my extended family and friends in India and the United States who have knowingly or unknowingly kept me going. Not to be forgotten is my girl friend in Delhi − Malvika Sharma who, with her absolute faith and trust in me, has shown extraordinary patience and handled this long distance relationship of ours, for over 2 years.

TABLE OF CONTENTS

page

LIST OF TABLES

LIST OF FIGURES

LIST OF ABBREVIATIONS

1MI	1-Methyl Imidazole
2MI	2-Methyl Imidazole
4MI	4-Methyl Imidazole
AZM	Acetazolamide
BCA	Bovine Carbonic Anhydrase
BZM	Brinzolamide
CA	Carbonic Anhydrase
CAI	Carbonic Anhydrase Inhibitor
CD	Circular Dichroism
CHESS	Cornell High Energy Synchrotron Source
CNS	Central Nervous System
DMSO	Dimethyl Sulfoxamide
DSC	Differential Scanning Calorimetry
DTC	Dithiocarbamate
DZM	Dorzolamide
EC	Enzyme Commission number
GOL	Glycerol
HCA	Human Carbonic Anhydrase
IOP	Intra-Ocular Pressure
MCA	Murine Carbonic Anhydrase
MD	Molecular Dynamics
NIH	National Institute of Health
NMR	Nuclear Magnetic Resonance
PDB	Protein Data Bank

PISA	Proteins, Interfaces, Surfaces, and Assemblies
RT	Room Temperature
SAR	Structure Activity Relationship
SDS	Sodium Dodecyl Sulfate
SUC	Sucrose
wt-CA	Wild Type Carbonic Anhydrase

Abstract of Dissertation Presented to the Graduate School
of the University of Florida in Partial Fulfillment of the
Requirements for the Degree of Doctor of Philosophy

INSIGHTS INTO HUMAN CARBONIC ANHYDRASE INHIBITOR DESIGN

By

Mayank Aggarwal

August 2013

Chair: Robert McKenna
Co-Chair: David N. Silverman
Major: Medical Sciences - Biochemistry and Molecular Biology

Carbonic anhydrases (CAs) are a family of metalloenzymes (EC 4.2.1.1) found in all organisms, catalyzing the reversible reaction of CO_2 hydration to bicarbonate and a proton. In humans, CA exists as 12 catalytically active isoforms that differ in their distribution and localization. Of special interest is CA IX that has been shown to play a critical role in cancer proliferation, and its overexpression in certain types of cancers has led to its use as a biomarker for cancer diagnosis and prognosis. In addition, much knowledge has been acquired on CA II inhibition for various classes of diuretics, anti-epileptics, and systemically acting antiglaucoma agents. The differences in the active sites of CA isoforms are subtle and this causes non-specific CA inhibition which leads to various side effects. Experimental studies on different groups of CA inhibitors (CAIs) are performed, and presented. Various structural features (such as buried surface area, hydrogen bonds etc.), have been mapped and correlated to the inhibition of CA II and CA IX, to provide structure activity relationships (SARs) that may help in understanding the varied binding affinities of these CAIs. Two different approaches to drug designing:

Protein Data Bank (PDB) Mining and Fragment Addition have been used that take into account the amino acid differences in the active site of CA II and CA IX.

The PDB was mined for previously solved CA-CAI complexes, and a sub-set of selected structures were superposed with the structure of CA IX to study SARs. On the other hand, X-ray crystal structures of four small "fragments" (imidazole, 1-methyl imidazole, 2-methyl imidazole and 4-methyl imidazole) were solved. Few of the multiple binding sites observed with these fragments could be exploited for drug designing by chemically linking the fragments bound at regions that are different in different CA isoforms. This data will be used to guide *in silico* design of new CAIs that would preferentially bind to one CA isoform (on-target) over others (off-target).

CHAPTER 1
INTRODUCTION TO CARBONIC ANHYDRASES[1]

Classification

Carbonic Anhydrases (CAs, EC 4.2.1.1) are a family of metalloenzymes that catalyze the reversible hydration/dehydration of carbon dioxide/bicarbonate ion.[2,3] CAs are found in both prokaryotes and eukaryotes, and are involved in many physiological processes such as respiration, bone resorption, calcification, and photosynthesis.[4]

CAs have been divided into five distinct classes (α, β, γ, δ and ζ). The α-class is found in mammals, β is found in plants and some prokaryotes, γ is present only in archaeabacteria and two other rare classes (that are similar to class β), δ and ζ are found in diatoms.[5–10] The three main classes (α, β and γ) of CA are structurally dissimilar and are thought to have evolved independently, possibly as a result of convergent evolution.

Structure and Function of Human CAs

Structure

There are 15 isoforms of human (h) α-CA of which, three are acatalytic and will be discussed later. The 12 catalytic isoforms differ from each other in activity, tissue localization and distribution (Table 1-1) in forms of cytosolic (hCAs I-III, VII, XIII), membrane bound (hCAs IV, IX, XII, XIV), secretory (hCA VI) or mitochondrial (hCAs VA, VB).[8,11–26] Overall, most hCA isoforms (except hCA VI, IX and XII) exist in monomeric forms composed of 7 right handed α-helices, and a twisted β-sheet formed by 10 β-strands (two parallel and eight antiparallel). The CA catalytic domains in

---

Adapted from: Aggarwal, M.; Boone, C.D.; Kondeti, B.; McKenna, R; Structural annotation of human carbonic anhydrases; *J Enzyme Inhib Med Chem.* 2013, 28, 267-77.

transmembrane hCA IX and hCA XII have a similar, but dimeric structure. Figure 1-1 shows a primary sequence alignment of all the isoforms of hCA, and Table 1-2 and Table 1-3 summarize the primary sequence identity and structural similarity, respectively. A superposition of all the catalytic isoforms of hCA shows high similarity in the main chain (Figure 1-2).

HCA II is the most well studied of all CA isoforms and its active site can be described as a cone-shaped cavity formed of a hydrophobic region (Val121, Val143, Leu198, Val207 and Trp209), and a hydrophilic region (Tyr7, Asn62, His64, Asn67, Thr199 and Thr200). At the base of the cavity lies the Zn^{2+}, tetrahedrally coordinated by three conserved histidines (His94, His96 and His119) and a solvent molecule (Figure 1-3). Although the core of the active site in α-CAs is highly conserved, there is variability in the polarity and hydropathicity of its periphery. The conservation of polar and non-polar residues on the surface of catalytic isoforms of hCA is shown in Figure 1-4 and Figure 1-5, respectively.

Catalytic Mechanism

CAs follow a two-step ping pong catalytic mechanism for the hydration and dehydration of CO_2 and HCO_3^-, respectively:

Step 1: $EZnOH^- + CO_2 \leftrightarrow EZnHCO_{3-} \leftrightarrow EZnH_2O + HCO_3^-$

Step 2: $EZnH_2O + B \leftrightarrow EZnOH^- + BH^+$

The first step of the reaction involves the binding of a CO_2 molecule in the active site. Molecular dynamics (MD) data suggest the existence of three CO_2 binding sites within the active site, one of which is found in the hydrophobic region (3-4 Å away from Zn^{2+}), and the other two are found 6-7 Å away from the Zn^{2+}. Energy analysis suggests that the two binding sites that are 6-7 Å away may act as intermediates guiding CO_2 into

the hydrophobic region.[27] However, the recent X-ray crystal structure (PDB ID: 3D92)[3] reveals a single binding site for CO_2 in the active site of hCA II with one of the oxygens of the CO_2 interacting with the amide of Thr199 (3.5 Å) and displacing a water molecule whereas, the other oxygen is positioned between the Zn^{2+} and Val121. This arrangement places both of the oxygens nearly equidistant from the zinc bound OH^- ($Zn\text{-}OH^-$), and the carbon 2.8 Å from the $Zn\text{-}OH^-$.[3] Once positioned within the hydrophobic region, the CO_2 undergoes a nucleophillic attack by the $Zn\text{-}OH^-$, forming zinc bound bicarbonate ($Zn\text{-}HCO_3^-$). This $HCO_{3-}$is then displaced with a water molecule ($Zn\text{-}H_2O$) and the former diffuses into the bulk solvent. In the second step, the $Zn\text{-}OH^-$ is regenerated as a result of the transfer of a proton from the $Zn\text{-}H_2O$ generated in step one, to the bulk solvent (or buffer).[9]

Kinetic studies show differences in catalytic efficiency among hCAs (Table 1-1) which may be attributed to the varying speed of proton shuttling (the rate determining step of catalysis) in step two.[27] The proton shuttling step is said to occur by two key events. The first event involves the transfer of the proton via a network of ordered water molecules in the active site to a nearby residue, while the second subsequently releases the proton into the bulk solvent.[28]

One of the key amino acid residues in proton shuttling is His64 (hCA II numbering), which is conserved in all of the catalytic hCAs except III and V. In X-ray crystal structures[29] and MD studies[30], His64 has been found to exist in a dual conformation: inward (7.5 Å away from the Zn^{2+}) and outward (12.0 Å away from the Zn^{2+}) suggesting that the residue acts as a shuttle, accepting the proton then transferring it to the bulk solvent by a flipping mechanism. Although, there exists

another hypothesis according to which it is not the flipping of the side chain of His64, but its tautomerism that results in proton transfer.[31] Absence of His64 in hCAs III and V could well be argued as the reason for their relatively slowed catalytic efficiency. However, the rate of proton transfer also depends on the number of water molecules involved in proton transfer, as well as the distance between the proton donor and acceptor.[32]

In hCA III, mainly three residues are speculated to affect catalysis: Lys64, Arg67, and Phe198 in place of His64, Asn67 and Leu198 (hCA II numbering).[33] The replacement of His64 for a much more basic Lys, and presence of bulkier Arg67 and Phe198 causes a reduction in the active site cavity volume affecting the binding of CO_2, thereby resulting in a lower rate of catalysis.[34] However, the exact mechanism of how the proton leaves the active site and the exact role of these residues is still unanswered. In CA V, presence of larger residues, Tyr and Phe, in place of His64 and Ala65 (CA II numbering) respectively, makes the region very hydrophobic and thus these residues are believed to be not involved in proton transfer. It is speculated however, that the proton travels through another network possibly involving either Tyr131 or Lys132.[35]

Up until now, the primary reaction i.e. reversible hydration of CO_2 to bicarbonate ion has been discussed. However, CA has been known to be involved in a variety of other reactions (Table 1-4), mechanisms and physiological functions of which are yet to be ascertained.[4]

Physiological Functions

The isoforms of hCA are found throughout the body in various tissues and sub-cellular locations and have varied physiological roles (Table 1-1). HCAs I, II, and III share a high sequence similarity, and have been extensively studied. HCAs I, II and IV

are involved in the efficient transportation of CO_2. HCA II is the most widely expressed isoform and participates in processes ranging from bone resorption to respiration and pH regulation. In astrocytes, monocarboxylate protein 1 (MCT1) and CA II are located in close proximity. CA II may therefore act as a H^+-collecting antenna for MCT1 in astrocytes, which mediates the exchange of H^+ between the transporter pore and protonatable residues near the astrocyte inner plasma membrane. This is how Lactate flux in astrocytes is enhanced by a non-catalytic action of CA II.[36] HCA III is believed to serve an antioxidant role in cells which have high rates of oxidation such as adipose tissues, hepatocytes, and skeletal muscle fibers.[37]

HCA V is found in the mitochondrial matrix, existing in two forms: VA and VB. HCA VA provides bicarbonate for gluconeogenesis, and fatty acids for pyrimidine base synthesis.[4] It is found in the mitochondria of the heart, lung, kidney, spleen and intestines. HCA VB on the other hand, is present in the mitochondria of the pancreas, kidney, and salivary glands playing an intermediate role in metabolism.[38]

HCA VI is the secretory isoform expressed in saliva, milk, nasal secretions, and the epithelial lining of digestive organs. The physiological function of hCA VI is yet to be fully understood, but studies show a correlation between the loss of taste and a decrease in hCA VI secretion.[39] HCA VII (cytosolic) is speculated to play a role in cerebrospinal fluid production in the CNS.[38] HCA XIII is another cytosolic isoform that is expressed among tissues in the reproductive organs and is speculated to play a role in pH regulation, and ensuring proper fertilization.[40]

Among the three transmembrane hCAs, isoforms IX and XII are expressed in the gastrointestinal mucosa. However, they have also been found to be over expressed in

epithelial tumors including tumors of the cervix, lungs, kidneys, prostate, and breast. In addition, these isoforms are implicated in allowing tumors to acclimate to a hypoxic microenvironment and promoting metastasis.[41] HCA XIV is present in the brain and retina and is believed to aid in the removal of CO_2 from the neural retina and help modulate photoreceptor function.[42]

CA-Related Proteins (CA-RPs)

The hCA family, besides the catalytic isoforms, includes a subclass of three non-catalytic isoforms (hCAs VIII, X and XI) called CA-related proteins (CA-RPs), based on sequence similarity with the catalytic isoforms. The reason behind these isoforms being non-catalytic has been attributed to the absence of one or more histidines that coordinate the Zn^{2+} ion in the active site of a catalytic hCA isoform. In hCA-RP VIII, for example, the Zn-coordinating His94 (hCA II numbering) is replaced by Arg116 (hCA-RP VIII numbering)[43] which precludes CO_2 hydration in the first step of CA catalysis.[44] Although the biological functions of CA-RPs remain undefined, these isoforms continue to gain scientific interest. To date, X-ray crystal structure of only one hCA-RP (hCA-RP VIII) has been determined.[45] HCA-RP VIII is highly expressed in the cerebellum[46], and has been identified as a binding partner for the inositol 1,4,5 triphosphate (IP3) receptor type 1.[47]

With a sequence identity of 41%, the overall structure of hCA-RP VIII has an r.m.s.d. of 1.3 Å with the hCA II isoform. The X-ray crystal structure of hCA-RP VIII (PDB ID: 2W2J)[45] reveals a unique glutamate rich loop (E loop; a.a. 24–36) that is not seen in other hCAs. The core domain of hCA-RP VIII adopts the classical architecture of other α-CAs, namely a 10-stranded central β-sheet flanked by 7 short α-helices.

A sequence similarity of 98% between murine (m) CA VIII and hCA-RP VIII may well form the hypothesis that over the course of evolution the loss in CA activity is coupled to a gain of a new, though unidentified, cellular function. One possibility is the modulation of biological functions via protein–protein interactions. The type 1 IP3 receptor, identified as a hCA-RP VIII binding protein, contains an electropositive IP3 binding site.[48] It is possible that the electronegative surface in hCA-RP VIII, unique among hCAs, forms a charge-complementary binding site for the receptor, thereby regulating IP3-dependent Ca^{2+} release.[49] Consistent with this, a protein-interaction function has been reported for the CA like domain in receptor protein tyrosine phosphatase β which serves as the contact in binding site.[50]

Stability of α-CAs

Stability is an important factor that influences the practical application of a protein. Resistance to various environmental stresses including heat, proteolytic degradation and high concentrations of denaturing agents, e.g. sodium dodecyl sulfate (SDS), acid, urea and guanidine-hydrochloride (GuHCl) are some of the factors that define the stability of any protein. Mostly, thermal and chemical stability are strongly correlated[51,52], but this trend is not a valid assumption in many cases.[53,54] Previous studies involving denaturation and folding of CA have provided an insightful understanding of its folding pathway.[9]

Cytosolic hCAs: I and II

Nearly 30 years after the discovery of CA in erythrocytes[55], the first detailed denaturation studies on hCAs I and II with concentrated solutions of urea and GuHCl were conducted.[56] These and later experiments revealed that isoforms from the same species have varying midpoint concentrations of inactivation (C_m) for GuHCl: 1.5 M for

hCA I versus 0.9 M for hCA II.[57] This also coincides with the same isoform from different species having different stability: bovine (b) CA II denatures in GuHCl at a C_m of 1.6 M[58] and has also been shown to be less susceptible to denaturation at high pH than hCA II.[59,60] With the sequence similarity of hCA I, hCA II and bCA II being ~60%, the differences seen in stability between these isoforms seem to arise from as little as two to three amino acid substitutions in the primary sequence. Several studies examining the affect of point mutations in the stability of hCA II in GuHCl show varying destabilization in these variants with C_m values ranging from 0.9 M to < 0.1 M.[61–66]

Early studies involving GuHCl denaturation also revealed that the unfolding pathway of hCA I, hCA II and bCA II occurs in two well-defined transition states via a stable molten-globule intermediate composed of the central β-strands.[56,67] Studies involving mutagenesis of residues in this hydrophobic core into radio-labeled cysteines revealed that some portion of this region of hCA II remained folded up to solubility limit of GuHCl (~6 M).[61,68,69] Interestingly, the same point mutations mentioned above that showed varying stability of the native structure had little to no effect on the stability of the molten globule state and, in some cases, actually increased the C_m value for the intermediate.[61–66] Truncation of the first five amino acid residues in the N-terminus of hCA II results in a moderate destabilization (ΔC_m = 0.5 M compared to that of wild-type hCA II) of the native state.[66] Further truncation of the N-terminus up to 24 residues does not significantly destabilize the native or the molten globule state of the enzyme. This suggests that there are only one or more residues within the first 24 amino acids that interact(s) with the rest of the protein and contribute(s) minimum stabilization energy (~5 kcal/mol).[66] In contrast, digestion of the first three C-terminus residues of hCA I with

carboxypeptidase revealed a significant decrease in stability from a C_m of 1.5 M GuHCl for the native enzyme to 0.6 M for the truncated variant.[70]

The metal in the active site of CAs also affects the stability of the enzyme. According to the differential scanning calorimetry (DSC) studies performed on the native and apo-form of hCA II, the enzyme is destabilized by approximately 7 °C when comparing the melting temperature (T_m) of the two forms (58 °C versus 51 °C for native and apo-hCA II, respectively), resulting in a destabilization of about 12 kcal/mol.[71] Cobalt can replace the zinc in the active site of hCA II without major structural changes or significant loss of activity and stability[72,73] whereas, the C_m-value decreases by approximately 0.2 M GuHCl for cobalt-substituted hCA I and bCA II[74] as compared to hCA II.

Studies involving tryptophan fluorescence confirmed the absence of a molten-globule intermediate in the denaturation pathway of hCA II with a C_m value of 4.4 M urea.[75] The authors predict that the difference in denaturation between urea and GuHCl is due to the ionic character of GuHCl. The high ionic strength of NaCl may help to weaken the ionic interactions in the native state of hCA II which could explain the similar results seen between denaturation using GuHCl and urea with high salt concentrations.

Circular dichroism (CD) studies performed on hCA I and II suggest approximately 20% α-helix characterization below pH 4, which is much higher than that of the protein near neutral pH.[76] During the second transition, measurements of the intrinsic viscosity (η) of a solution of bCA II suggests that only partial denaturation occurs at pH 2 (η = 8.4 cm^3/g)[77], unlike that seen with GuHCl or urea (η = 29.6 cm^3/g) which is consistent with the viscosity of a solution containing random coil characteristics (η = 29 cm^3/g).[78] This

partial denaturation in acidic conditions was also observed in hCA I and II with the stability showing a strong dependence on the ionic strength of the buffer.[60,79] Incomplete denaturation of CA in acidic conditions could be due to electrostatic repulsions that fail to overcome hydrophobic forces, salt bridges and other favorable interactions.

Other Cytosolic hCAs: III, VII and XIII

The stability of the other hCAs have not been as extensively studied as hCAs I and II, but what has been reported to date in the literature reveals some similarities and interesting differences between the isoforms. CD studies on bCA III showed a similar profile to that of hCA II, with a molten-globule intermediate occurring at a C_m value of 1.0 M GuHCl and a completely unfolded state at a C_m of 2.6 M GuHCl.[80] Although bCA III contains five free cysteine residues that could form inter- and/or intra-molecular disulfide bridges during the unfolding process, the CD spectra of bCA III in reducing conditions was similar to those without dithiothreitol (DTT). This suggests that these cysteines do not form linkages during denaturation. Interestingly, hydratase and esterase activity studies on CA III isolated from mice (mCA III) at various ages revealed that the mCA III from older mice show a significant tolerance to thermal denaturation compared to the young mice.[81] This is believed to be a result of glutathiolation resulting in an unusual disulfide linkage between cysteine residues and glutathione and could provide protection against the highly oxidative environment.[81]

The X-ray crystal structure of hCA VII shows a disulfide bond between residues 54 and 178 (hCA VII numbering).[82] However, the authors were careful to note that these two cysteines are not conserved in other α-CAs and that disulfide bonds are rare among cytosolic proteins. It was concluded, therefore, that this disulfide bond could be a result of the oxidizing conditions that arise during protein handling. As of present, there have

been no stability studies done with hCA VII but, based on the sequence identity to hCA I (51%), hCA II (56%) and hCA III (53%) (Table 1-2) similar stability characteristics could be assumed.

Recently, the heat dependency of hCA XIII denaturation has been reported.[83] It was shown by DSC studies that hCA XIII undergoes a two-state denaturation phase change from native to a completely unfolded state, similar to those previously reported for hCA I[84] and hCA II[71,85], with a T_m at approximately 59 °C. It was also seen that when complexed with a tight-binding inhibitor of CA, ethoxyzolamide, the T_m increased to 72 °C, a common trend seen with other inhibitors of hCA II.[9]

The Extracellular hCAs: IV, VI, IX, XII and XIV

The X-ray crystal structure of hCA IV[86] revealed that the presence of two disulfide linkages between 6-11G and 23-203 (hCA IV numbering) may contribute to its stability in 5% SDS.[87,88] The latter disulfide linkage stabilizes an important loop in the active site containing Thr199, which hydrogen bonds to and orients the zinc-bound hydroxide for catalysis.[86] A disulfide bridge between residues 23 and 203 was engineered in hCA II. Additionally, Cys206 was mutated to Ser in order to avoid 23-206 disulfide formation. An enhancement in stability of this triple mutant was observed: ΔC_m = 0.8 M GuHCl[89] and ΔT_m = 13 °C. (Boone CD et al 2013; accepted in *Acta Crystallogr. D Biol. Crystallogr*)

This disulfide (23-203) linkage is conserved in hCAs VI, IX, XII and XIV[39,90–92], but these isoforms are more sensitive to SDS than hCA IV. This suggests that the additional disulfide bridge between residues 6 and 11G in hCA IV accounts for the enhanced SDS-resistance.[92] Additionally, the X-ray crystal structure of hCA IX reveals a dimeric complex that is linked together via an intermolecular disulfide bridge at residue

41 (hCA IX numbering).[90] The implications on stability of this linkage are not yet fully understood, but hCA IX has been associated with tumor cells which are surrounded by a highly acidic environment compared to those of other hCAs.[93]

The CA-RPs: hCAs VIII, X and XI

Unfolding studies on hCA-RP VIII with GuHCl showed that this isoform, like hCA II, unfolds in two distinct transitions, but was more sensitive to GuHCl chemical denaturation than hCA II (C_m = 0.4 M for hCA-RP VIII, and C_m = 0.9 M for hCA II).[43] Based on near-UV CD experiments, it was concluded that the destabilization of hCA-RP VIII could be due to an extended N-terminus, giving it a less compact tertiary structure as compared to hCA II. The sensitivity of hCA-RP VIII to GuHCl could be due to the high ionic character found on the surface (E-loop and α3-β15 loop), as the proposed mechanism of GuHCl denaturation occurs via disruption of ionic charges on the surface of hCA II.[75] Additionally, the lack of a metal coordinating to the active site has shown to have destabilizing effects in both hCA II and bCA II.[71,94] Stability studies and high-resolution structures of hCA-RPs X and XI are not yet available, but it may be predicted that the lack of a metal-coordinating ion in the active site of these proteins would have similar destabilizing effects as those seen with hCA-RP VIII, apo-hCA II and bCA II.

Discussion

The determination of crystal structures for all the catalytically active α-CAs (i.e., hCA I[95], hCA II[29], hCA III[34], hCA IV[86], mCA VA[35], hCA VI (unpublished, PDB ID: 3FE4), hCA VII (unpublished, PDB ID: 3MDZ), hCA IX[90], hCA XII[91], hCA XIII[40] and mCA XIV[92] will provide a better understanding of the mechanisms of inhibition of different hCAs. This has initiated significant advances in the development of CAIs and their administration in humans.[96]

Most tumors experience a structurally and functionally disturbed microcirculation of oxygen which pathophysiologically causes an inadequate supply of oxygen (a condition called hypoxia).[6,97–102] There is evidence that hCA IX expression allows tumors to acclimate to a hypoxic microenvironment, promoting tumor cell proliferation, and that hCA IX expression is related to poor survival in patients.[41,103] HCA IX is a transmembrane protein with a extracellular hCA catalytic domain. This domain is very similar to hCA II and acts as an off-target for most CA inhibitors (CAIs). The only known structure of hCA IX (PDB ID: 3IAI)[90] has an r.m.s.d. of 1.5 Å with hCA II (PDB ID: 3KS3)[29]. However, the existence of certain amino acid differences on the surface, referred to as the “selective pocket”, in hCA IX[104] could be exploited for design of isoform specific CAIs. Apart from the catalytic CAs, determination of crystal structure of hCA-RP VIII (PDB ID: 2W2J)[45] has reinforced the efforts to study the other two hCA-RPs and investigate the possible role of these acatalytic CA isoforms.

The biophysical properties of CAs that contribute to the stability and folding pathway have been extensively studied. While these studies have mainly focused on hCAs I and II, the conclusions can be applied to other protein families in which these characteristics remain elusive. Further research is needed to fully characterize the stability of several human isoforms, namely the extracellular hCAs (IV, VI, IX, XII and XIV) as well as the mitochondrial hCAs (VA and VB). All of these isoforms experience unique environments compared to those of the cytosolic hCAs (I, II, III, VII and XIII).

The favorable properties of hCA II (high kinetic parameters, easy expression, high solubility, intermediate heat resistance) have made it an attractive candidate for numerous industrial applications[85]; however, there are few prokaryotic extremophilic

CAs (such as SspCA and SazCA) recently discovered in *Sulfurihydrogenibium yellowstonense* that show comparable enzymatic activity and higher thermostability.[105,106] There is an increasing industrial interest in using hCA II as a bio-catalyst for carbon sequestration of flue-gas from coal-fired power plants. Also, there are established protocols utilizing CA found in algae to capture carbon dioxide and convert it into biofuels and other valuable products.[107,108] There is also interest in using apo-CAs as a bio-sensor for zinc and other transition metals in sea water or human serum.[109]

For industrial applications, small improvements in stability without detriment to yield, activity or solubility, can accelerate the development of hCA II as a better bio-catalyst. Use of the free enzyme in solution can also have disadvantages, as the low-stability can limit recycling and cost-efficiency in an industrial setting.[110] As such, there are numerous studies underway to enhance the stability of hCA II while also retaining its characteristic high catalytic efficiency. One such study deals with mutating some residues to Cys in wild-type hCA II in order to form disulfide linkages.[89] Figure 1-6 shows regions in hCA II where Cys residues can possibly be engineered, based on their presence in other hCAs. Other studies include immobilization of hCA II on a variety of surfaces[110,111] and directed-evolution of the enzyme involving mutagenesis of surface hydrophobic residues into hydrophilic moieties.[85] Further research is needed to maximize the stability of hCA II in a wide array of environments without the loss of catalytic efficiency for industrial use.

The overall goal of this research is to study and report new insights into how an inhibitor binds in the active site of human CAs. Reported in the following chapters of this

dissertation are several X-ray crystal structures of hCA II in complex with sulfoamide and non-sulfonamide inhibitors, H64A hCA II in complex with imidazole derivatives, a neutron structure of hCA II in complex with acetazolamide, and several inhibitors manually docked into the active sites of other isoforms of hCA. It is proposed that the information gathered from these structures, along with CA kinetics data provided by collaborating labs in the University of Florida (USA) and the University of Florence (Italy) may be crucial in helping design novel, more isoform specific inhibitors of CA that can be eventually be developed as clinical drugs.

Table 1-1. Catalytic efficiency and distribution of hCA isoforms.

Isoform	k_{cat} (s^{-1})	K_M (mM)	k_{cat}/K_M ($M^{-1}s^{-1}$)	Localization		Ref
				Sub-cellular	Tissue/Organ	
hCA I	2.0×10^5	4.0	5.0×10^7	Cytosol	RBCs, GI tract	6,10,97
hCA II	1.4×10^6	9.3	1.5×10^8	Cytosol	RBCs, GI tract, Eyes, Osteoclasts, Kidneys, Lungs, Testes, Brain	6,10,97
hCA III	1.0×10^4	33.3	3.0×10^5	Cytosol	Skeletal muscles, Adipocytes	6,10,97
hCA IV	1.1×10^6	21.5	5.1×10^7	Membrane-bound	Kidneys, Lungs, Pancreas, Brain, Capillaries, Colon, Heart muscles	6,10
hCA VA	2.9×10^5	10.0	2.9×10^7	Mitochondria	Liver	13
hCA VB	9.5×10^5	9.7	9.8×10^7	Mitochondria	Heart and Skeletal muscles, Pancreas, Kidneys, GI tract, Spinal cord	13
hCA VI	3.4×10^5	6.9	4.9×10^7	Secretory (milk/saliva)	Salivary and Mammary glands	14
hCA VII	9.5×10^5	11.4	8.3×10^7	Cytosol	CNS	15
hCA-RP VIII			-	Cytosol	CNS	6,10,97
hCA IX	3.8×10^5	6.9	5.5×10^7	Trans-membrane	Tumors, GI mucosa	97,98
hCA-RP X			-	Cytosol	CNS	6,10,97
hCA-RP XI			-	Cytosol	CNS	6,10,97
hCA XII	4.2×10^5	12.0	3.5×10^7	Trans-membrane	Renal, Intestinal, Reproductive epithelia, Eye, Tumors	91
hCA XIII	1.5×10^5	13.8	1.1×10^7	Cytosol	Kidneys, Brain, Lungs, Gut, Reproductive tract	19
hCA XIV	3.1×10^5	7.9	3.9×10^7	Trans-membrane	Kidneys, Brain, Liver	92

Table 1-2. Primary sequence identity (upper right) and number of conserved residues (lower left) among hCA isoforms.

	I	II	III	IV	V	VI	VII	IX	XII	XIV
I	-	60.5	54.4	28.8	43.7	30.9	50.6	31.3	29.8	32.6
II	158	-	58.9	32.4	49.4	32.5	55.9	31.4	28.4	36.0
III	142	153	-	30.2	43.3	32.8	52.9	29.5	27.3	33.0
IV	78	88	82	-	27.9	31.3	33.1	29.4	26.0	34.2
V	114	129	113	76	-	28.6	47.9	29.0	24.3	32.6
VI	83	87	88	85	77	-	35.3	41.0	35.4	41.4
VII	132	146	138	90	125	95	-	34.6	31.6	36.3
IX	85	85	80	80	79	110	94	-	31.2	41.9
XII	79	75	72	70	64	93	84	83	-	37.8
XIV	86	82	88	93	87	110	97	113	99	-

Table 1-3. Structural main chain r.m.s.d. (Å) among hCA isoforms.

	I	II	III	IV	V	VI	VII	IX	XII	XIII	XIV
I	-	0.98	0.87	2.48	1.02	1.55	0.99	2.02	2.07	0.85	1.52
II		-	0.96	2.29	0.98	1.48	0.77	2.05	2.17	0.76	1.50
III			-	2.37	1.01	1.69	0.86	1.79	1.99	0.85	1.41
IV				-	1.65	1.52	2.36	2.81	2.78	1.39	2.48
V					-	1.47	0.83	1.82	1.89	1.30	1.42
VI						-	1.52	1.35	1.58	1.58	1.49
VII							-	1.79	1.97	0.77	1.42
IX								-	1.87	2.06	1.88
XII									-	1.17	1.86
XIII										-	1.18
XIV											-

Table 1-4. Reactions that CAs are believed to be involved in.[4]

$O=C=O + H_2O \leftrightarrow HCO_{3^-} + H^+$
$O=C=NH + H_2O \leftrightarrow H_2NCOOH$
$HN=C=NH + H_2O \leftrightarrow H_2NCONH_2$
$RCHO + H_2O \leftrightarrow RCH(OH)_2$
$RCOOAr + H_2O \leftrightarrow RCOOH + ArOH$
$RSO_3Ar + H_2O \leftrightarrow RSO_3H + ArOH$
$ArF + H_2O \leftrightarrow HF + ArOH$
Ar = 2,4 – dinitrophenyl
$PhCH_2OCOCl + H_2O \leftrightarrow PhCH_2OH + CO_2 + HCl$
$RSO_2Cl + H_2O \leftrightarrow RSO_3H + HCl$
R = Methyl or Phenyl (Ph)

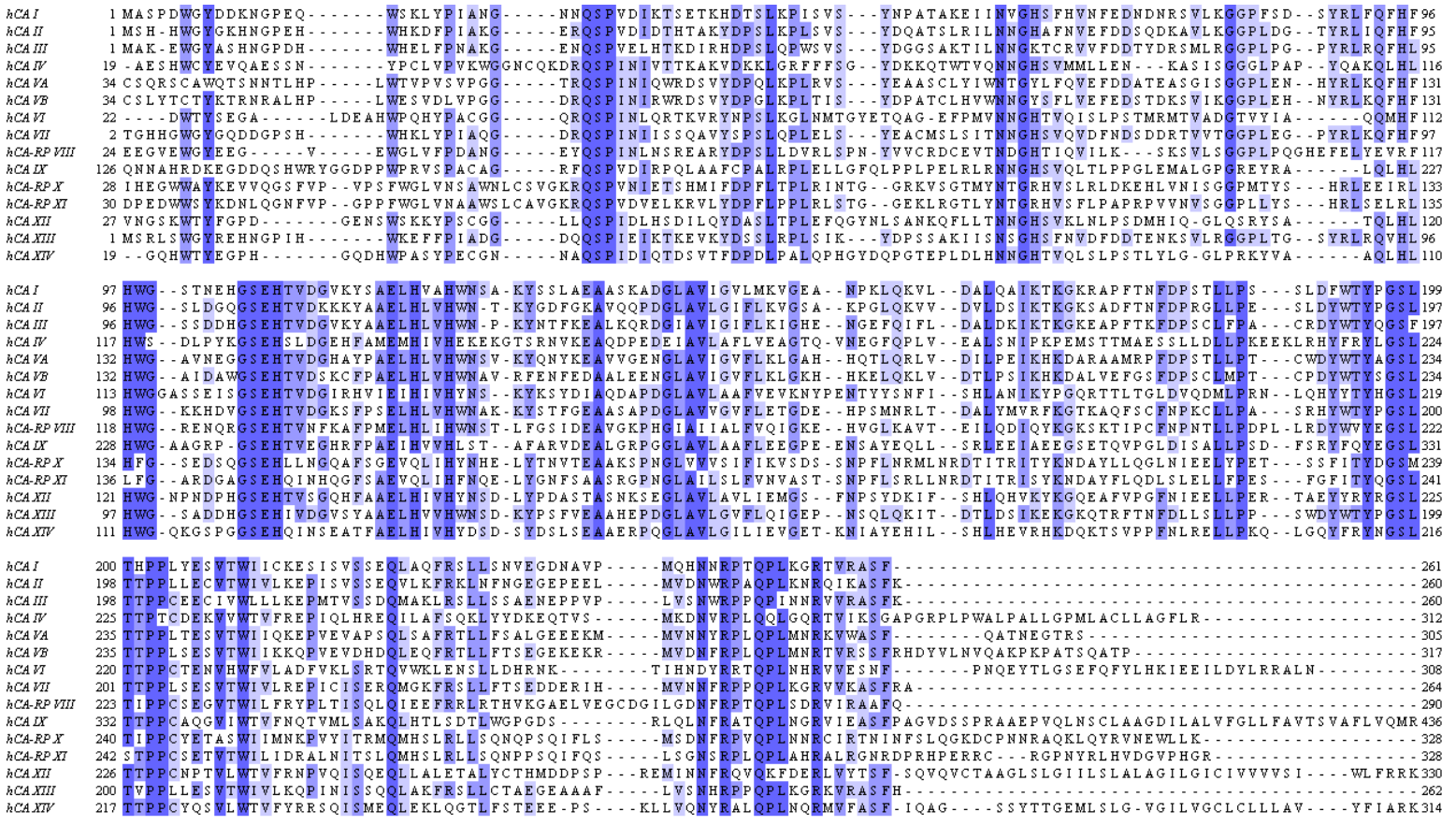

Figure 1-1. Multiple sequence alignment of the hCA isoforms. Gradients of blue represent sequence conservation from most (dark blue) to least conserved (light blue).

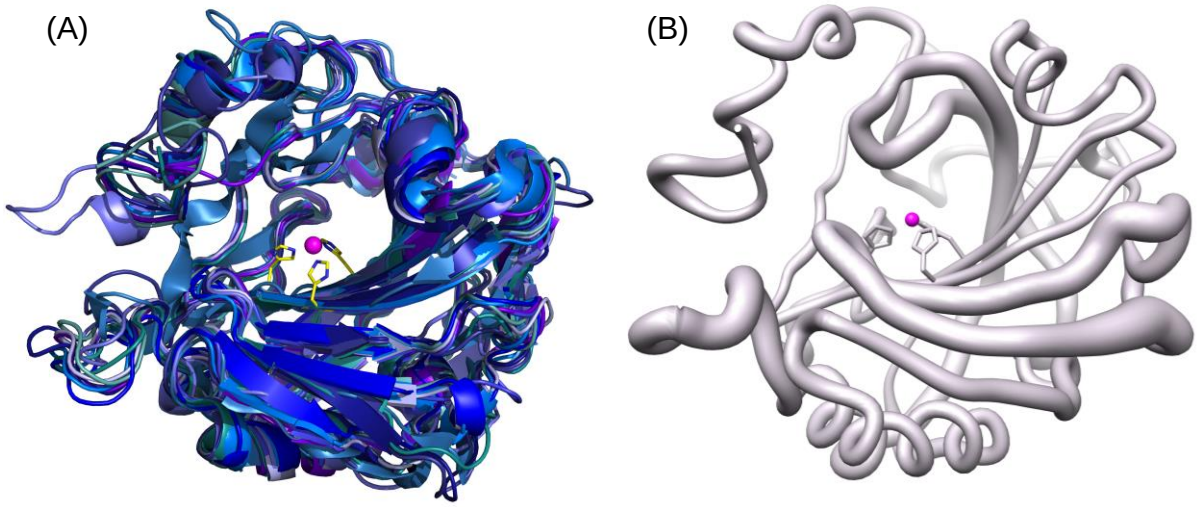

Figure 1-2. (A) Cartoon representation of superposition of the 11 catalytic isoforms of α-CA, in shades of blue. The histidines (94, 96 and 119) that coordinate the Zn^{2+} are shown as yellow sticks. (B) Worm representation of main chain r.m.s.d. of the 11 catalytic isoforms. Thicker regions represent more deviation in the main chain. Figure was made using Chimera.[112]

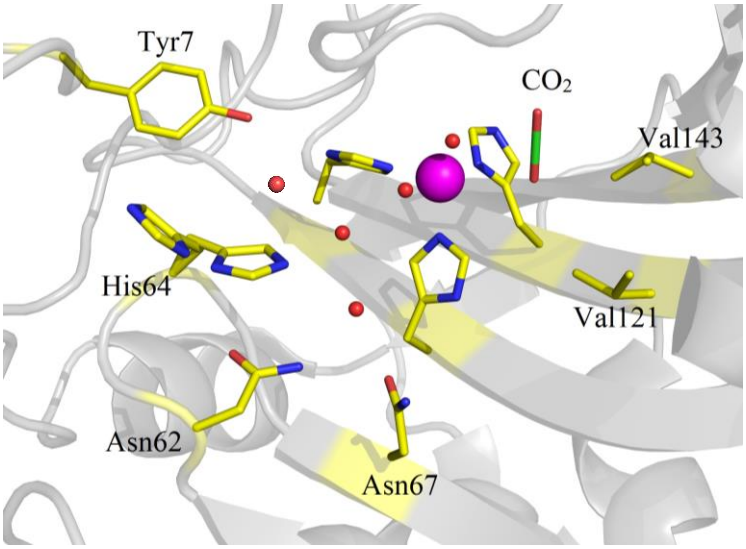

Figure 1-3. Stick representation of the active site of hCA II (PDB ID: 3D92)[3] showing key residues that are involved in CO_2 binding and proton transfer during catalysis.

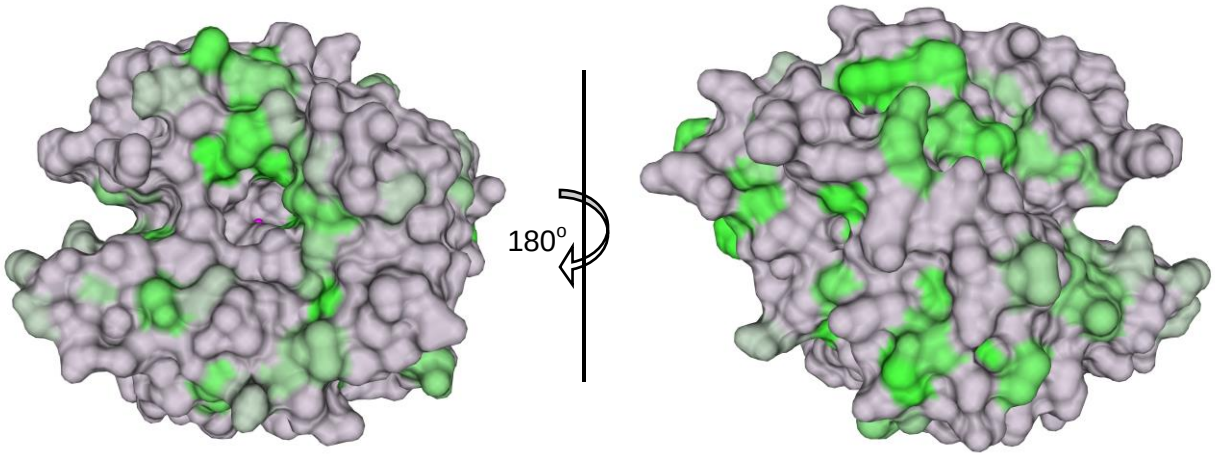

Figure 1-4. Surface representation of conservation of hydrophobic amino acids among the catalytic α-CAs. The conserved residues are colored in a gradient of dark (most conserved) to light (least conserved) green.

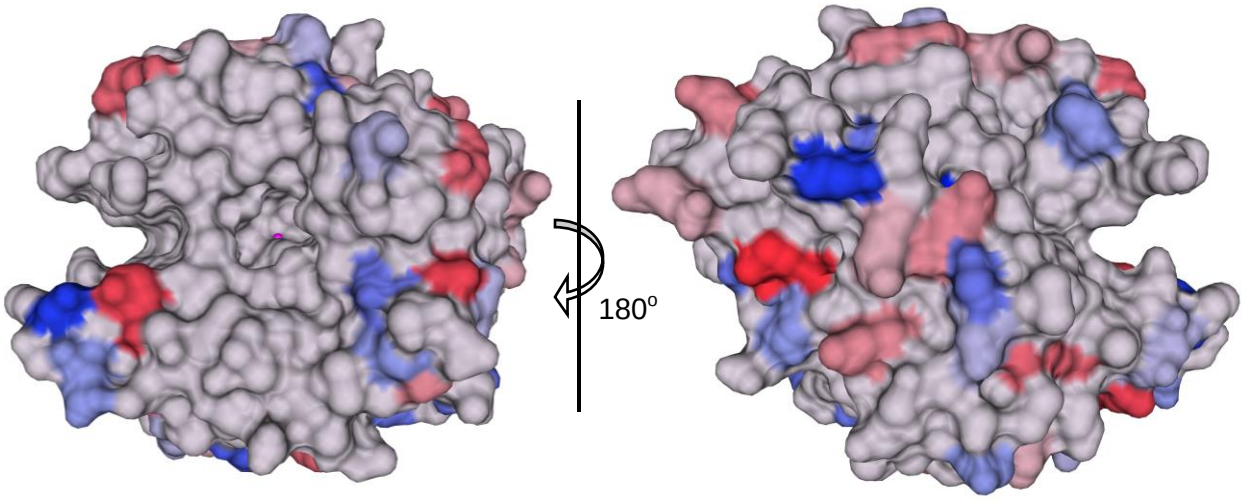

Figure 1-5. Surface representation of conservation of hydrophilic amino acids among the catalytic α-CAs. The conserved residues are colored in a gradient of red (negatively charged) and blue (positively charged), from dark (most conserved) to light (least conserved).

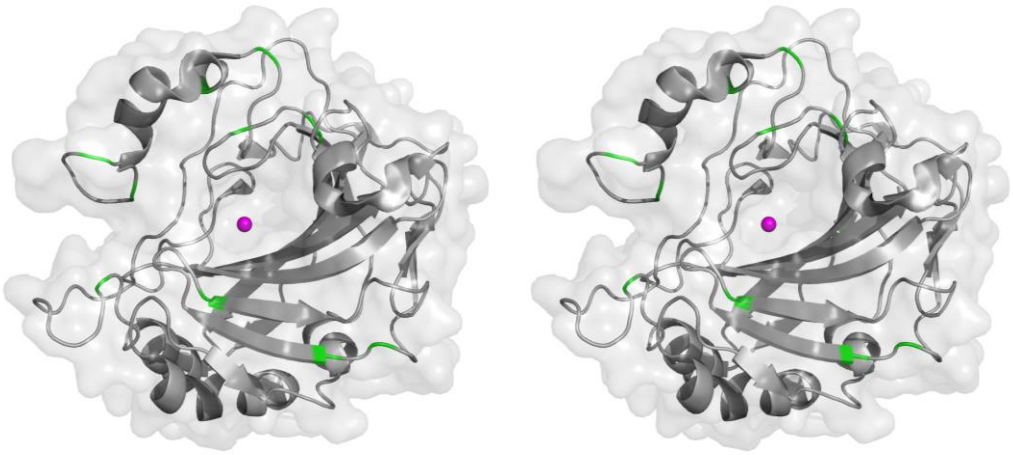

Figure 1-6. Stereo cartoon-surface representation of hCA II (gray) showing the analogous positions of cysteines (green) present in all the catalytic hCAs.

CHAPTER 2
MATERIALS AND METHODS

Expression and Purification of CA II

The recombinant gene for CA II was cloned into a pET-32(b) plasmid vector with an ampicillin resistance gene[113] and expressed in *E. coli* BL21 (DE3) cells. The culture was grown at 37 ºC in the presence of ampicillin (100 µg/mL) until they reached an OD_{600} of 0.6, and thereafter induced with IPTG (100 µg/mL) for protein expression. The lysate was then purified using affinity chromatography using a p-aminomethyl benzene sulfonamide column.[114] Non-specifically bound proteins were washed off the column using buffers (200 mM sodium sulfate) at pH 7.0 and pH 9.0, finally eluting the protein with elution buffer (400 mM sodium azide). The enzyme was thereafter buffer exchanged to remove sodium azide, and concentrated to 15 mg/mL (450 µM) using a 10 kDa filter.

Site Directed Mutagenesis

The wild-type cDNA of CA II containing H64A point-site mutation was prepared from a pET-32(b) vector containing the enzyme coding region with an ampicillin resistance gene. This was done via site-directed mutagenesis using the Stratagen QuikChange II kit and primers from Invitrogen. The variant vector was transformed into *E. coli* XL1-Blue supercompetent cells, and confirmed by DNA sequencing of the entire coding region. The recombinant H64A CA II gene was cloned in *E. coli* BL21 (DE3) cells.

Co-crystallization and X-ray Data Collection

Co-crystals of CA II − ligand complexes were obtained using the hanging drop vapor diffusion method. Drops of 10 µL (0.3 mM CA II, 0.7 mM ligand, 0.1% (v/v)

DMSO, 0.8 M sodium citrate, 50 mM Tris-HCl at pH 7.8) were equilibrated against the precipitant solution (1.6 M sodium citrate, 50 mM Tris-HCl at pH 7.8) at RT (298 K). Imidazoles and dithiocarbamates are soluble in water and hence DMSO was absent from their crystallization conditions. Since the binding affinity of imidazoles is much lower than that of any other inhibitor studied, their concentration was around 150 mM in the crystal drops. Crystals were observed after 5 days. Based on appearance, the best crystals were selected for diffraction studies. Data was either collected at: (1) the national X-ray facility of Cornell High Energy Synchrotron Source (CHESS) on F1 beamline at 100 K, crystal to detector distance maintained at 100 mm, 1^{o} oscillation steps and 1 second exposure per image; or (2) in-house at 298 K mounted in quartz capillary; or (3) in-house at 100 K. In case of data collection at 100 K, cryoprotection was performed by quick immersion into 20% (w/v) sucrose or 20% (v/v) glycerol precipitant solution and flash-cooled by exposing to a gaseous stream of liquid nitrogen at 100 K. In-house data collection was performed with R-AXIS IV^{++} image plate system on a Rigaku RU-H3R Cu rotating anode (λ = 1.5418 Å) operating at 50 kV and 22 mA, using Osmic Varimax HR optics. The detector-crystal distance was set to 80 mm and oscillation steps were 1° with a 5 min exposure per image, for both the datasets.

Structure Determination

The diffraction data were indexed, integrated, and scaled using *HKL2000*.[115] Starting phases were calculated from PDB ID: 3KS3[29] with waters removed. The *PHENIX*[116] package was used for refinement with 5% of the unique reflections selected randomly and excluded from the refinement data set for the purpose of R_{free} calculations.[117] Manual refitting of the model was performed in *COOT*.[118]

Ligand-Binding Studies by PDBePISA

The buried surface area of all ligands in their respective crystal structures were calculated using the online algorithm of "Proteins, Interfaces, Surfaces and Assemblies", provided by Protein Data Bank in Europe (PDBePISA).[119] The ΔG values provided by this algorithm indicate the solvation free energy gain upon formation of the interface, in kcal/mol. The value is calculated as difference in total solvation energies of isolated and interfacing structures. Negative ΔG corresponds to hydrophobic interfaces, or positive protein affinity. However, this value does not include the effect of satisfied hydrogen bonds and salt bridges across the interface.

Differential Scanning Calorimetry (DSC)

DSC experiments were performed using a VP-DSC calorimeter (Microcal, Inc., North Hampton, MA) with a cell volume of approximately 0.5 mL. All CA II − ligand samples were buffered in 50 mM Tris-HCl, pH 7.8 at protein concentrations of ~30 μM. Samples were degassed while stirring for at least 10 min prior to data collection. DSC scans were collected from 20 − 100 °C with a scan rate of 60 °C/hr. The calorimetric enthalpies of unfolding were calculated by integrating the area under the peaks in the thermograms after adjusting the pre- and post-transition baselines. The thermograms were fit to a two-state reversible unfolding model to obtain van't Hoff enthalpies of unfolding. The melting temperature (T_m) values of the CA II − ligand samples were obtained from the midpoints on the DSC curves, indicating a two-state transition. All samples were measured in triplicate with a buffer baseline subtracted.

Enzyme Kinetics Measurements − ^{18}O Exchange

The experiment will be carried out to study the kinetics of catalyzed reaction of CO_2 hydration with CA II and CA IX in presence and absence of selected inhibitors. The

method relies on the depletion of ^{18}O from species of CO_2 as measured by membrane inlet mass spectrometry using an Extrel EXM-200 mass spectrometer.[120] In the first stage of catalysis, the dehydration of labeled bicarbonate has a probability of labeling the active site with ^{18}O (eq 1). In a following step, protonation of the zinc-bound ^{18}O-labeled hydroxide results in the release of $H_2{}^{18}O$ to the solvent and loss of signal from the isotopic species (eq 2).

$$HCOO^{18}O^- + EZnH_2O \rightleftarrows EZnHCOO^{18}O^- \rightleftarrows COO + EZn^{18}OH^- \quad (2\text{-}1)$$

$$H^+His64\text{-}EZn^{18}OH^- \rightleftarrows His64\text{-}EZnH_2{}^{18}O \rightarrow His64\text{-}EZnH_2O + H_2{}^{18}O \quad (2\text{-}2)$$

This approach yields two rates: The R_1, the rate of CO_2 and HCO_{3-} interconversion at chemical equilibrium (Equation 2-1), as shown in Equation 2-3, and R_{H2O}, the rate of release from the enzyme of water with labeled substrate oxygen (eq 2).

$$R_1/[E] = k_{cat}{}^{ex}\,[CO_2]/(\,K_{eff}{}^{CO2} + [CO_2]) \quad (2\text{-}3)$$

In Equation 2-3, $k_{cat}{}^{ex}$ is a rate constant for maximal interconversion of CO_2 and bicarbonate, $K_{eff}{}^{CO2}$ represents a binding constant for the substrate to enzyme. The ratio $k_{cat}{}^{ex}/K_{eff}{}^{CO2}$ is considered equivalent in value to k_{cat}/K_M from steady state experiments, and is a measure of the successful binding and interconversion of substrate and product.

The second rate, R_{H2O}, is the component of the ^{18}O exchange that is dependent upon the donation of protons to the ^{18}O-labeled zinc-bound hydroxide. In such a step, His64 as a predominant proton donor in the catalysis provides a proton (Equation 2-2). The value of R_{H2O} can be determined and considered as the rate constant for proton transfer from His64 to the zinc-bound hydroxide according eq 4, in which k_B is the rate constant for proton transfer to the zinc-bound hydroxide and $(K_a)_{donor}$ and $(K_a)_{ZnH2O}$ are

ionization constants of the proton donor, His64, and zinc-bound water. The least-squares determination of kinetic constants of Equation 2-3 and Equation 2-4 was carried out using Enzfitter (Biosoft).

$$R_{H2O}/[E] = k_B/([1 + (K_a)_{donor}/[H^+]][1 + [H^+]/(K_a)_{ZnH2O}]) \quad (2\text{-}4)$$

The uncatalyzed and carbonic-anhydrase-catalyzed exchanges of ^{18}O between CO_2 and water at chemical equilibrium were measured in the absence of buffer (to prevent interference from the second intermolecular proton transfer reaction) at a total substrate concentration of 25 mM and 25 °C.

CHAPTER 3
CARBONIC ANHYDRASE INHIBITION STUDIES

Introduction to Carbonic Anhydrase Inhibition

Carbonic anhydrases (CAs) are involved in various physiological reactions including respiration, pH regulation, Na^+ retention, calcification, tumorigenesis, electrolyte secretion, gluconeogenesis, ureagenesis, lipogenesis.[6,11–19,121] Being involved in a number of processes, human (h) CA isozymes are therapeutic targets for inhibition to treat diseases such as glaucoma, edema, altitude sickness, epilepsy and obesity. Broadly, CA inhibitors (CAIs) are divided into two main classes which act in either of two different mechanisms, as shown in Figure 3-1: (1) making a trigonal-bipyramidal species (e.g. cyanates) by adding an extra functional group to the already hydroxyl bound zinc, or (2) forming tetrahedral adducts (e.g. sulfonamides) with zinc, by displacing the zinc-bound hydroxyl. In the last couple of decades, novel applications of CAIs have emerged such as systemic anticonvulsants and topically acting anti-glaucoma agents; additionally, more interest has been drawn towards anti-obesity, anti-pain and anti-tumor effects of CAIs.[5–8,10,86,98] Discussed below are X-ray crystal structures and docking studies performed on hCA isoforms with different inhibitors (Figure 3-2).

Selective Pocket Binding by 4-Substituted-UreidoBenzeneSulfonamides[122]

My contribution: Expression of hCA II, its purification, crystallization in complex with 5 sulfonamide inhibitors, structure determination, structural analyses, figure making, and manuscript writing.

Adapted from: Pacchiano, F.; Aggarwal, M.; Avvaru, B. S.; Robbins, A. H.; Scozzafava, A.; McKenna, R.; Supuran, C. T. Selective hydrophobic pocket binding observed within the carbonic anhydrase II active site accommodate different 4-substituted-ureido-benzenesulfonamides and correlate to inhibitor potency. *Chem. Commun. (Camb.)* **2010**, *46*, 8371–8373.

Introduction

The crystal structures of hCA II complexed with compounds **101–105** were determined to a resolution of ~ 1.5 Å (Table 3-1). All five compounds were well ordered and refined with full occupancy, and B-factors that were comparable to the solvent within the active site (Figure 3-3 and Table 3-1). Similar to other sulfonamide inhibitors of hCA II,[26,123–126] the ureido-substituted sulfonamides are buried deep in the active site, displacing solvent molecules (Figure 3-3A), with the sulfonamide amine nitrogen binding directly to the active site zinc atom and accepting a hydrogen bond from OG1 of Thr199 and with the O2 of the sulfonamide accepting a hydrogen bond from the main-chain nitrogen atom of Thr199 at a distance of 2.9-3.0 Å. The overall $Zn(N)_4$ coordination can be described as a distorted tetrahedron. The compound moieties protrude out of the active site and are stabilized by both hydrophilic and hydrophobic residues (Figure 3-3 and Figure 3-4). As in other hCA II complexes, for all five compounds, additional electron density consistent with a bound glycerol molecule, from the cryoprotectant solution used during data collection, was observed adjacent to the aromatic ring of the benzene sulfonamide (data not shown).

Crystal Structure Details

For all five compounds the benzene core is at van der Waals distance from the side chain of Leu198, and is sandwiched on the other side by the glycerol molecule, and atoms from Val121 and Gln92. Hydrogen bonds from the O1 and O2 hydroxyl groups of the glycerol anchor it to the side chain atoms of Asn67 and Asn62. Other than **104** there are no direct hydrogen bonds between the compounds and the active site other than those linking the sulfonamide to the surrounding amino acids. Two bridging solvent molecules link O8 to NE2 of Gln92 and N7 to the main chain carbonyl oxygen of

Pro201, respectively. All the compounds are non-planar and exhibit a twisted shape that can be ascribed to two torsion angles, C5–C4–N7–C8 (orange arrow) and C8–N9–C10–C15(C11) (blue arrow) (Figure 3-3).

For **101**, the C5–C4–N7–C8 and C8–N9–C10–C15 torsion angles are -30° and -38°, respectively. This allows the terminal fluorine atom F13 to make hydrophobic contacts with side chain carbon atoms of Pro202 and Leu204. Other hydrophobic interactions are between N9, C10 and C15 with the CE2 carbon atom of Phe131 in a face-to-edge interaction, C14 with CB and CG of Pro202 and CD1 of Leu198, and C13 with CB and CG of Pro202 (Fig. 3-3B). For **102**, the C5–C4–N7–C8 and C8–N9–C10–C11, torsion angles are -18° and -45°, respectively. This allows the pentafluorophenyl atoms C12, C13, F12, and F13 to make hydrophobic contacts with the CB and CG atoms of Pro202 (Figure 3-3C).

With **103**, the C5–C4–N7–C8 and C8–N9–C10–C11, torsion angles are 5° and -66°, respectively. The overall shape of the inhibitor brings the isopropyl methyl carbon atom C18 into hydrophobic contacts with methyl carbon atoms of Val135 and the CD1 atom of Leu198, respectively. Other hydrophobic interactions are between the ring atoms of the isopropylphenyl group with the CE2 carbon atom of Phe131 in a face-to-edge interaction (Figure 3-3D). Compound **104** differs from **101**, **102**, **103** and **105** in that a direct hydrogen bond is observed between the inhibitor and the active site, in addition to those linking the sulfonamide to the surrounding amino acids. This interaction, which does not involve a solvent bridge, is between Gln92 NE2 and O8 of the inhibitor at a distance of 2.8 Å (Figure 3-3E). Again, **104** exhibits nonplanarity with the C5–C4–N7–C8 and C8–N9–C10–C15, torsion angles being -34° and -19°,

respectively. This allows the terminal nitro atoms N16, O16 and O17 to make hydrophobic contacts with side chain carbon atoms of Ile91, Glu69, and Gln92 (Figure 3-3E). Other hydrophobic interactions for **104** are observed between the aromatic ring of the nitrophenyl group and a dimethyl sulfoxide (DMSO) C1 carbon atom (used to dissolve the compounds). The ring is also in a partial stacking interaction with Phe131 and these interactions make the orientation of **104** uniquely different from the other compounds (Figure 3-3E and Figure 3-4).

With **105**, the C5–C4–N7–C8 and C8–N9–C10–C11, torsion angles are -164° and -175°, respectively. The torsion angles allow the cyclopentyl group of **105** to make hydrophobic contacts with side chain carbon atoms of Pro202 and Phe131. Both N9 and N7 are within hydrogen bond distance of a water molecule, which also is a bridge solvent to the main chain O atom of Pro201 (Figure 3-3F).

Discussion and Conclusion

The X-ray data for the five hCA II adducts of sulfonamides **101–105** presented above show that the benzenesulfonamide part of the molecules is very much superposable between the five adducts, whereas the ureido and aryl/cycloalkyl moieties are much less so. Data of Figure 3-4 clearly show that three of the five compounds (**101**, **102** and **105**) bind in a rather similar manner, with the 4-fluorophenyl, pentafluorophenyl and cyclopentyl moieties observed in the same active site region. This is a rather well defined hydrophobic pocket observed in other hCA II–sulfonamide adducts.[125,126]

By comparing the inhibition constants of the five inhibitors (Figure 3-1)[122] with their superposition when bound to the enzyme (Figure 3-4), a very interesting fact emerges: the three inhibitors binding in the same hydrophobic pocket (compounds **101**,

102 and **105**) are the weaker ones (K_Is in the range of 50–200 nM) in the small series of derivatives investigated here. Compounds **103** and **104** that bind in a different pocket are much more effective hCA II inhibitors (K_I of 3 and 15 nM, respectively). As above, the differences of activity between the most active **103** and the least active **105** sulfonamides investigated here are significant, a factor of 68, and this difference can be directly attributed to the rather diverse binding of the substituted ureido tails of these compounds in the various hydrophobic pockets/regions of the enzyme.

Another aspect that should be stressed here, which probably explains the rather variable binding patterns of these structurally similar compounds to hCA II, is related to the presence of the ureido fragment (NHCONH) which connects the benzenesulfonamide part of the molecule to the aryl/cycloalkyl tails. As seen from the crystallographic data, the torsion angles between these two fragments of the scaffold are different in the five compounds investigated here. This probably allows the flexibility of the inhibitor to select the most energetically favorable hydrophobic pocket to bind into and avoid steric clashes[23] and/or to make as many as possible favorable interactions with amino acid residues within the enzyme cavity. Most of the hCA inhibitors (CAIs) of sulfonamide type investigated earlier contained CONH or SO_2NH linkers instead of the ureido one present in **101–105**. These two different linkers allow less flexibility for the inhibitor scaffold, and probably this is the reason why most of those compounds bind in the canonical hydrophobic pocket. It is thus rather obvious that even a very minor moiety (in this case the linker) from the scaffold of a CAI may contribute significantly to the overall potency of the compound.

In conclusion, this study demonstrates the importance of the hydrophobic pockets/regions within the hCA II active site for the binding of a series of structurally related sulfonamides possessing various ureido substitutions. These findings can be extended to other classes of CAIs, and probably also to other hCA isoforms, less well investigated than hCA II, with the possibility of designing inhibitors with a better selectivity for the various isoforms with medicinal chemistry applications.

Conformational Variability of Sulfonamides with Thienyl-Acetamido Moieties[127]

My contribution: Expression of hCA II, its purification, crystallization in complex with two sulfonamide inhibitors, structure determination, docking of these compounds with hCAs I, III, VII and XIII, structural analyses, figure making, and manuscript writing.

Introduction

Recently, a class of aromatic, heterocyclic sulfonamides incorporating 2-thienylacetamido moieties in their molecule was reported, which showed good selectivity ratios for inhibiting some hCA isoforms, such as hCA VII over hCA I and II.[128,129] Among these derivatives, sulfonamides **106** and **107** differing only by a supplementary fluorine atom triggered our attention for several reasons. Both **106** and **107** were observed to be low nanomolar hCA VII inhibitors (K_Is ~ 7 nM), and recently it has been established that this brain-associated cytosolic isoform may be the target of drugs against neuropathic pain.[130] In addition, **106** and **107** were less effective as inhibitors of other two cytosolic isoforms, hCAs I and II, which are widespread in many tissues and thus constitute off-targets when the inhibition of other such enzymes are

---

Adapted from: Biswas, S.; Aggarwal, M.; Güzel, Ö.; Scozzafava, A.; McKenna, R.; Supuran, C. T. Conformational variability of different sulfonamide inhibitors with thienyl-acetamido moieties attributes to differential binding in the active site of cytosolic human carbonic anhydrase isoforms. *Bioorg. Med. Chem.* **2011**, *19*, 3732–3738.

required. Indeed, **106** and **107** showed inhibition constants in the range of 60–160 nM against hCA I and of 50–400 nM against hCA II.[129] Two issues thus rose regarding the inhibitory properties of these two structurally related compounds: why the presence of a fluorine atom in **107** leads to an hCA II inhibitor ~8 times less effective compared to **107**? The second question is: why these two compounds show highly effective hCA VII inhibitory activity? In order to address these questions we report here the X-ray crystal structure of the two compounds in complex with hCA II as well as a detailed study for their interactions with all cytosolic hCA isoforms, that is, hCAs I, II, III, VII and XIII.

Crystal Structure Details

The crystal structures were determined to 1.6 and 1.7 Å resolution. Both compounds were refined with full occupancy, and B-factors that were comparable to the side chains within the hCA II active site (Table 3-3). Compounds **106** and **107** had a buried surface area of ~350 $Å^2$ (74%) and ~360 $Å^2$ (74%), respectively, at the interface with hCA II active site. For **106**, the C5–C4–N7–C8 and C8–N9–C10–C11 torsion angles are -1° and -125°, respectively. The C5–C4–N7–C8 torsion angle is essentially planar and the O8 carbonyl oxygen points towards Gln92, on the Phe131 side of the active site. While the C8–N9–C10–C11 torsion angle permits the preceding thiophene ring to be orientated with the sulfur, S14, pointing toward Pro202, on the opposite side of the active site to Phe131 (Figure 3-5A). In case of **107**, the C5–C4–N7–C8 and C8–N9–C10–C11 torsion angles were 158° and 124°, respectively. The C5–C4–N7–C8 torsion angle is almost 180° to that of **106**. This torsion angle change can be attributed to the fluorine atom, F5, attached to the benzene ring, as having both the F5 and O8 atoms in a cis-configuration would create steric hindrance. This has the effect of placing the O8 carbonyl oxygen towards Pro202, away from Phe131.

In addition, the C8–N9–C10–C11 torsion angle is rotated which rotates the thiophene ring, to be almost perpendicular to its position observed in **106**, although the S14 atom occupies the same spatial location (Figure 3-5B). Superposition of the two structures (Cα r.m.s.d. 0.05 Å) reveals that they almost occupy the same volume of the hCA II active site, though the orientation of the O8 carbonyl oxygen points in opposite directions of the active site and the thiophene ring is closer to the Pro202 and Val135 for **107** (Figure 3-5). Thus, the placement of a fluorine atom on the benzene ring causes a steric clash for **107** which is elevated by a cis−trans transition of the carbonyl oxygen atom and a torsional angle adjustment of the thiophene ring.

Docking onto hCAs I, III, VII and XIII

Compound **107** investigated in the present study was a weaker inhibitor than **106** against hCA II, probably because of the presence of the supplementary fluorine atom, which is located in a hydrophobic environment in close proximity to residues Phe131 and Val121 in the hCA II active site. The hydrophobic nature of these residues is conserved across all hCA isoforms investigated here. It is conceivable that the presence of a polar atom (fluorine) in a hydrophobic enzyme pocket makes **107** a weaker inhibitor in comparison to **106**, which has no halogen atom attached to it. In addition, the carbonyl oxygen O8 of **107** points towards the carbonyl group of Pro201 of hCA II, thus placing it in a charge repulsive environment, which is not seen in the hCA II–**106** complex. This is an example of how a relatively minor change in the chemical structure of a sulfonamide CAI can have significant consequences to its affinity for the enzyme, strongly influencing its binding within the active site.

Among all isoforms studied here, the inhibition of hCA III was weaker than the others (Table 3-2). The rationale for this is clear, as hCA III has a bulky hydrophobic

residue (Phe198) in the middle of the active site cavity, which is a leucine in the other four studied isoforms. This bulky residue effectively prevents a large inhibitor to bind into the active site (Figure 3-6). The present data also showed that the best inhibition with **160** and **107** was against hCA VII (Table 3-2). This potent inhibition is probably due to the presence of Lys93 in hCA VII, an amino acid residue which is unique only to this isoform, providing a hydrophilic and flexible amino acid residue in the middle of the active site, which furnishes an additional interaction point for the inhibitor.

Based on a model generated using *COOT*,[118] Lys93 can have an alternate conformation leading to the formation of a hydrogen bond with either the carbonyl oxygen of **106** or the fluorine atom present in **107**, thereby further stabilizing the inhibitor – hCA VII complexes. When this residue is replaced by a bulky side chain such as Arg91 (in the case of hCA XIII and hCA III) the inhibition with **106** and **107** is weaker compared to hCA VII, most likely because the flexibility of Arg91 is reduced compared to that of the lysine present in hCA VII, also leading to steric clashes. In addition, hCA VII also has a smaller side chain (Ala137) close to the active site instead of hydrophobic, bulkier Val135 (present in hCA II and XIII), which might facilitate the binding of inhibitors within the hCA VII active site.

Discussion and Conclusion

The X-ray crystal structure of hCA II complexed with two aromatic sulfonamides incorporating 2-thienylacetamido moieties was reported. The two inhibitors only differ by the presence of an additional 3-fluoro substituent on the 4-amino-benzenesulfonamide scaffold of one of them, but their inhibition profiles against the cytosolic isoforms hCA I, II, III, VII and XIII are quite different. These differences were rationalized based on the obtained X-ray crystal structures. Specific interactions between the structurally different

inhibitors and amino acid residues present only in some of these isoforms have been shown, which explain the high affinity of the 2-thienylacetamido benzenesulfonamides for some pharmacologically relevant CAs such as isoforms II and VII, and might be useful for the drug design of isoform-selective sulfonamide inhibitors of various CAs. Collectively these results help us understand the affinity/selectivity of different sulfonamide inhibitors towards the cytosolic hCA isoforms, which show a great variation in their inhibition profile for this class of pharmacologically important compounds even in the presence of minimal structural changes of inhibitors.

Anticonvulsant 4-Aminobenzenesulfonamide Derivatives[131]

My contribution: Expression of hCA II, its purification, crystallization of hCA II in complex with three sulfonamide inhibitors, their docking with hCAs I, VII and XIV, structure determination, structural analyses, figure making, and manuscript writing.

Introduction

Epilepsy is one of the most common neurological disorders.[132] Triggering mechanisms by which seizures form remain unclear but are related to a rapid change in ionic composition, including an increase of intracellular potassium concentration and pH shifts within the brain.[133–136] The pH buffering of extra- and intracellular spaces is mainly carried out by the CO_2/HCO_3-system, and this equilibrium is regulated by CA. However, the link between hCA inhibition and seizures is poorly understood primarily because many hCA isoforms (such as CAs I, II, III, IV, VB, VII, VIII, X, XI, XII, and XIV) are

Adapted from: Hen, N.; Bialer, M.; Yagen, B.; Maresca, A.; Aggarwal, M.; Robbins, A. H.; McKenna, R.; Scozzafava, A.; Supuran, C. T. Anticonvulsant 4-aminobenzenesulfonamide derivatives with branched-alkylamide moieties: X-ray crystallography and inhibition studies of human carbonic anhydrase isoforms I, II, VII, and XIV. *J. Med. Chem*. 2011, 54, 3977–3981.

present in the brain.[6,137–139] Several, such as CAs II, VII and XIV, have been noted for their contributions to epileptiform activity.[6,137–139] Several studies have investigated the design/synthesis of sulfonamide/sulfamate CAIs as potential anticonvulsants.[140–144] A study has been performed on the inhibition of the hCA isoforms thought to be involved in epileptogenesis, i.e., hCAs I, II, VII, and XIV, with a series of benzenesulfonamides CAIs incorporating branched aliphatic carboxamide moieties in the para position of the aromatic ring (Table 3-3). Furthermore, the X-ray crystal structures of adducts of three such compounds with the physiologically dominant isoform hCA II have led to new insights for the design of potent inhibitors of these metalloenzymes.

Crystal Structure Details

The crystal structures of hCA II complexed with compounds **108**, **109**, and **110** were determined (Figure 3-6) to a resolution of ~ 1.5 Å. All three compounds were well ordered and refined with occupancies between 0.7 and 1.0, and B-factors that were comparable to that of the solvent within the active site. Protruding from the active site, the tails of the compounds are stabilized predominantly by hydrophobic residues. All three structures are at a van derWaals distance from the side chains of Val135, Phe131, Leu198, and Pro202 (Figure 3-7). Hence, **108**, **109**, and **110** bury approximately the same amount of protein surface area of 140, 125, and 125 $Å^2$, respectively. Compound **12** exhibits the lowest average B-factor of 13 $Å^2$ compared to **110** and **109** whose average B-factors are 24 and 21 $Å^2$, respectively (Table 3-4). Also, **110** refines with a lower occupancy of 0.7 than the other two compounds and the bifurcated hydrophobic tail is less ordered and more solvent exposed at the mouth of the active site. However, all these compounds have very similar inhibitory action against hCA II, with K_I ~ 10 nM.

Although the overall structures of hCAs I, II, VII, and XIV are similar, there are several differences in the type and spatial arrangement of amino acids within the active sites (Figure 3-8). Of particular note are the three hydrophobic residues (Phe131, Val135, and Leu204) on the surface of hCA II that play an important stabilizing role when interacting with the longer hydrophobic termini R- groups of sulfonamide inhibitors. The weaker binding of **108-110** with hCA XIV compared to hCA II can be directly attributed to these amino acid differences, which are Leu131, Ala135, and Tyr204 in hCA XIV. The overall reduction in hydrophobicity of the active site appears to have a significant effect and reduces the affinity of these compounds to hCA XIV (Figure 3-8A, Table 3-3). The amino acids differences between hCAs I and II in the regions where the R- groups of **108** & **109** interact seem to compensate each other. The hydrophobicity decreases with Phe131 and Val135 in hCA II replaced with Leu31 and Ala135, respectively, in hCA I; but increases with Ile91 and Leu204 in hCA II replaced with Phe91 and Tyr204, respectively, in hCA I; these compensatory changes may account for why the two compounds show similar affinities for hCAs I and II. Of note is that the R- group of **110** is less hydrophobic than **108** or **109**. Thus, the reduced modulation in hydrophobicity of amino acids (F131L, V135A, and L204Y) in hCA I that are in proximity to **110** may cause a cumulative effect and weaken its K_I to hCA I compared to hCA II with **108** and **109** (Figure 3-8B, Table 3-3).

In hCA VII, the hydrophilic Ser206, Tyr22 and less hydrophobic Ala137 are Leu204, Phe20, and Val135 in hCA II, respectively, and this reduced hydrophobicity could explain the weak K_I of **108** and **109** to hCA VII compared to hCA II. However, Lys93 in hCA VII (which is the hydrophobic residue Phe in hCA I, Ile in hCA II, and Ala

in hCA XIV) can be modeled to hydrogen bond with the carbonyl group of **110**. The presence of strong hydrophobicity at the inhibitor interaction regions of **108** and **109** (which are more hydrophobic) precludes Lys93 of hCA VII from adopting this conformation (Figure 3-8C, Table 3-3). Therefore, the SARs between the hCA isoforms clearly imply that small differences in the hydrophobicity of the hCA isoform active sites modulate the affinity of the inhibitors' various aliphatic chains.

Discussion and Conclusion

A novel class of anticonvulsant aromatic amides obtained by the coupling of 4-amino-benzenesulfonamides or 4-alkylamino-benzenesulfonamides (alkyl = methyl or ethyl) with phenylacetic acid or branched aliphatic carboxylic acids were recently reported by us.[145] In the current study the most active compounds were **2**, **4**, **13**, **16**, and **17** and were more potent inhibitors of hCAs VII and XIV than hCAs I and II. The hydrophobicity differences in hCA isoforms studied clearly show that small differences in hydrophobic residues in hCA active sites modulate the affinity of the inhibitors with various aliphatic chains, but in this series of 4-aminobenzenesulfonamide derivatives there seems to be little correlation between anticonvulsant activity and inhibition of hCAs I, II, VII, or XIV.

Tricyclic Sulfonamides Incorporating Pyrazole[146]

My contribution: Expression of hCA II, its purification, crystallization in complex with a tricyclic sulfonamide inhibitor, docking of this inhibitor along with celecoxib and

---

Adapted from: Marini, A. M.; Maresca, A.; Aggarwal, M.; Orlandini, E.; Nencetti, S.; Da Settimo, F.; Salerno, S.; Simorini, F.; La Motta, C.; Taliani, S.; Nuti, E.; Scozzafava, A.; McKenna, R.; Rossello, A.; Supuran, C. T. Tricyclic Sulfonamides Incorporating Benzothiopyrano[4,3-c]pyrazole and Pyridothiopyrano[4,3-c]pyrazole Effectively Inhibit α- and β-Carbonic Anhydrase: X-ray Crystallography and Solution Investigations on 15 Isoforms. *J. Med. Chem.* **2012**, *55*, 9619–9629.

valdecoxib onto hCAs I, II, IX and XII, structure determination, structural analyses, figure making, and manuscript writing.

Introduction

For the first time tricyclic sulfonamides **3a−e** incorporating the poorly investigated benzothiopyrano [4,3-c] pyrazole (**3a−c**) and pyridothiopyrano [4,3-c] pyrazole (**3d−e**) systems, as well as the classical benzenesulfonamide moiety responsible for binding to the catalytically crucial metal ion were explored. The lead compounds used in the present drug design study were the clinically used derivatives celecoxib (**CLX**) and valdecoxib (**VLX**), initially launched as cyclooxygenase 2 (COX-2) specific inhibitors,[147–149] and later shown also to act as potent CAIs (Table 3-5)[150–152] Both compounds possess a benzenesulfonamide group linked to a five-membered, substituted heterocyclic ring. The presence of the SO_2NH_2 moiety seems not to be necessary for COX-2 inhibition, but it is essential for the hCA inhibition.[147–152] The two compounds were shown to possess interesting and isoform-selective hCA inhibitory action, and their X-ray crystal structures in complex with hCA II have also been reported earlier.[151,152] The rationale for designing the new compounds **3a−e** reported here was to use the benzenesulfonamide as a zinc binding moiety connected to a pyrazole moiety annealed with a bulky heterocyclic ring in order to explore both alternative chemotypes and the possibility to further enhance the isoform selectivity observed with **CLX** and **VLX** as CAIs.[147–152] Furthermore, compounds **3a−e** may be regarded as geometrically constrained analogues of the two reference leads **CLX** and **VLX**.

Crystal Structure Details

The crystal structure was determined to a resolution of 1.5 Å and compound **3e** was refined with occupancy of 0.8. Residual density adjacent to **3e** was observed in the final Fo−Fc electron density map, revealing a possible second conformer, but refinement efforts to fit this weaker binding site were unsuccessful as the electron density was too diffuse to fit a reliable ordered second molecule. The sulfur atom caused a pucker in the ring geometry but was not directly involved in any interaction with hCA II. Protruding out of the active site, the inhibitor's hydrophobic rings were stabilized predominantly by hydrophobic residues that line the active site cavity, engaging good van der Waals interactions with the side chains of Val121, Phe131, Leu198, Pro202, and His64 (the proton shuttle residue of hCA II). **3e** was buried within the active site with 407 $Å^2$ (78%) of its surface area in contact with hCA II (Figure 3-9). The crystallographic parameters and data collection statistics are shown in Table 3-6.

Docking Studies

The superposition of the hCA II−3e structure was carried out with **CLX** (PDB ID: 1OQ5)[151] and **VLX** (PDB ID: 2AW1)[152] also in complex with hCA II using *COOT*.[118] The most striking feature of this comparison, given that all the inhibitors are tethered to the active site zinc, is the capacity of their tail groups to occupy very different surface locations of the active site (Figure 3-10). Notably, the hydrophobic phenyl ring of the ligand **VLX** pushes the Phe131 out of the hydrophobic pocket compared to inhibitors **3e** and **CLX** (Figure 3-9B, compared to Figure 3-9A and Figure 3-10C). In a similar manner, the pendant hydrophobic phenyl ring of **CLX** forces Asn67 to change conformation differently from inhibitors **3e** and **VLX** (Figure 3-10C compared to Figure 3-9A and Figure 3-9B). In addition, **CLX** has both a fluorine rich hydrophilic region and a

hydrophobic phenyl ring at its terminus. Interestingly, the fluorine rich group is located in the hydrophilic pocket (Leu204, Pro202, Phe131, and Val135) and the hydrophobic phenyl ring is positioned in the hydrophilic pocket (Asn62, Asn67, Glu69, and Gln92). This unusual orientation could be attributed to the bulky nature of the ligand, bearing a large phenyl group in the 5-position of the heterocyclic ring, which may cause a steric hindrance in the relatively small pocket in the active site of hCA II (Figure 3-10B).

On the other hand, the hydrophilic nitrogen atom in the fused pyridine ring of **3e** may be involved in hydrogen bonding with the bulk solvent and hence does not need to stay in the Phe131 hydrophobic pocket. Despite the different conformational changes in hCA II side chains induced by the ligand binding and their distinctly different orientations within the active site (Figure 3-10), all three inhibitors, **3e**, **CLX**, and **VLX** bury approximately the same amount of surface area of the protein: 405, 450, and 410 $Å^2$ respectively. The crystal structure determination of **3e** complexed to hCA II raised several other questions related to the CAI's specificity.

Although the overall structures of hCAs I, II, IX, and XII are similar, compound **3e** behaves as a highly effective hCAs I and II inhibitor, with reduced affinity against hCAs IX and XII (Table 3-5). To investigate the reasons of such binding profile, the crystal structures of hCA I (PDB ID: 2NMX)[153] hCA IX (PDB ID: 3IAI)[90] and hCA XII (PDB ID: 1JCZ)[91] were superimposed with the structure of hCA II in complex with **3e** (PDB ID: 3QYK)[146], highlighting that the differences in affinities could be attributed to a reduction in hydrophobicity in the hydrophobic pockets within the active sites of hCAs IX and XII. Namely, Val131 and Ala204 in hCA IX and Ala131 and Asn204 in hCA XII cause a decrease in hydrophobicity compared to their equivalent amino acids in hCAs I and II

(Table 3-7). Moreover, Arg62 in hCA IX, and residues Lys67, Thr91, Ser135, and Asn204 in hCA XII impart hydrophilic properties to the otherwise hydrophobic region in hCAs I and II (Table 3-7). HCA II (PDB ID: 3QYK)[146] had an r.m.s.d. (main chain) of 0.8 Å with hCA I (PDB ID: 2NMX)[153] 1.5 Å with hCA IX (PDB ID: 3IAI)[90] and 1.1 Å with hCA XII (PDB ID: 1JCZ).[91]

The crystal structure determination of **3e** complexed to hCA II raised several other questions related to the CAI's specificity. Although the overall structures of hCAs I, II, IX, and XII are similar, compound **3e** behaves as a highly effective hCA I and II inhibitor, with reduced affinity against hCA IX and XII (Table 3-5). To investigate the reasons of such binding profile, the crystal structures of hCA I (PDB ID: 2NMX)[153] hCA IX (PDB ID: 3IAI)[90] and hCA XII (PDB ID: 1JCZ)[91] were superimposed with the structure of hCA II in complex with **3e** (PDB ID: 3QYK)[146], highlighting that the differences in affinities could be attributed to a reduction in hydrophobicity in the hydrophobic pockets within the active sites of hCA IX and XII. Namely, Val131 and Ala204 in hCA IX and Ala131 and Asn204 in hCA XII cause a decrease in hydrophobicity compared to their equivalent amino acids in hCAs I and II (Table 3-7). Moreover, Arg62 in hCA IX, and residues Lys67, Thr91, Ser135, and Asn204 in hCA II impart hydrophilic properties to the otherwise hydrophobic region in hCAs I and II (Table 3-7).

Discussion and Conclusion

The new compounds **3a−e**, obtained by an original synthesis, have been designed by using **CLX** and **VLX** as lead molecules. The most interesting feature of this new class of sulfonamides was their capacity to predominantly exert strong inhibition of only hCAs I and II, as well as of the mycobacterial β-class enzymes (Rv1284, Rv3273, and Rv3588c), whereas their inhibitory activity against hCAs III, IV, VA, VB, VI, VII, IX,

XII, XIII, and XIV was at least 2 orders of magnitude lower. The combination of X-ray crystal structure of the hCA II−compound **3e** adduct, and homology modeling explained this peculiar inhibition profile, which is also quite different from those of **CLX** and **VLX**. Thus, the benzenesulfonamides **3a−e** constitute a highly interesting class of compounds which, inhibiting only a restricted number of physiologically relevant hCA isoforms among the 12 catalytically active human enzymes, should lead to fewer side effects. In addition, the good inhibition profile of some of the new derivatives (**3d−e**) against mycobacterial CAs is also to be considered as relevant because these enzymes are less inhibited by other classes of sulfonamides.

Finally, the sulfonamido type CAIs, **CLX** and **VLX**, are known to act also as potent COX-2 inhibitors, with serious concerns about their cardiovascular side effects. Consequently, the high selectivity toward hCA isoforms of compounds **3a−e**, which do not show any inhibitory activity against COX-2, may be regarded as an important clinical advantage.

Table 3-1. Crystal Structure Details − Ureido-Benzene Sulfonamides.

Compound ID	**101**	**102**	**103**	**104**	**105**
PDB ID	3N4B	3N0N	3N3J	3N2P	3MZC
Data-collection statistics					
Temperature (K)	100	100	100	100	100
Wavelength (Å)	1.5418	1.5418	1.5418	1.5418	1.5418
Space group	$P2_1$	$P2_1$	$P2_1$	$P2_1$	$P2_1$
Unit-cell parameters (Å, °): *a, b, c, β*	42.5, 41.4, 72.0, 104.1	42.4, 41.5, 72.0, 104.2	42.3, 41.4, 71.8, 104.2	42.3, 41.3, 72.0, 104.2	42.5, 41.5, 72.0, 104.1
Total theoretical reflections	32224	39029	38826	29334	39139
Unique measured reflections	30065	36024	36469	28366	35773
Resolution (Å)	19.9-1.6 (1.7-1.6)*	20.0-1.5 (1.6-1.5)	19.9-1.5 (1.6-1.5)	19.9-1.6 (1.7-1.6)	19.9-1.5 (1.6-1.5)
[a]R_{sym} (%)	6.7 (55.0)	7.6 (37.4)	9.0 (17.7)	5.7 (53.9)	4.1 (25.3)
I/σ(I)	13.0 (3.5)	19.2 (5.1)	40.7 (3.3)	12.8 (3.8)	24.4 (4.9)
Completeness (%)	93.3 (90.1)	92.3 (87.4)	93.8 (97.3)	96.7(93.5)	91.4 (87.9)
Redundancy	7.0 (7.1)	7.1 (6.9)	2.3 (2.1)	7.0 (6.8)	3.8 (3.9)
Final Model Statistics					
[b]R_{cryst} (%)	14.1	14.6	15.3	15.2	15.6
[c]R_{free} (%)	17.0	17.4	17.4	17.6	18.7
Residue numbers	3-261	3-261	3-261	3-261	4-261
[d]No. of atoms: *Protein, inhibitor, water*	2133, 21, 258	2104, 25, 308	2087, 23, 359	2085, 23, 218	2085, 19, 306
R.M.S.D.: *Bond lengths* (Å), *bond angles* (°)	0.010, 1.3	0.009, 1.4	0.009, 1.3	0.012, 1.4	0.010, 1.4
Ramachandran statistics (%): *Most favored, allowed, outliers*	89.4, 10.6, 0.0	87.6, 12.5, 0.0	87.1, 12.9, 0.0	88.9, 11.1, 0.0	88.9, 11.1, 0.0
Average B-factors (Å^2): *Main chain, side chain, inhibitor, solvent*	14.2, 18.6 14.8, 29.2	12.8, 17.8 20.8, 27.6	15.1, 19.8 17.6, 29.4	16.8, 22.5 18.1, 30.3	13.4, 17.8 16.4, 29.1

[a]$R_{sym} = \Sigma |I - \langle I \rangle| / \Sigma \langle I \rangle$. [b]$R_{cryst} = (\Sigma ||Fo| - |Fc|| / \Sigma |F_{obs}|) \times 100$. [c]$R_{free}$ is calculated in same manner as R_{cryst}, except that it uses 5% of the reflection data omitted from refinement. [d]Includes alternate conformations. *Values in parenthesis represent highest resolution bin.

Table 3-2. Crystal Structure Details − Thienyl-Acetamido Sulfonamides.

Compound ID	**106**	**107**
PDB ID	3R16	3R17
Data-collection statistics		
Temperature (K)	100	100
Wavelength (Å)	1.5418	1.5418
Space group	$P2_1$	$P2_1$
Unit-cell parameters (Å, °): *a, b, c, β*	42.4, 41.4, 72.0, 104 .0	42.4, 41.3, 71.9, 104.0
Total theoretical reflections	114473	45252
Unique measured reflections	30225	23896
Resolution (Å)	50.0-1.6 (1.7-1.6)[d]	50.0-1.7 (1.8-1.7)
[a]R_{sym} (%)	7.0 (27.0)	4.0 (13.0)
I/σ(I)	20.7 (4.9)	16.6 (6.9)
Completeness (%)	93.0 (87.8)	89.0 (86.5)
Redundancy	3.8	1.9
Final Model Statistics		
[b]R_{cryst} (%)	15.1	15.1
[c]R_{free} (%)	17.3	19.4
Residue numbers	4-261	4-261
[d]No. of atoms: *Protein, drug, water*	2129, 18, 327	2113, 19, 283
R.M.S.D.: *Bond lengths* (Å), *bond angles* (°)	0.006, 1.13	0.006, 1.07
Ramachandran statistics (%): *Most favored, allowed, outliers*	97.0, 3.0, 0.0	97.0, 3.0, 0.0
Average B-factors (Å^2): *Main chain, side chain, inhibitor, solvent*	16.0, 12.4, 15.7, 19.6, 28.3	19.0, 15.8, 19.1, 22.2, 29.9

[a]$R_{sym} = \Sigma |I - \langle I \rangle| / \Sigma \langle I \rangle$. [b]$R_{cryst} = (\Sigma ||Fo| - |Fc|| / \Sigma |F_{obs}|) \times 100$. [c]$R_{free}$ is calculated in same manner as R_{cryst}, except that it uses 5% of the reflection data omitted from refinement. [d]Includes alternate conformations. *Values in parenthesis represent highest resolution bin.

Table 3-3. Inhibition of hCA I, II, VII and XIV (h= human, recombinant isozymes) with compounds **1-21**, by a stopped flow, CO_2 hydrase assay.

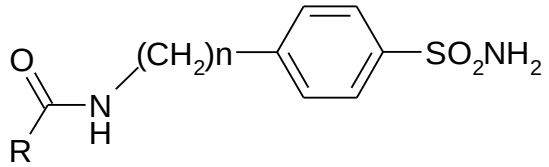

1-8, **10**, **13-18,** n = 0; **11 & 20,** n = 1; **21,** n = 2

ID	R	MES-ED_{50} µmol/kg	K_I (nM)			
			hCA I	hCA II	hCA VII	hCA XIV
1	*t*-Bu	165 (89-338)	6000	2500	7200	700
2	$(Et)_2CH$	37 (24-54)	4000	2800	900	600
3	$(i\text{-}Pr)_2CH$	N.A.	2500	200	8400	700
4	*n*-Pr(Me)CH	40 (27-57)	1700	200	600	600
5	(*i*-Pr)(*n*-Pr)CH	139 (80-213)	1800	200	600	700
6	(*i*-Pr)(sec-Bu)CH	N.A.	100	100	50	60
7	(*n*-Pr)(sec-Bu)CH	115 (83-141)	4300	200	5100	600
8	$(i\text{-}PrCH_2)(Et)CH$	56 (28-86)	700	100	60	60
109*	$(Et)(Me)CHCH_2$	61 (44-81)	10	10	50	80
10	(*n*-Bu)(Et)CH	80 (55-109)	10	10	5	5
11	$(Et)_2CH$	87 (57-120)	80	100	70	80
110*	$PhCH_2$	55 (29-86)	10	10	50	50
13	Me(Et)CH	30 (18-41)	2200	300	60	80
14	Et(*t*-Bu)CH	N.A.	3600	10	50	800
15	i-Pr(*t*-Bu)CH	58 (26-128)	3000	200	500	5
16	$t\text{-}BuCH_2$	35 (20-65)	2100	3500	60	70
17	(*n*-Pr)(Et)CH	41 (17-66)	1600	300	60	5
18	(*sec*-Bu)(Et)CH	N.A.	2500	100	50	5
108*	(*n*-Pr)(*t*-Bu)CH	N.A.	3800	10	5	70
20	t-Bu	N.A.	300	30	5	60
21	$(Et)_2CH$	N.A.	400	30	50	700
AZM	**-**	239 (174-327)	250	10	5	40
ZNS	**-**	100 (84-120)	60	30	100	5200
TPM	**-**	10 (6-15)	250	10	5	1500

*These structures are provided in Figure 3-2

Table 3-4. Crystal Structure Details − 4-Aminobenzene Sulfonamides.

Compound ID	**108**	**109**	**110**
PDB ID	3OY0	3OYQ	3OYS
Data-collection statistics			
Temperature (K)	100	100	100
Wavelength (Å)	1.5418	1.5418	1.5418
Space group	$P2_1$	$P2_1$	$P2_1$
Unit-cell parameters (Å, °): *a, b, c, β*	42.2, 41.3, 72.0, 104.1	42.3, 41.3, 72.0, 104.2	42.4, 41.4, 72.0, 104.1
Unique measured reflections	28795	40285	36083
Resolution (Å)	20.6-1.6 (1.7-1.6)*	23.2-1.4 (1.5-1.4)	23.9-1.5 (1.6-1.5)
[a]R_{sym} (%)	7.7 (15.9)	5.5 (17.3)	4.4 (10.9)
I/σ(I)	11.9 (5.2)	23.4 (7.8)	33.8 (15.0)
Completeness (%)	89.7 (89.5)	97.6 (93.6)	99.6 (99.6)
Redundancy	2.5 (2.4)	5.0 (4.8)	6.9 (6.4)
Final Model Statistics			
[b]R_{cryst} (%)	15.6	16.5	15.6
[c]R_{free} (%)	19.2	18.2	17.4
Residue numbers	4-261	4-261	4-261
[d]No. of atoms: *Protein, inhibitor, water*	2096, 21, 177	2104, 19, 175	2079, 20, 177
R.M.S.D.: *Bond lengths* (Å), *bond angles* (°)	0.013, 1.47	0.011, 1.44	0.012, 1.47
Ramachandran statistics (%): *Most favored, allowed, outliers*	97.7, 2.3, 0.0	97.3, 2.7, 0.0	98.1, 1.9, 0.0
Average B-factors (Å^2): *Main chain, side chain, inhibitor, solvent*	17.4, 22.1, 24.7, 30.5	13.8, 18.2, 21.7, 23.8	13.3, 17.9, 12.8, 25.0

[a]$R_{sym} = \Sigma |I - \langle I \rangle| / \Sigma \langle I \rangle$. [b]$R_{cryst} = (\Sigma ||Fo| - |Fc|| / \Sigma |F_{obs}|) \times 100$. [c]$R_{free}$ is calculated in same manner as R_{cryst}, except that it uses 5% of the reflection data omitted from refinement. [d]Includes alternate conformations. *Values in parenthesis represent highest resolution bin.

Table 3-5. Inhibition of hCA isoforms I-XIV and mycobacterial β-CAs Rv1284, Rv3273 and Rv3588c with sulfonamides **3a-e**, celecoxib (**CLX**) and valdecoxib (**VLX**) by a stopped flow CO_2 hydrase assay.[154]

Isoform	K_I (nM)*						
	3a	**3b**	**3c**	**3d**	**3e**	**CLX**	**VLX**
hCA I	60	200	300	200	150	50000	54000
hCA II	120	30	200	70	50	20	40
hCA III	22000	32000	28600	6400	7900	7400	78000
hCA IV	8800	7200	7100	300	7500	900	1300
hCA VA	900	400	300	500	1000	800	900
hCA VB	1000	3100	3200	3200	3300	100	90
hCA VI	7000	9300	9300	8000	8100	100	600
hCA VII	600	600	600	900	900	2200	3900
hCA IX	2200	1800	2600	2300	3200	20	20
hCA XII	4500	5600	6700	5500	5900	20	10
hCA XIII	900	2800	700	4300	4600	100	400
hCA XIV	900	800	500	700	800	700	100
Rv1284	800	400	600	100	100	10000	13000
Rv3273	700	300	200	300	200	7800	7800
Rv3588c	600	200	300	300	100	700	700

* Mean from 3 different assays. Errors were in the range of ± 10 of the reported values (data not shown).

Table 3-6. Crystal Structure Details − Benzothiopyrano Sulfonamide.

Compound ID	**3e**
PDB ID	3QYK
Data-collection statistics	
Temperature (K)	100
Wavelength (Å)	1.5418
Space group	$P2_1$
Unit-cell parameters (Å, ^{o}): *a, b, c, β*	42.3, 41.4, 72.3, 104.2
Unique measured reflections	39832
Resolution (Å)	50.0 - 1.4 (1.5 - 1.4)*
[a]R_{sym} (%)	5.6 (19.0)
I/σ(I)	23.7 (7.2)
Completeness (%)	96.0 (92.0)
Redundancy	4.9 (4.8)
Final Model Statistics	
[b]R_{cryst} (%)	15.7
[c]R_{free} (%)	17.7
Residue numbers	4-261
[d]No. of atoms: *Protein, inhibitor, water*	2288, 24, 265
R.M.S.D.: *Bond lengths* (Å), *bond angles* (^{o})	0.010, 1.40
Ramachandran statistics (%): *Most favored, allowed, outliers*	88.4, 11.6, 0.0
Average B-factors (Å^2): *Main chain, side chain, inhibitor, solvent*	12.1, 14.9, 13.3, 29.2

[a]$R_{sym} = \Sigma |I - \langle I \rangle| / \Sigma \langle I \rangle$. [b]$R_{cryst} = (\Sigma ||Fo| - |Fc|| / \Sigma |F_{obs}|) \times 100$. [c]$R_{free}$ is calculated in same manner as R_{cryst}, except that it uses 5% of the reflection data omitted from refinement. [d]Includes alternate conformations. *Values in parenthesis represent highest resolution bin.

Table 3-7. Amino acid differences in the active site of hCAs I, II, IX and XII (hCA II numbering).

Residue #	CA I	CA II	CA IX	CA XII
62	Val	Asn	Arg	Asn
67	His	Asn	Gln	Lys
91	Phe	Ile	Leu	Thr
121	Ala	Val	Val	Val
131	Leu	Phe	Val	Ala
135	Ala	Val	Leu	Ser
204	Tyr	Leu	Ala	Asn

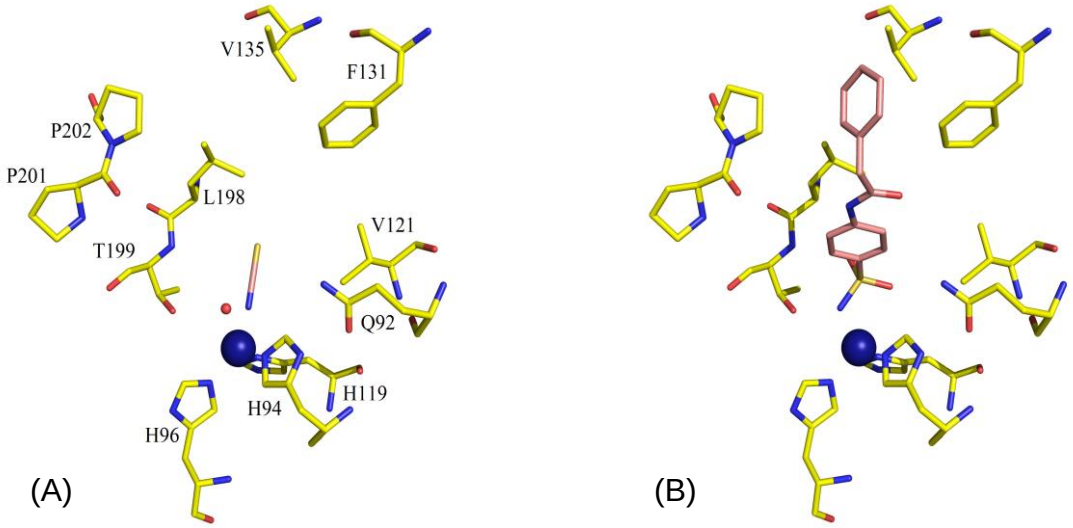

Figure 3-1. Stick representation of hCA II (yellow) in complex with two different kinds of inhibitors (pink): (A) Cyanate and water molecule (red sphere), PDB ID: 2CA2[155], (B) Sulfonamide, PDB ID: 3OYS.[131]

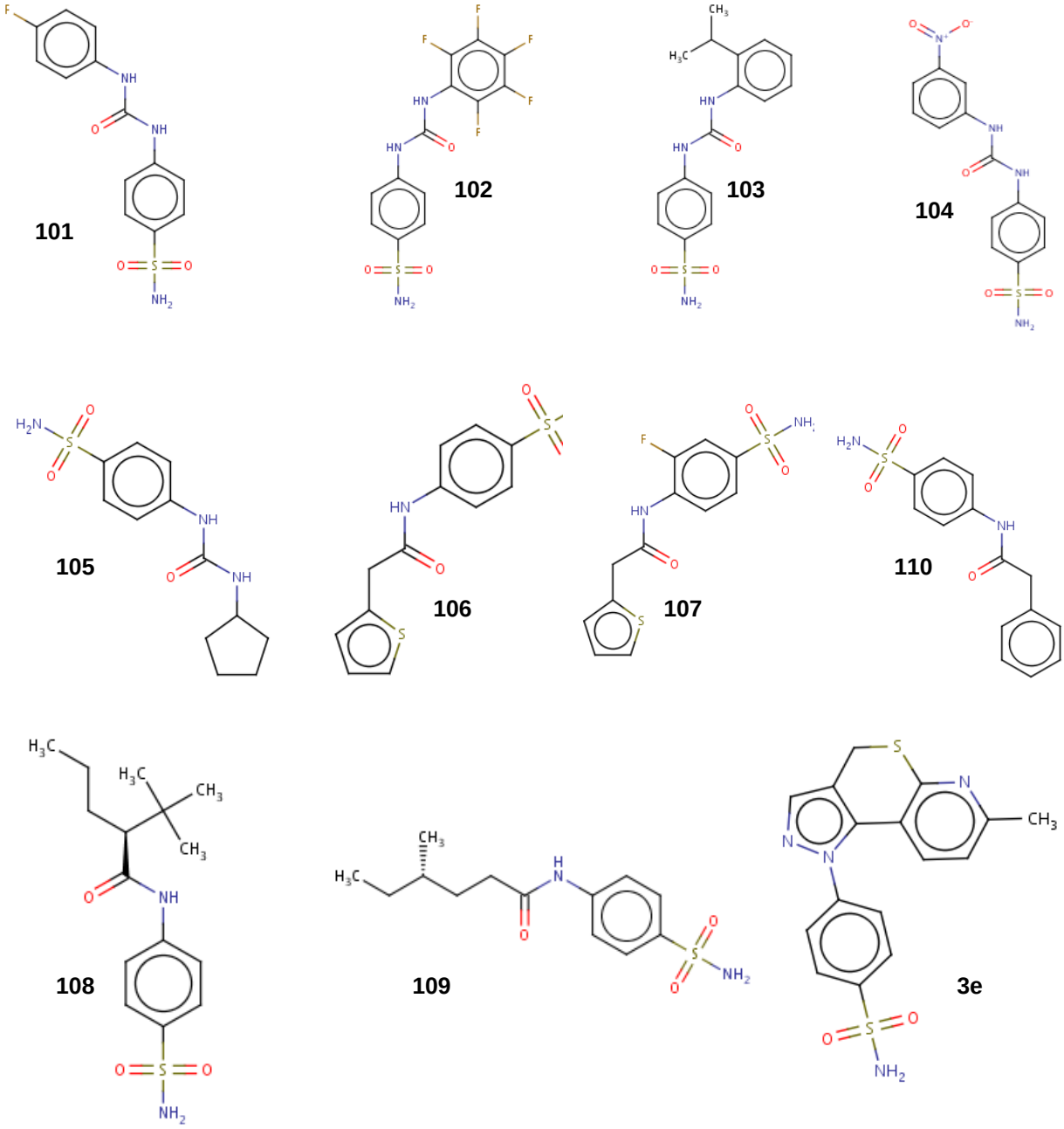

Figure 3-2. Chemical structures of inhibitors.

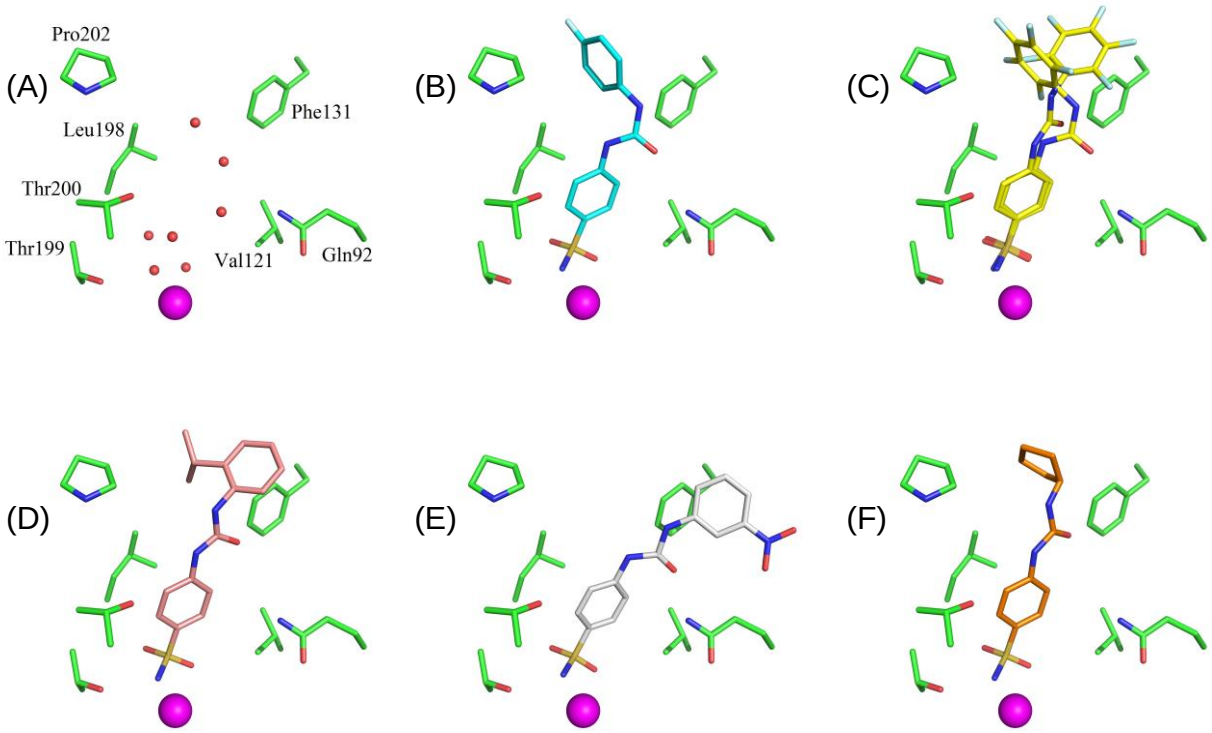

Figure 3-3. hCA II active site (A) unbound (PDB ID: 3KS3)[29], (B) with compound **101** (cyan, PDB ID: 3N4B)[122], (C) **102** (yellow, PDB ID: 3N0N)[122], (D) **103** (pink, PDB ID: 3N3J)[122], (E) **104** (gray, PDB ID: 3N2P)[122], and (F) **105** (orange, PDB ID: 3MZC)[122].

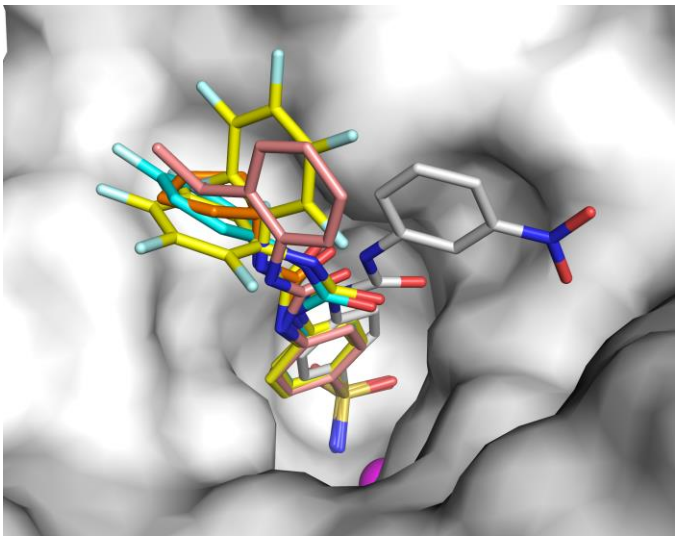

Figure 3-4. View of compounds **101-105** superposed in the active site of hCA II (gray surface).

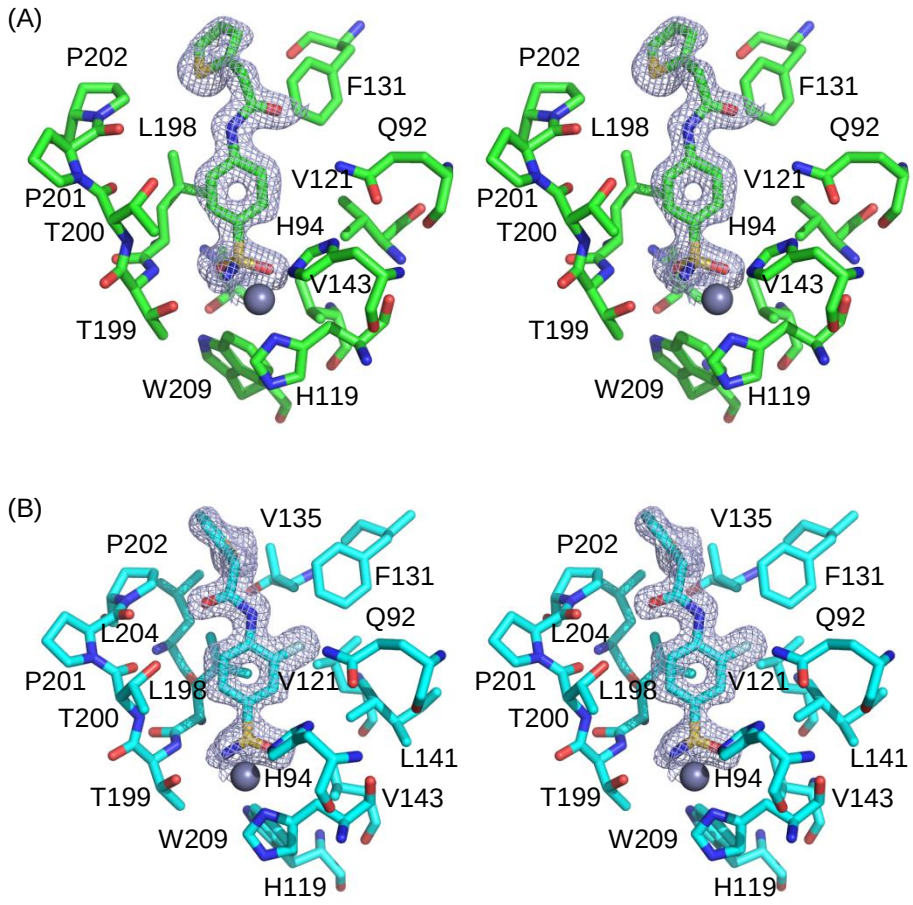

Figure 3-5. Stereo stick representation of hCA II active site complexed with (A) **106** (green) and (B) **107** (cyan). The 2Fo-Fc electron density is contoured at 1.2 σ.

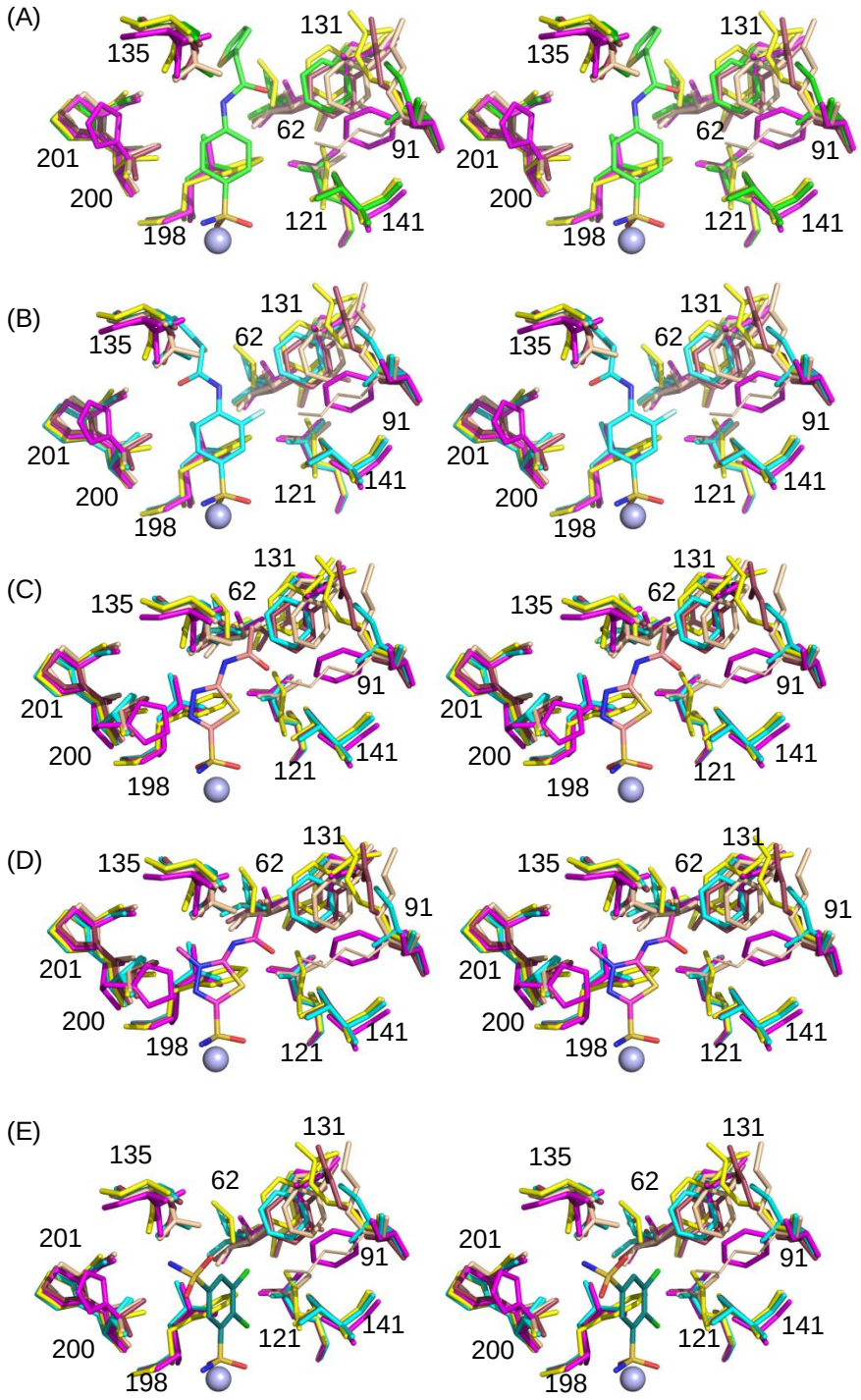

Figure 3-6. Stereo stick representation of the superposition of hCA I (pink), hCA II (green), hCA III (yellow), hCA VII (wheat), and hCA XIII (purple) active sites complexed with (A) **106**, (B) **107**, (C) **AZM**, (D) **MZM**, and (E) **DCP.**[127]

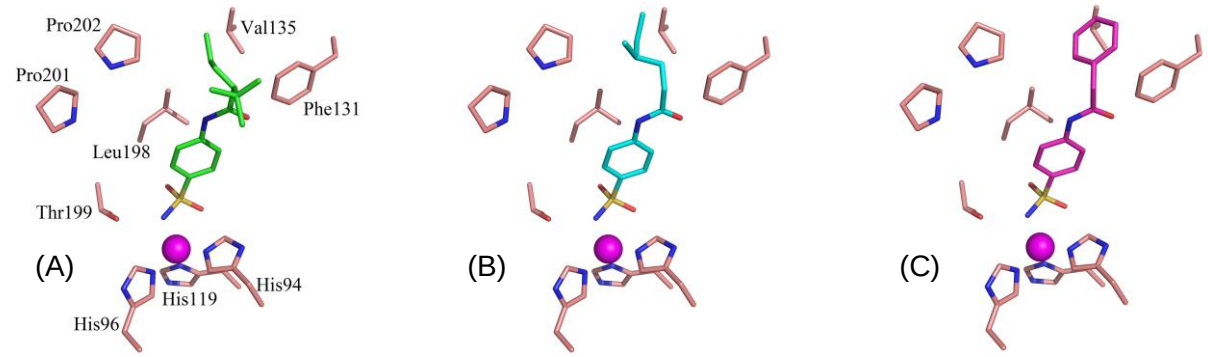

Figure 3-7. Stick representation of hCA II active site with compounds (A) **108,** (B) **109**, and (C) **110**. Residues in (B) and (C) are same as labeled in (A).

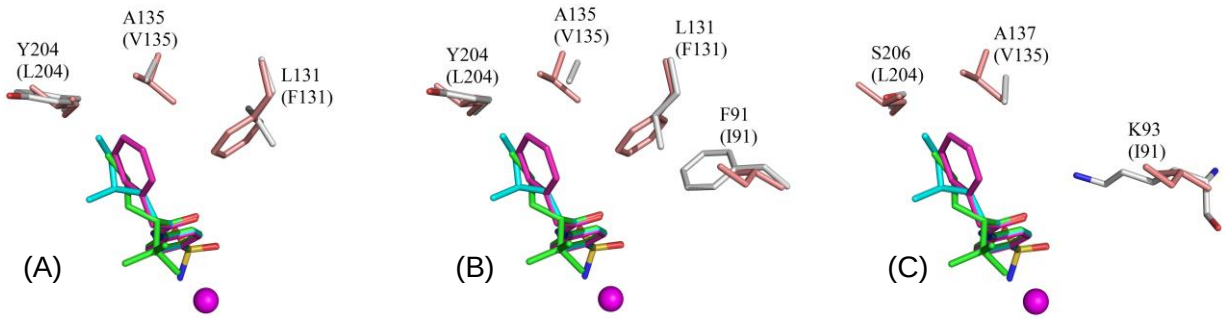

Figure 3-8. Stick representation of (A) hCA XIV, (B) hCA I, and (C) hCA VII active sites superimposed onto hCA II (salmon) complexed with compounds **108** (green), **109** (cyan), **110** (pink). Amino acids are as labeled, hCA II residues are labeled in parenthesis.

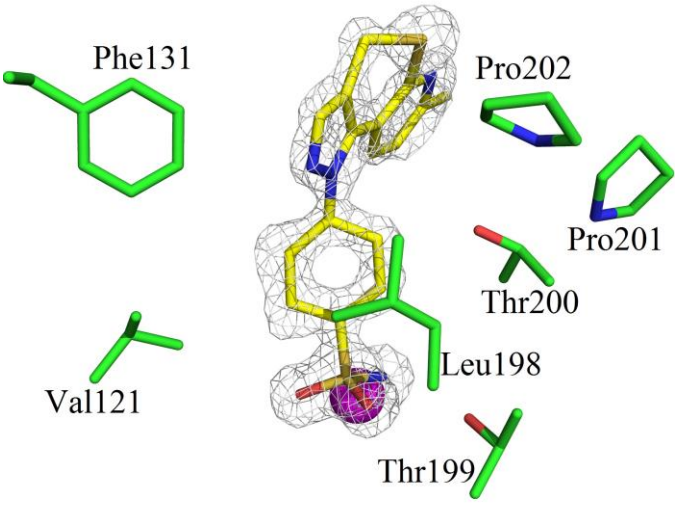

Figure 3-9. Stick representation of hCA II active site (green) complexed with **3e** (yellow). The 2Fo-Fc electron density is contoured at 1.2 σ.[146]

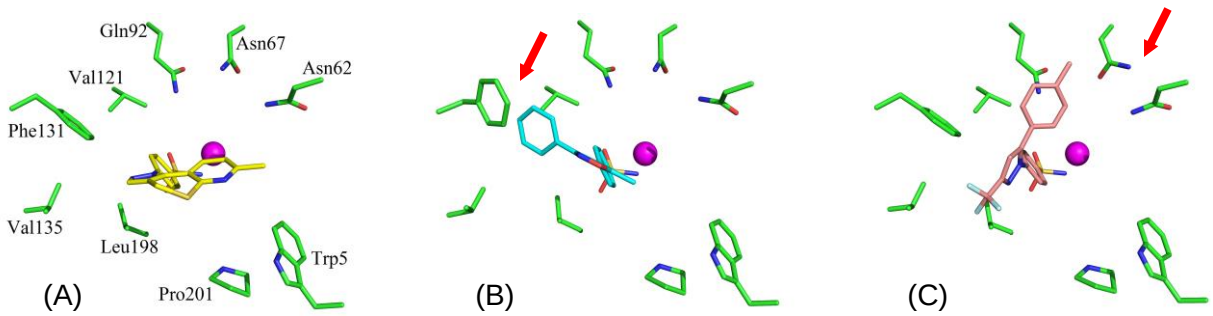

Figure 3-10. Stick figure of inhibitors (A) **3e** (yellow)**,** (B) valdecoxib **VLX** (cyan), and (C) celecoxib **CLX** (pink), superposed in the active site of hCA II. View looking into the active site of hCA II. Red arrows indicate hCA II conformational change on inhibitor binding.

CHAPTER 4
DITHIOCARBAMATES − NOVEL ANTIGLAUCOMA INHIBITORS[156,157]

Introduction

Carbonic anhydrase (CA) inhibitors (CAIs) of the sulfonamide type such as dorzolamide (**DZM**) or brinzolamide (**BZM**) are topically used antiglaucoma agents[158–166], whereas the older drugs, such as acetazolamide (**AZM**) or dichlorophenamide (**DCP**) show the same action through systemic administration, which, however, leads to a wide range of side effects due to inhibition of the enzyme from other organs than the target one, that is, the eye. CA XII, a transmembrane isoform with an extracellular active site, was shown to be overexpressed in glaucomatous patients eyes.[167]

Trithiocarbonate (TTC) (CS_3^{2-}), an anion similar to carbonate, has recently been investigated and shown to constitute a "lead" for novel CAIs.[168,169] The X-ray crystal structure for the adduct of TTC, bound to hCA II, has recently been reported (Figure 4-1).[124,168,169] The inhibitor binds to the Zn^{2+} in the hCA II active site in a slightly distorted tetrahedral geometry of the metal ion, occupying a position similar to that observed in the case of the hCA II−bicarbonate complex. The TTC was monocoordinated to the Zn(II) ion by means of one of the sulfur atoms. The same sulfur made a hydrogen bond to the OH of Thr199, whereas a second sulfur atom participated with another hydrogen bond to the NH group of the same amino acid residues, Thr199. This binding mode explains the low micromolar affinity of this inhibitor to many of the CA isoforms

---

Adapted from: Carta, F.; Aggarwal, M.; Maresca, A.; Scozzafava, A.; McKenna, R.; Supuran, C. T. Dithiocarbamates: a new class of carbonic anhydrase inhibitors. Crystallographic and kinetic investigations. *Chem. Commun. (Camb.)* **2012**, *48*, 1868–1870.

Adapted from: Carta, F.; Aggarwal, M.; Maresca, A.; Scozzafava, A.; McKenna, R.; Masini, E.; Supuran, C. T. Dithiocarbamates strongly inhibit carbonic anhydrases and show antiglaucoma action in vivo. *J. Med. Chem.* **2012**, *55*, 1721–1730.

investigated to date. On the basis of this binding mode of a millimolar inhibitor, TTC, compounds incorporating this new zinc-binding function, CS_2^-, may act as even stronger CAIs. Dithiocarbamates (DTCs), compounds possessing the general formula R1R2N-CS2 −M+, have recently been demonstrated in a preliminary communication to act as highly efficient CAIs.[156] This is the first detailed study of the DTCs as a class of potent CAIs, with a mechanism of action different of that of the sulfonamides. Furthermore, some of these highly water-soluble compounds possess excellent intraocular pressure (IOP) lowering properties in an animal model of glaucoma, making them interesting candidates for developing antiglaucoma drugs.

Indeed, DTCs are well known metal complexing agents and they also possess interesting biomedical and agricultural applications.[170,171] However, few studies investigated their interactions with metalloenzymes.[172] One such work has investigated the inhibition of N,N-diethyl-DTC with bovine CA.[173] By using Co(II)-substituted CA, Morpurgo et al.[173] showed that the inhibitor does not extrude the metal ion from the enzyme active site and that it binds to it in a trigonal-bipyramidal geometry of the Co(II) ion. No other DTCs were subsequently investigated for their interaction with CAs till our group reported that trithiocarbonate, which contains a new ZBG, (CS_2^-) as well as diethyl-DTC, inhibit several CA isoforms in the low micromolar or submicromolar range.[124,168,169] Those findings are hereby extended, showing that a wide range of DTCs incorporating various aliphatic and/or aromatic moieties at the nitrogen atom, act as low nanomolar and even subnanomolar CAIs. The mechanism of action of this new class of potent CAIs is elucidated by X-ray crystal structures of three DTCs in complex with hCA II. The investigated DTCs (**11a**–**27a**) were prepared by reacting amines with CS_2 in the

presence of sodium hydroxide. Four CA isoforms were included in this study: the cytosolic hCAs I and II, and the tumor-associated transmembrane hCAs IX and XII.

Results

Carbonic Anhydrase Inhibition (Performed by collaborators at the University of Florence, Italy)

Compounds **11a-27a** were assayed[154] for the inhibition of four physiologically relevant CA isoforms, hCAs I, II, IX and XII. All of them are drug targets: hCAs I, II and XII for ophthalmologic diseases, mainly glaucoma[9,164–166], whereas CA IX and XII for antitumor drugs/tumor imaging agents.[9,103,174–179] Comparison of these inhibition data with the clinically used agent acetazolamide (**AZM**) are also reported in Table 4-1.

Carbonic anhydrase II

The physiologically dominant cytosolic isoform hCA II showed an interesting inhibition profile with these DTCs. Several of them (**16a, 21a, 24a** and **25a**) were excellent hCA II inhibitors, with K_Is < 5 nM, being more effective (even one order of magnitude) than the clinically used sulfonamide **AZM** (Table 4-1). It may be observed that these compounds incorporate aromatic, arylakyl, hetaryl, alkyl and hydroxyalkyl moieties substituting the nitrogen atom from the DTC moiety. Another rather large group of derivatives, such as **12a, 15a, 17a-20a, 22a, 23a, 26a** and **27a**, were slightly less effective hCA II inhibitors, but still possessed a high efficacy, with K_Is in the range of 13-55 nM. They incorporate various types of substituents, such as alkyl, aryl, aralkyl, and hetaryl ones. It is obvious that small structural changes in the DTC scaffold influence dramatically the biological activity. For example, the isomeric pair **16a-18a**, which differ only by the nature of the aliphatic chain (*iso*-Bu moieties in the first compound and *n*-Bu in the second derivative), have K_Is which differ by a factor of ~54. The length of the alkyl

chain also strongly influence activity, with compounds possessing a medium chain (e.g., **15a-20a**) being more effective than the ones with shorter chains, such as **13a** and **14a**, which are rather ineffective as hCA II inhibitors (K_Is > 5 μM). Also the glycine DTC **11a** was a medium potency hCA II inhibitor, with a K_I of 300 nM.

Carbonic anhydrase IX

The tumor-associated isoform hCA IX was highly inhibited by the DTCs investigated here, with K_Is in the range of 5 nM - 1.5 mM. The simple aliphatic DTCs **13a**/**14a** and the bulky cyclic derivative **26a**, were the least effective inhibitors (K_Is of 0.7-1.4 μM), and four other compounds (**11a**, **15a, 17a** and **18a**) were effective, medium potency inhibitors, with K_Is in the range of 50-70 nM. They incorporate the carboxyalkyl moiety present in glycine (**11a**), the five-membered aliphatic ring (from **15a**) and 3-or 4-carbon atom *n*-alkyl chains (**17a** and **18a**). All the remaining derivatives showed highly effective hCA IX inhibitory properties, with K_Is < 30 nM. Thus, a rather high structural diversity (aliphatic, aromatic, aralkyl, hetaryl moieties) present in primary/secondary DTCs lead to highly effective hCA IX inhibitors, with minor structural changes drastically affecting enzyme inhibition. Many DTCs were more effective hCA IX inhibitors compared to acetazolamide (Table 4-1).

Carbonic anhydrase XII

A rather similar structure activity relationship (SAR) as the one discussed above for hCA IX, was observed for the inhibition of the second transmembrane isoform, hCA XII. Compounds **13a**/**14a** and **26a** were the least effective inhibitors (K_Is in the range of 200 nM - 1 mM), whereas the remaining DTCs were highly effective hCA XII inhibitors, with K_Is < 30 nM (Table 4-1). Among the best hCA XII inhibitors (subnanomolar inhibition constants) were the di-isobutyl-DTC **16a** and the piparazine-bis-DTC **25a**.

Again, the main conclusion is that a large number of substitution patterns, incorporating varied moieties lead to highly effective hCA XII inhibitors.

Crystal Structure Details

In order to explain the potent CA inhibitory properties of the DTCs, X-ray crystal structures of hCA II in complex with the inhibitors **23a**, **24a**, and **26a** were solved. The compounds are buried deep into the active site, displacing the catalytic zinc-bound solvent, such that one of the sulfur atoms coordinates directly to the zinc ion of the enzyme. The overall zinc coordination (3N from the coordinating histidine residues 94, 96 and 119, and 1S from the inhibitor ligand) can be described as a distorted tetrahedron (Figure 4-2). The details of this tetrahedral geometry are provided in Table 4-2. The zinc bound sulfur also interacts with the O atom of Thr199 in a similar manner to that observed in the more classical clinically used sulfonamides and sulfamates CAIs.[90,125,127,131,146,180]

Compound **23a** is at a van der Waals distance from the side chains of Asn62, His64, Glu92, His94, Val121, Phe131, Leu198, Thr200 and Pro202 (Figure 4-2). With an average B-factor of 20 $Å^2$ (Table 4-3), **23a** was refined with an occupancy of 0.8. Around 28 $Å^2$ (8%) of the surface area of the compound is buried at the interface with the protein. **24a** which possesses a puckered ring, binds with a slightly higher B-factor of 24 $Å^2$, but was refined with full occupancy. The compound has a buried surface area of 33.3 $Å^2$ (11.3%). In contrast to **23a**, **24a** interacts with and is kept in place by the side chains of only two residues His64 and Thr200. Within the active-site, the oxygen atom of the compound lies at a hydrogen bond distance from two water molecules. **26a** possesses a nitrogen atom which hydrogen bonds with a surrounding water molecule and the side chains of Asn67 and Gln92, and consequently buries 77 $Å^2$ (18%) of its

surface area. The hydrophobic cyclohexane ring at the distal end of the drug protruding outwards from the active site is stabilized by the side chains of Phe131, Leu198 and Pro202.

For a structural comparison the three compounds were superposition onto each other. In unbound hCA II, the side chain conformation of His64 has been shown to be dependent upon the buffer pH, which affects the protonation state of the imidazole ring. It is widely believed that this side chain flips from an “in” to “out” conformation as part of the proton transfer mechanism in hCA II, hence two conformations of the residue are often observed in crystal structures.[29,181] His64 in the hCA II structure in complex with compounds **26a** (PDB ID: 3P5L)[156] and **24a** (PDB ID: 3P5A)[157] has a dual conformation. In the case of **26a**, the terminal six-membered hydrophobic ring sits close to Phe131, Val135 and Pro202 at the rim of the active site in a hydrophobic pocket of hCA II. Whereas, for **24a** the six-membered ring does not extend far enough out of the active site to either reach this hydrophobic pocket or close enough to the in-conformation of His64. Hence compounds **24a** and **26a** are at 5.6 and 5.0 Å respectively, from His64 and therefore do not affect its dual conformation. Whereas, in the hCA II structure in complex with **23a** (PDB ID: 3P58)[156], the six-membered planar ring forms a T-shaped π-stacking with the imidazole ring of His64 and stabilizes His64 in the “in” conformation. In addition **24a** is positioned 3.2 Å from Thr200 but does not form hydrogen bonds with either the protein main- or side-chain. However, the endocyclic oxygen atom in the tail ring of **24a** is within hydrogen bond distance of two water molecules (Figure 4-2B) which probably also contribute to its high affinity to hCA II.

In vivo Studies on Rabbits (Performed by collaborators at the University of Florence, Italy)

Compound **24a** was investigated *in vivo*, for its ability to lower intraocular pressure (IOP) in carbomer-induced glaucoma in rabbits.[166] Normal IOP in rabbits, like in humans is of around 15-20 mm Hg. In this model, the IOP is quite elevated, thus mimicking the pathologic situation observed in the human disease. Clinically used drugs such as **DZM**, induce a maximal IOP lowering of 4-5 mm Hg.[164–166] DTC **24a** was chosen due to its excellent enzyme inhibitory activity *in vitro* and good water solubility, being formulated at 2% eye drop solution at neutral pH (due to its salt character, whereas **DZM** is formulated at pH 5.5, as hydrochloride salt, and induces eye irritation). In fact, water solubility of eye drugs is a significant problem[163], with many classes of drugs achieving an acceptable solubility only as salts with strong acids, such as HCl, which leads to acidic pH values causing eye irritation (**DZM** is a well known such case).

Rabbits were treated with 2% solution of DTC **24a** and their IOP was monitored for 48 h. The contralateral eye was treated with vehicle and was used as control. Effective time-dependent reduction in elevated IOP was observed, for a rather long period. The maximal effect (of 6-10 mm Hg) was observed after 2 hours post administration, and it lasted for up to 8 hours, being almost double that reported for **DZM** (of 4-5 mm Hg, and lasting only for about 3-4 hours).[164–166]

Conclusions

DTCs represent a novel class of highly effective CAIs. They are easy to prepare from simple starting materials, they can incorporate a very high chemical diversity, and act as inhibitors of several physiologically relevant CA isoforms, with potencies from the subnanomolar to the micromolar. The SARs for the inhibition of isoforms hCA I, II, IX

and XII were straightforward and slightly different, with small modifications in the backbone of the compound leading to dramatic changes of biological activity. The inhibition mechanism of the DTCs was also explained, by resolving the X-ray crystal structure for hCA II complexed with a heterocyclic DTC. The CS_2-moiety present in DTCs represents a new zinc-binding function. It is directly coordinated to the Zn(II) ion from the enzyme active site and also participates in an interaction (hydrogen bond) with the OH moiety of Thr199, an amino acid essential for the binding of many classes of CAIs (and of the substrates). The organic scaffold of the DTC is deeply buried within the enzyme active site and also participates in favorable interactions with it, which leads to a high stabilization of the enzyme-inhibitor adduct. Some of the most potent CAIs detected here showed favorable IOP lowering effects in an animal model of glaucoma. Being water soluble, with pH of the solution in the neutral range, and with duration of action lasting up to 48 h, this new class of CAIs may constitute interesting candidates for developing novel antiglaucoma therapies, a field in which no new drug emerged in the last 18 years.

Table 4-1. CA I, II, IX and XII inhibition data with DTCs **1a-27a** by a stopped-flow, CO_2 hydrase assay.[154]

Compound	K_I (nM)[#]			
	hCA I	hCA II	hCA IX	hCA XII
11a	10	300	60	5
12a	10	20	5	5
13a	700	6900	700	800
14a	800	3100	1400	1100
15a	1	30	70	50
16a	1	1	5	1
17a	1800	50	50	10
18a	40	50	50	5
19a	50	50	30	20
20a	150	30	30	10
21a	10	5	5	5
22a	40	20	30	10
23a	70	20	50	5
24a	1	1	5	5
25a	10	1	40	1
26a	50	40	700	200
27a	5	20	5	5
AZM	250	10	20	5

*Tris-dithiocarbamate; **(*S*)-proline dithiocarbamate; [#]Mean from 3 different assays. Errors were within 5-10 % of the reported values (data not shown).

Table 4-2. Geometry of Zn and bound sulfur atom for DTCs **23a**, **24a** and **26a**.

	23a	**24a**	**26a**
Distance (Å)	2.3	2.3	2.3
Angle (^{o}) with His94	111.3	107.3	108.8
Angle (^{o}) with His96	114.2	112.2	112.9
Angle (^{o}) with His119	119.4	128.3	126.1

Table 4-3. Crystal Structure Details − DTCs.

Compound ID	**23a**	**24a**	**26a**
PDB ID	3P58	3P5A	3P5L
Data-collection statistics			
Temperature (K)	100	100	100
Wavelength (Å)	1.5418	1.5418	1.5418
Space group	$P2_1$	$P2_1$	$P2_1$
Unit-cell parameters (Å, °): *a, b, c, β*	42.2, 41.1, 71.9, 104.4	42.3, 41.2, 72.1, 104.2	42.3, 41.3, 72.2, 104.4
Unique measured reflections	39387	39632	39014
Total theoretical reflections	38521	39395	38468
Resolution (Å)	50.0-1.5 (1.6-1.5)*	50.0-1.5 (1.6-1.5)	50.0-1.5 (1.6-1.5)
[a]R_{sym} (%)	6.4 (39.7)	6.4 (18.1)	6.7 (37.1)
I/σ(I)	20.2 (3.3)	17.5 (5.8)	16.3 (3.2)
Completeness (%)	97.8 (91.7)	99.4 (95.7)	98.6 (96.3)
Redundancy	4.3 (4.0)	3.7 (3.4)	3.4 (3.2)
Final Model Statistics			
[b]R_{cryst} (%)	15.0	14.8	16.6
[c]R_{free} (%)	17.1	16.9	19.0
Residue numbers	4-261	4-261	4-261
[d]No. of atoms: *Protein, inhibitor, water*	2114, 12, 291	2078, 9, 300	2123, 17, 172
R.M.S.D.: *Bond lengths* (Å), *bond angles* (°)	0.013, 1.53	0.012, 1.49	0.012, 1.44
Ramachandran statistics (%): *Most favored, allowed, outliers*	87.9, 12.1, 0.0	89.4, 10.7 0.0	87.5, 12.5, 0.0
Average B-factors (Å^2): *Main chain, side chain, inhibitor, solvent*	17.0, 21.5, 20.0, 32.2	13.6, 18.1, 23.9, 29.4	14.7, 17.8, 20.7, 25.3

[a]$R_{sym} = \Sigma |I - \langle I \rangle| / \Sigma \langle I \rangle$. [b]$R_{cryst} = (\Sigma ||Fo| - |Fc|| / \Sigma |F_{obs}|) \times 100$. [c]$R_{free}$ is calculated in same manner as R_{cryst}, except that it uses 5% of the reflection data omitted from refinement. [d]Includes alternate conformations. *Values in parenthesis represent highest resolution bin.

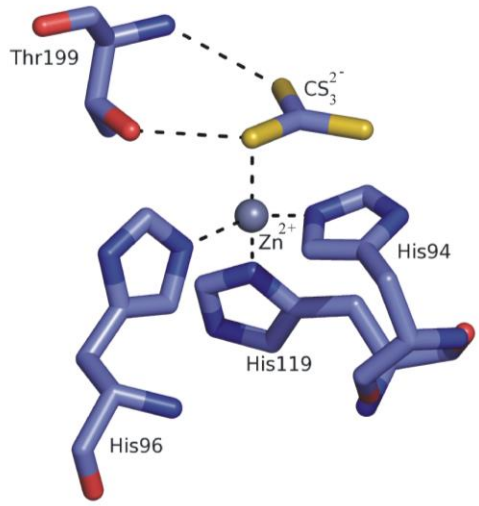

Figure 4-1. Trithiocarbonate (CS_3^{2-}) bound in the hCA II active site in a slightly distorted tetrahedral geometry of the metal ion (PDB ID: 3K7K).[124]

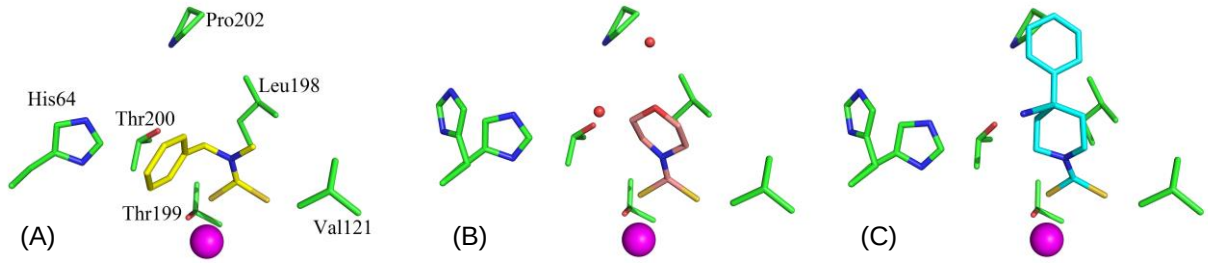

Figure 4-2. Stick representation of hCA II active site (green) with compounds (A) **23a** in yellow**,** (B) **24a** in pink, and (C) **26a** in cyan. Water molecules are depicted as small red spheres.[156,157]

CHAPTER 5
NEUTRON STUDIES ON CARBONIC ANHYDRASE II − ACETAZOLAMIDE[182]

Introduction

Carbonic Anhydrase Inhibition

Carbonic anhydrase (CA) isoforms are prominent clinical targets for treating various diseases. The clinically used acetazolamide (**AZM**) is a sulfonamide that binds with high affinity to human CA isoform II (hCA II). Most structure-based carbonic anhydrase inhibitor (CAI) designs have focused on hCA II X-ray crystallographic studies. There are numerous crystal structures in the Protein Data Bank (www.rcsb.pdb.org) of CAs bound to a variety of CAIs: the sulfonamides, their bioisosteres, small molecule anions, phenols, coumarins, and polyamines.[183,184] Sulfonamides are still of significant interest with more than 30 derivatives being used clinically.[97]

The primary sequence conservation among CA isoforms causes cross-reactivity of CAIs and this necessitates the development of isoform-specific drugs.[6] A detailed understanding of the water patterns and H-bonding in the active site provided by this neutron diffraction study gives a new avenue for the rational structure-based drug design effort.

States of AZM

AZM dissolved in water has three possible protonation states with two associated pK_a values (7.2 and 8.7) that are relevant to physiological pH (Figure 5-1). It is thought that any of these forms can bind to hCA II.[185,186] There have been no crystallographic

---

Adapted from: Fisher, S. Z.; Aggarwal, M.; Kovalevsky, A. Y.; Silverman, D. N.; McKenna, R. Neutron Diffraction of Acetazolamide-Bound Human Carbonic Anhydrase II Reveals Atomic Details of Drug Binding. *J. Am. Chem. Soc.* **2012**, *134*, 14726–14729.

studies to definitively observe the charged state of **AZM** bound to hCA II and it is unknown which form dominates in the crystalline state. This is despite the availability of very high resolution (1.1 Å resolution) X-ray data.[187] However, results from past ^{15}N NMR studies have shown that it is the sulfonamido anion (Form 3 in Figure 5-1) that binds to hCA II in solution.[188]

There is limited explicit information available about the H-bonding interactions between enzymes and inhibitors/drugs and the role of solvent orientations. Besides the current neutron study of hCA II-**AZM**, there are only two other reports of a similar nature: *E. coli* Dihydrofolate reductase (DHFR) : methotrexate and HIV protease:KNI-272.[189,190] While methotrexate is a widely used chemotherapy agent, the reported neutron structure is in complex with a bacterial DHFR homologue. Similarly, the inhibitor KNI-272 bound to HIV protease has no clinical significance as it is not a drug currently in use. To determine the charged state and binding mode of **AZM**, a single H/D exchanged crystal of hCA II, co-crystallized with **AZM** was prepared.

Neutron Crystallography

Neutron diffraction gives an advantage over conventional X-ray diffraction techniques in that even at medium resolution (1.5 – 2.0 Å) it is the only direct method available for unambiguously visualizing H (or D) atomic positions. Neutrons scattering off atomic nuclei lead to H/D atoms being as visible as heavier N, C, or O atoms. In contrast, X-ray diffraction occurs from the electron cloud making it very challenging to observe light H/D atoms with any confidence. A systematic study by Gardberg et al. carried out on a limited set of X-ray and neutron structures revealed a trend that at sub-atomic resolution (~ 1 Å) only a fraction of H atoms are observed in electron density

maps. This is in dramatic contrast to the case for nuclear density maps where almost all H/D atoms are observed at medium resolution.[191]

Data Collection

A large single crystal (~2 mm^3 volume) was mounted in a quartz capillary, with D_2O mother liquor placed at one end of the capillary prior to sealing. The crystal was left to undergo H/D exchange for ~4 weeks before data collection was started. Bennett *et al.* reported that most labile H atoms are exchanged by D atoms fairly rapidly with ~80% amide backbone exchange happening in about a month.[192] The crystal was transported to the Protein Crystallography Station (PCS) for neutron data collection. Time-of-flight, wavelength-resolved neutron Laue diffraction images were collected at room temperature. The sample was mounted on a Huber κ-circle goniometer and 33 settings were recorded on the position sensitive ^{3}He-filled neutron detector. Each frame corresponds to 16 hrs exposure and corresponds to 22 days total beam time.

A room temperature X-ray diffraction data set was collected from a similar crystal from the same drop. This crystal was also subjected to in-capillary H/D exchange prior to data collection. Data were collected on an in-house Rigaku HighFlux home source equipped with 007 Micromax optics and an R-AXIS IV++ image plate. The source was a Cu rotating anode operated at 40 kV and 30 mA. The crystal-detector distance was 100 mm and the oscillation steps were 0.5° with a 2 minute exposure per frame. Data processing and reduction were done using *HKL3000*.[193] X-ray data was collected to 1.6 Å resolution from 240 frames. The data set statistics are shown in Table 5-1.

Structure Determination

Data Processing Structure Refinement

Each image was processed using a version of *d*TREK*[194] modified for wavelength-resolved Laue neutron protein crystallography.[195] The integrated reflections were wavelength normalized using *LAUENORM*[196] and then merged using *SCALA* incorporated into the *CCP4i*.[197–200] The wavelength range was restricted to 0.6-6.2 Å so as to eliminate the least accurately measured reflections. The overall completeness was ~86% to 2.0 Å, with an R_{sym} of ~ 26% and redundancy of 3.2 (Table 5-1).

Density Visualization

The **AZM** molecule was clearly observed in omit F_o-F_c electron density maps and after placement and refinement was found to bind in the same overall configuration as reported previously.[187] A series of omit F_o-F_c and $2F_o$-F_c nuclear density maps reveal the positions of the two exchangeable D atoms of **AZM** (Figure 5-2), information not obtainable from the X-ray data alone. The joint X-ray and neutron structure refinement approach exploits the strengths of each technique: the use of X-ray data to refine "heavy" (non-H) atoms in proteins and complementing this with neutron data to refine "light" (H/D) atoms (Figure 5-2).[201] Highly complementary joint X-ray and neutron studies give very accurate and elusive details regarding H-bonding, solvent molecule orientation, and the protonation states of residues.[202,203] The neutron structure reported here clearly shows the charged state of **AZM** as well as H-bonding between hCA II and **AZM**, information not obtainable from numerous high-resolution X-ray studies (Figure 5-2).[187,204]

Omit F_o-F_c nuclear density maps calculated without the two exchanged D atoms – one each on the acetoamido and sulfonamido groups – clearly revealed that **AZM** was

in the anionic form, with the negatively charged sulfonamido group coordinated to the zinc (Form 3 in Figure 5-1; Figure 5-2 and Figure 5-3). There are four H-bonded waters in the vicinity of the **AZM** binding site that are displaced upon drug binding (Figure 5-4).[202] The waters serve as a chemical template for where the drug binds, in that the O of the waters superimpose with the N and S atoms of **AZM**.

Crystal Structure Details

The lone pair of sulfonamide N is involved in a coordinating bond with the zinc of ~2.4 Å distance (Figs. 3 and 5). This leads to a H-bonding scheme where the single D atom on the sulfonamide group acts as a H-bond donor to Thr199, which in turn acts as a H-bond donor to Glu106. The –OD of Thr200 participates as a bifurcated H-bond donor to both W1120 and the carbonyl of Pro201. W1120 forms an H-bond bridge between **AZM** and hCA II, acting as H-bond acceptor from the protonated acetoamido group and as a donor to the backbone carbonyl of Pro201 (Figure 5-3 and Figure 5-5).

Figure 5-5 illustrates the complementarity between electron and nuclear density maps. The neutron scattering length for S is quite small at only 2.7 fm. This is evident in the nuclear density maps where there is no nuclear density for the two S atoms of **AZM** at a 1.5 σ contour level (Figure 5-5A). In contrast to this and as expected, there is very strong density for S in the electron density maps (Figure 5-5B). The neutron scattering magnitude for D is comparatively large at 6.7 fm and this is evident by the excellent density observed for both D atoms.

As expected, the terminal $–CH_3$ group was not visible in the neutron densities as there is significant signal cancellation at 2.0 Å resolution due to the presence of non-exchangeable H atoms (negative 3.7 fm scattering length) in such groups. However, it is

not visible in the electron density map either. Although, electron density for the terminal $-CH_3$ is seen in the highest resolution structure (PDB ID: 3HS4)[187] of hCA II bound to **AZM**. In this case, the higher resolution X-ray data was not more informative for a heavy atom C compared to the neutron data.

A direct comparison of the hCA II[29] and hCA IX[90] active sites shows that the only differences are at residues Phe131 and Val135, with Val and Leu at these positions in hCA IX, respectively (Figure 5-6). Phe131 (in hCA II) is involved in very weak hydrophobic interactions with **AZM** and its absence in hCA IX could, in part, explain the small 2-fold difference in binding constants for **AZM** between hCA II and IX.[6]

Discussion and Conclusion

We have solved the first neutron structure of hCA II in complex with a sulfonamide inhibitor. This is the first example of a clinically used inhibitor bound to a human enzyme target to be studied with neutron diffraction. This study adds explicit details about the charged form of the drug that binds to hCA II, H-bonding to the target and water displacement when **AZM** binds. A comparison of the current neutron structure with **AZM** bound to another neutron structure of unbound hCA II (PDB ID: 3TMJ)[202] reveals that four water molecules in the active site (Figure 5-4) that were bound to either the zinc or H-bonded to other water molecules in the active site are displaced by the binding of **AZM** (Figure 5-3). This structure provides insightful observations regarding H-bonds and hydrophobic interactions that play a key role in binding of **AZM** to hCA II. Neutron diffraction is the only technique that can directly reveal these details and is expected to contribute greatly to structure-based drug design in the future.

Table 5-1. Crystallographic details of CA II – **AZM** structures.

	X-ray	Neutron
PDB ACCESSION #	-	4G0C
Data-collection statistics		
Source	Rotating Cu Anode	LANSCE, PCS
Temperature (K)	298	298
Wavelength (Å)	1.5418	0.6 – 6.2
Space group	$P2_1$	$P2_1$
Unit-cell parameters (Å, ^{o}): *a, b, c, β*	42.8, 42.7, 72.9, 104.6	42.8, 42.7, 72.9, 104.6
Unique measured reflections	31126 (2989)[#]	14486 (1782)
Resolution (Å)	40.0 – 1.6 (1.6 – 1.6)	20.0 - 2.0 (2.1 - 2.0)
[a]R_{pim} (%)	N/A	14.9 (27.8)
I/σ(I)	33.8 (20.0)	6.9 (2.1)
Completeness (%)	93.6 (89.6)	85.7 (73.4)
Redundancy	5.1 (5.1)	3.2 (2.1)
Final Model Statistics		
No. of atoms: *Main-chain, side-chain, water*	N/A	1029, 3030, 498
Ramachandran stats (%): *Favored, allowed, outliers*	89.4, 10.6, 0.0	89.4, 10.6, 0.0
Average B-factors (Å^2): *Main chain, side chain, water*	N/A	15.3, 17.9, 43.5
Joint [b]R_{cryst}, [c]R_{free}	17.4, 18.9	26.8, 28.3

[a]$R_{pim} = (\Sigma\ [1/(N-1)]^{1/2}\ \Sigma|\ I - \langle I \rangle\ |\ /\ \Sigma\Sigma\ I) \times 100$. [b]$R_{cryst} = (\Sigma\ |Fo| - |Fc|/\ \Sigma\ |F_{obs}|\ ) \times 100$. [c]$R_{free}$ is calculated in same manner as R_{cryst}, except that it uses 5% of the reflection data omitted from refinement. [#]Values in parenthesis represent highest resolution bin.

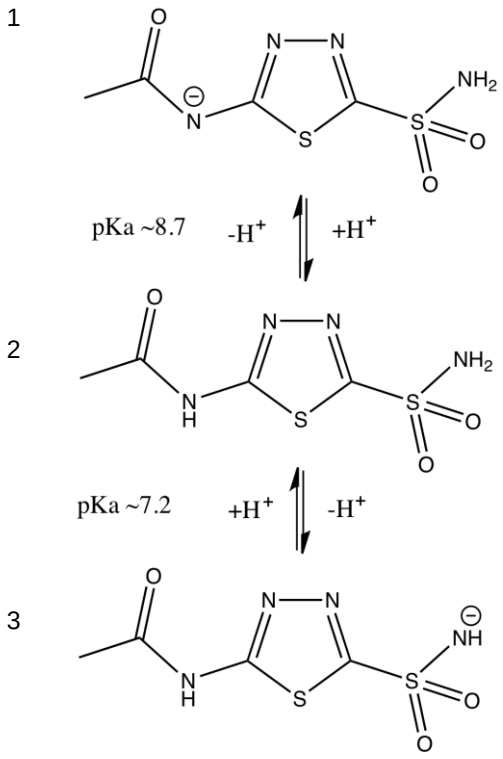

Figure 5-1. Ionization and pKa of acetazolamide (**AZM**) in water. These different charged states represent the relevant forms that may bind hCA II under physiological conditions.

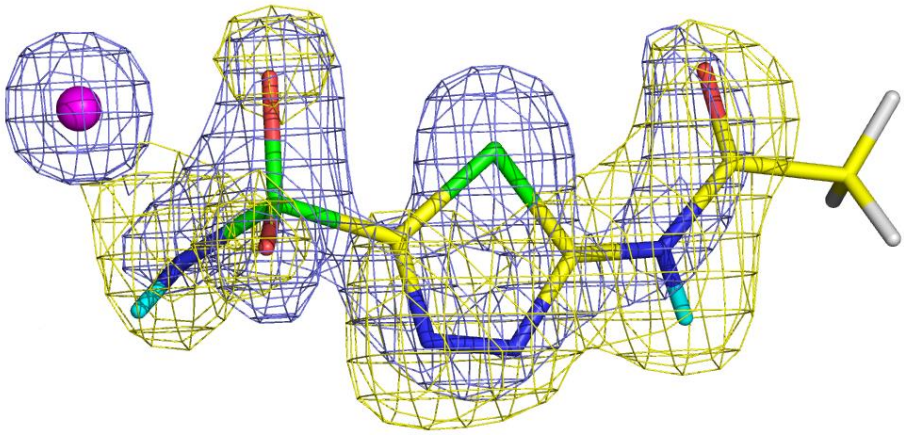

Figure 5-2. Stick representation of **AZM** bound to hCA II. Zinc is shown as a magenta sphere; D atoms are in cyan, H atoms in white. The nuclear density map is shown in yellow and is contoured at 1.5 σ, the electron density map is shown in blue and is contoured at 2.0 σ.[182]

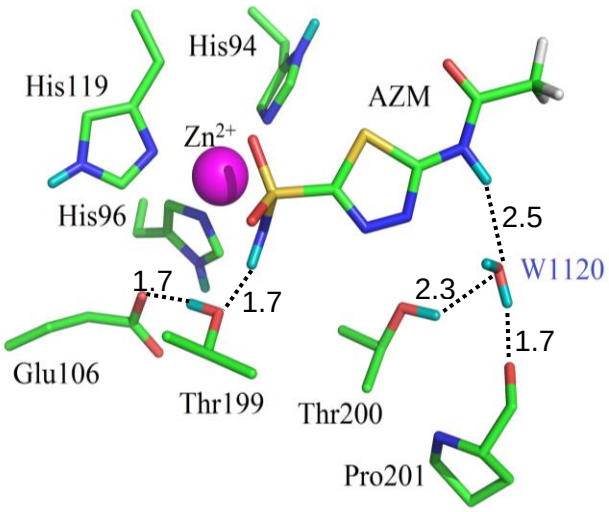

Figure 5-3. Stick representation of the neutron structure of the active site of hCA II-**AZM**. Exchanged D atoms are shown in cyan and unexchanged H atoms in white. Hydrogen bonds as observed in the nuclear maps are indicated by dashed lines with distances as indicated.

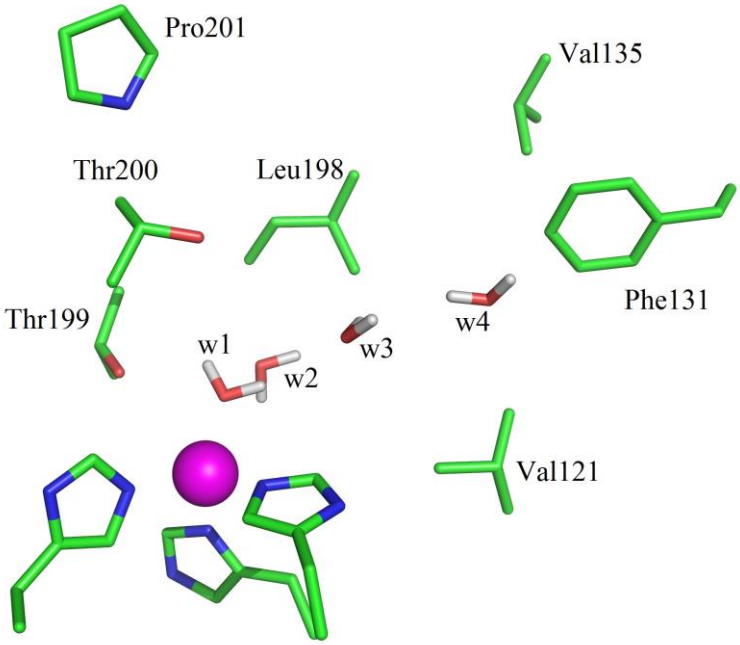

Figure 5-4. Stick representation of the active site of neutron structure of unbound hCA II (PDB 3TMJ)[202] showing well-ordered waters w1, w2, w3, and w4.

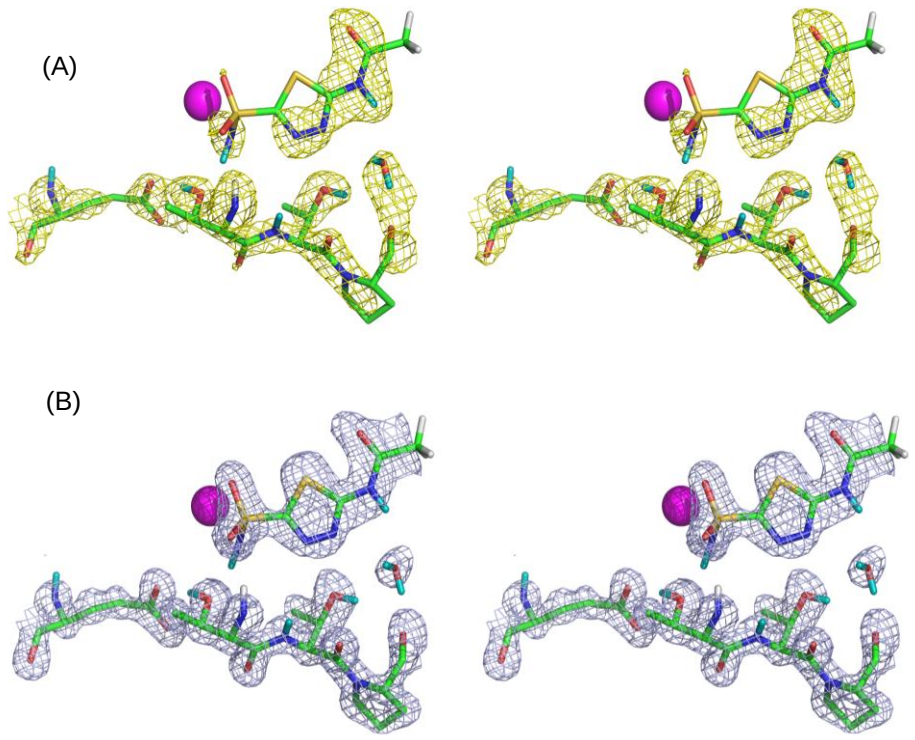

Figure 5-5. Complementarity of electron and nuclear density maps. Stereo stick representation of the active site of hCA II-**AZM** bound. (A) Nuclear density map is shown in yellow and is contoured at 1.5 σ; (B) Electron density map is shown in blue and is contoured at 2.0 σ. Color scheme and residue labeling is as shown in Figure 5-3.

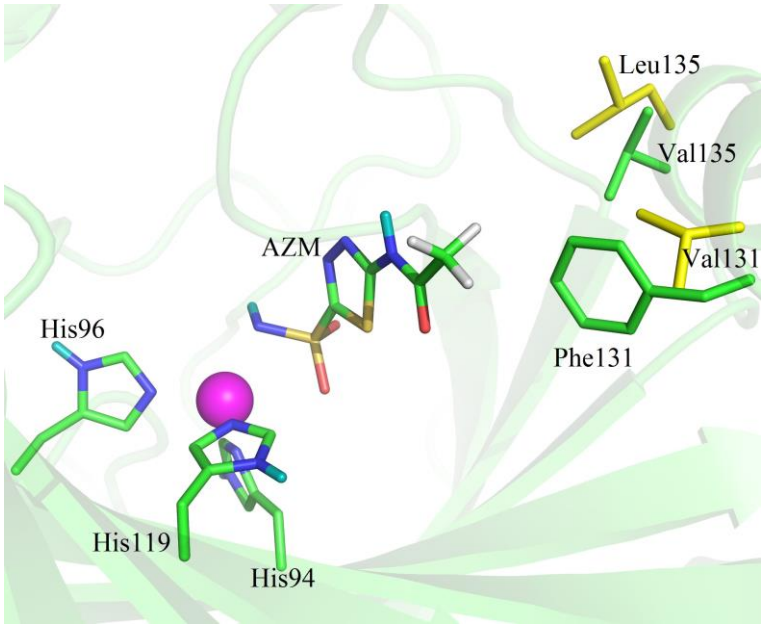

Figure 5-6. Active site of hCA II-**AZM** (green cartoon and sticks) superposed with hCA IX[90], showing key residues (yellow sticks) that are different among the two isoforms (Val131 and Leu135).

CHAPTER 6
ISOFORM SPECIFICITY − PDB MINING[104]

Introduction

Carbonic Anhydrase Isoform II

Carbonic anhydrase isoform II (CA II) is a monomeric 29 kDa protein composed of 260 amino acids with a mixed α/β globular protein fold. It is the best studied and most abundant isoform of CA present in humans, comprising a 10 β-strand sheet flanked by 7 α-helices. The active site zinc present at the base of the 15 Å deep conical cleft is tetrahedrally coordinated by three histidine residues (His94, His96 and His119) and a hydroxyl ion. The active site cavity is partitioned into two very different environments comprising a cluster of hydrophobic amino acids (Val121, Val143, Leu198, Val207 and Trp209) on one side, and hydrophilic amino acids (Tyr7, Asn62, His64, Asn67, Thr199 and Thr200) lining the surface on the other side.

The contrasting environments within the active site aid in enhancing the catalytic efficiency of the enzyme. Clustering of various amino acid residues in and around the rim of the active site of CA, forms various surface pockets (Figure 6-1A). The first step, hydration of CO_2 that occurs in the hydrophobic pocket (Figure 6-1B), is the nucleophilic attack on incoming CO_2 by a Zn-bound OH^- to produce HCO_3^-. The binding of HCO_{3-}at the metal is weak and accordingly is displaced by a water molecule. In the second step, the Zn-H_2O loses a proton (H^+) leaving the Zn in its original Zn-OH^- conformation through a network of well-ordered H-bonded waters to several hydrophilic residues (Tyr7, Asn62 and Asn67 in CA II) that line the active site (Figure 6-1B). These residues

---

Adapted from: Aggarwal, M.; Kondeti, B.; McKenna, R. Insights towards sulfonamide drug specificity in α-carbonic anhydrases. *Bioorg. Med. Chem.* **2013**, *21*, 1526–1533.

are found to be highly conserved among various isoforms of α-CA. This network stretches from the Zn-bound solvent to the proton shuttling residue His64.

Carbonic Anhydrase Isoform IX

CA isoform IX (CA IX) is a transmembrane protein.[98] Based on sequence similarity, CA IX has been recognized as a multidomain protein consisting of an N-terminal proteoglycan like (PG) domain, a CA catalytic domain, a transmembrane segment (TM), and an intracytoplasmic (IC) portion.[205] The CA catalytic domain presents a significant sequence identity (30-40%) to other catalytic CA isozymes. Both CA and PG domains are glycosylated[206]. A cDNA coding for the CA IX protein was first cloned by Pastorek et al[120], and the *CA9* gene was further characterized.[205] According to recent biochemical and structure reports, the CA IX is a dimer[206] and shows similarity with CA II not only in terms of catalytic efficiency, but also affinity for inhibitors[5,6,16,98] like sulfonamides[152,207–212] and sulfamates.[211–213]

So far, only one structure of CA IX[90] crystallized in complex with **AZM** (a classic inhibitor of CA) is available in the PDB. The structures of CA II (PDB ID: 3KS3)[29] and CA IX (PDB ID: 3IAI)[90] are very similar and have a Cα RMSD of 1.5 Å (Figure 6-2). However, there are several amino acid residues differences in and around the rim of the active site of the two isoforms. Ala65, Phe131, Asn67, Gln69, Ile91 and Leu204 in CA II are structurally equivalent to Ser65, Val131, Gln67, Thr69, Leu91 and Ala204 in CA IX, respectively. It is interesting to note that 3 of these differences lie in a region that forms a hydrophobic pocket on the rim of the active site where some of the already known inhibitors bind CA II.[122,210,214–224] It is these differences which could be exploited to design inhibitors which prefer binding to one CA compared to another. Differences in the active site residues of CA II and CA IX also account for a variation in the size of their

active site cavities. With a volume of 290 $Å^3$ and surface area of 245 $Å^2$, the active site of CA II is larger than that of CA IX (volume = 270 $Å^3$, surface area = 215 $Å^2$) These calculations were performed using the online web server of CASTp.[225]

CA IX and Cancer

Cancer continues to be the second most leading cause of death in the United States, after cardiovascular diseases. Accounting for more than 1.6 million cases in 2012, cancer was estimated to kill over 577,000 people in the U.S. alone.[226]

It has now been well documented that tumor hypoxia is associated with poor prognosis and increased tumor aggressiveness, and CA IX is an endogenous marker for tumor hypoxia, and its upregulation regulates the pH of tumor cells. In contrast to the other CA isoforms, CA IX has been implicated to play a role in regulation of cell proliferation, adhesion, and malignant cell invasion. Interestingly, CA IX is over expressed in human epithelial tumors derived from tissues that normally do not express these isoforms, including carcinomas of the cervix, lungs, kidneys, prostate, and breast. There is also evidence that CA IX allows tumors to acclimate to a hypoxic microenvironment, promoting tumor cell proliferation, and that CA IX expression is related to poor survival in patients.[41]

Most tumors experience a structurally and functionally disturbed microcirculation of oxygen which pathophysiologically causes an inadequate supply of oxygen (or hypoxia).[6,98–102,227] In tumors such as gliomas/ependymomas[6], mesotheliomas[6], tumors of kidney[228], carcinomas of bladder[229], uterus/cervix[230,231], pharynx[232], head/neck[233], breast[234–236], esophagus, follicles, brain, vulva, squamous/basal cells[6] and lungs[237], hypoxia or a mutation in von Hippel-Lindau (VHL) factor leads to an overexpression of CA IX (up to 150 fold)[6,98,234] through hypoxia inducible factor (HIF) cascade.[6,98–102,227,236]

Isoform Specific Drug Design

One of the major issues in targeting CA IX for the treatment of tumors is its structural similarity with CA II. In fact, most isoforms of CA bear only few differences in the active site which makes it difficult for designing inhibitors that would specifically bind to one isoform over the others. This non-specific binding (or off-target inhibition) to other isoforms of CA by clinically used (U.S. Food and Drug Administration approved) CA II inhibitory drugs is what causes various side effects during the course of treatment of glaucoma, such as eye irritation, watering, blurred vision, taste changes, constipation and diarrhea.[6] This has given rise to the need to get greater insights into the fine structural differences within the isoforms and exploit these to design novel and more specific inhibitors in order to circumvent the problem of off-target binding. Although, not many isoform specific inhibitors are known yet, but new sulfonamides and other non-sulfur based compounds are continuously being reported to find derivatives with better inhibition profiles as compared to the promiscuous, first generation inhibitors.[15,238,239] Various docking and kinetic studies to test and characterize novel and already existing inhibitors for isoform specificity are going on.[41,240]

Rational drug design or ligand design is the process of finding new compounds based on the knowledge of a biological target. However, once a ligand has been designed and proven to be effective in inhibiting or enhancing its appropriate target, there are certain issues that need to be resolved before the ligand can be used as a drug. These issues or rules were first defined as the *Lipinski's rule of five.*[241] The rule describes pharmacokinetic properties like absorption, distribution, metabolism, excretion (ADME) of an ideal orally administered drug. According to this rule, for a drug (ligand) to be orally administered, it should not violate more than one of the following criteria: the

ligand should have no more than 5 H-bond donors, 10 H-bond acceptors, 500 Dalton of molecular weight, and an octanol-water partition coefficient (log P) of 5. However, over the years there have been various changes to this rule, like the ones suggested by Ghose et al[242] and thus it is no longer followed verbatim. Some of the most successful results yielded by rational, structure based computer aided drug design have produced drugs like Saquinavir (HIV protease inhibitor)[243], Dorzolamide (CA inhibitor)[244,245] and Iminatib (tyrosine kinase inhibitor).[246]

One of the most common approaches that have been used for designing CAIs is referred to as the *ring approach* where an aromatic ring is attached directly to the sulfonamide group to enhance binding affinities. This approach has been calibrated and exploited over the last few decades.[10] There is already enough information available about high affinity inhibitors against CA and more compounds are added to an ever growing database. However, it is not the binding affinity but isoform-specificity that is lacking and hence, the ring approach has become less important. *Combinatorial chemistry* is another widely used, although not a very successful approach to rapidly synthesize or computationally simulate a large number of structurally related molecules. The failure to take molecular flexibility of drugs into account could well be considered as the biggest shortcoming of this approach.[247]

As mentioned earlier, CA IX has been observed to be a key player in tumorigenesis and tumor progression.[248] One of the major issues with cancer treatment is the inability of most drugs to distinguish cancerous cells from normal cells. Overexpression of CA IX specifically in cancerous cells makes it a good drug target.

Protein Data Bank (PDB)

The Protein Data Bank (PDB) is a repository for the 3-D structural data of large biological molecules, such as proteins and nucleic acids. The data, typically obtained by X-ray crystallography or NMR spectroscopy and submitted by biologists and biochemists from around the world, are freely accessible on the internet via the websites of its member organizations: PDBe (http://www.ebi.ac.uk/pdbe), PDBj (http://www.pdbj.org), and RCSB (http://www.rcsb.org/pdb/home/home.do). The PDB is overseen by an organization called the Worldwide Protein Data Bank. It is a key resource in areas of structural biology, such as structural genomics. Most major scientific journals, and some funding agencies, such as the National Institute of Health (NIH) in the U.S.A., now require scientists to submit their structure data to the PDB. If the contents of the PDB are thought of as primary data, then there are hundreds of derived (i.e., secondary) databases that categorize the data differently.

PDB Mining Approach

As shown in Figure 6-1A earlier, clustering of various amino acid residues in and around the active site of CA, forms various pockets. Different sulfonamide inhibitors' "tails" prefer different orientations and active site rim pockets as they extend out of from the Zn. Their orientation within a pocket depends largely on the interactions between the terminal tail atoms of the inhibitor and the residues that form the pocket. A list of all the inhibitors deposited in the PDB in complex with CA II, has been compiled. The inhibitors were then categorized based on their structural similarity and only one coordinate file for each inhibitor was included, shortening the original list of 400 structures to 145 non-redundant structures. Each of these structures were visualized in *COOT*[118] and analyzed based on which pocket the inhibitors bind in. As shown in the

flowchart (Figure 6-3), 115 inhibitors were found to bind in one general pocket, while 14 inhibitors (Figure 6-4) occupied a “selective” pocket (Figure 6-5). Based on the observed active site binding interactions of these inhibitors in the crystal structures and their respective inhibition constants, the goal is to structurally characterize aspects of these interactions that would lead to more potent, selective CA IX sulfonamide inhibitors.

The PDB deposited structure of CA IX, solved to a resolution of 2.2 Å, crystallized in $P6_1$ space group as a dimer. Coordinates of the aforementioned 129 inhibitors from the non-redundant list were used to model the respective inhibitors into the crystal structure of CA IX (PDB ID: 3IAI)[90]. The structures of CA II (PDB ID: 3KS3)[29] and CA IX (PDB ID: 3IAI)[90] are very similar although, there is a difference in three residues (N67Q, E69T and I91L) that form part of this “selective” pocket in the active site. It is this pocket where 14 inhibitors from the non-redundant list of PDBs were found to be bound. This raises opportunities for designing and altering the tails of these 14 inhibitors in a manner that might preferentially enhance their K_Is for CA IX over CA II.

With the objective of enhancing the CA II inhibitor database to enable studies using the tail approach, more and more crystal structures of CA II in complex with various novel inhibitors belonging to different structural classes are being solved.[122,127,131,156,157] To attain selective inhibition of CA IX and to relate its catalytic activity to extracellular acidification, the hypothesis is that the inhibition characteristics for CA IX will vary from CA II (based on crystal structures). The specific differences in amino acids projecting into the active site (namely, residues at positions 65, 67, 69. 91 and 131 (CA II numbering)) will have a direct effect on the specificity of inhibitor binding.

Among various other approaches that are currently under study, *tail approach* (a word coined by Supuran and co-workers)[10] can be used to enhance the aqueous solubility of inhibitors in order to decrease the side effects caused by drugs which are only soluble in highly acidic solvents. The approach (Figure 6-6) could also involve altering the terminal regions of an already known inhibitor such that the tail interacts specifically with residues on the surface of one isoform (CA IX) and not others.

Discussion and Conclusion

CA IX has been shown to play a critical role in cancer proliferation. Its overexpression in certain types of cancers has led to the use of CA IX as a biomarker for cancer diagnosis and prognosis. In addition, much knowledge has been acquired on CA II inhibition for various classes of diuretics and systemically acting antiglaucoma agents. The differences in the active sites of different isoforms of CA are subtle and this causes non-specific CA inhibition which leads to side effects. The PDB was mined for previously solved α-CA inhibitor complex structures (mainly CA II), and a sub-set of selected structures were superposed with the structure of CA IX. For example, the inhibitor from a CA II complex (PDB ID: 3N2P)[122] when modeled in CA IX (PDB ID: 3IAI)[90] appears to form one extra hydrogen bond with the protein (Figure 6-7). This is because Gln67 in CA IX is one C-C bond longer than the Asn67 in CA II and thus extends further towards the inhibitor to be close enough to form a H-bond. Surface area (SA) buried by an inhibitor in a crystal structure with CA II, has been compared with that of the same inhibitor modeled into CA IX. A reduction of buried SA by 10 $Å^2$ corresponds to a decrease in Gibbs free energy by 0.3 kcal/mol.[249] Although the buried SA in almost all the 14 inhibitors with CA IX is smaller (larger ΔG) than that with CA II, the presence of extra hydrogen bonds in the former compensates for the gain in ΔG by

a larger magnitude (H-bond energy values obtained from Wendler et al[250]). These findings can be hereafter correlated to the inhibition of CA II and CA IX to provide SARs that may help in understanding the varied binding affinities of the inhibitors toward different α-CA isoforms (Table 6-4). This data can further be used to guide *in silico* design of new CA inhibitors (CAIs) that would preferentially bind to CA IX (on-target) over others CAs (off-target).

Table 6-1. Differences in buried surface area, hydrogen bonds, and difference in Gibbs free energy (ΔG) associated with H-bonds among published CA II-inhibitor crystal complexes and modeled CA IX-inhibitor complexes.

PDB IDs	Buried Surface Area (Å^2)		Δ(ΔG) (kcal/mol)	# of Hydrogen Bonds	
	CA II	CA IX		CA II	CA IX
3N2P[122]	370	360	0.2	4	5
1I8Z[214]	440	425	0.6	5	5
1I91[214]	430	425	0.2	5	5
1IF9[215]	370	355	0.5	4	4
3BL1[216]	405	375	0.9	4	4
3FFP[217]	335	315	0.7	4	4
3HLJ[218]	340	315	0.7	3	3
1ZE8[210]	360	335	0.7	3	4
2FOU[219]	360	345	0.4	4	5
2HL4[220]	360	340	0.5	5	6
2WD3[221]	400	415	-0.4	5	5
3K34[222]	400	370	0.9	4	4
3MNU[223]	340	320	0.6	5	5
3HKT[224]	380	355	0.6	5	2

ΔG indicates the solvation free energy gain upon formation of the interface, in kcal/M. The value is calculated as difference in total solvation energies of isolated and interfacing structures.Negative ΔG corresponds to hydrophobic interfaces, or positive protein affinity. This value does not include the effect of satisfied hydrogen bonds and salt bridges across the interface.

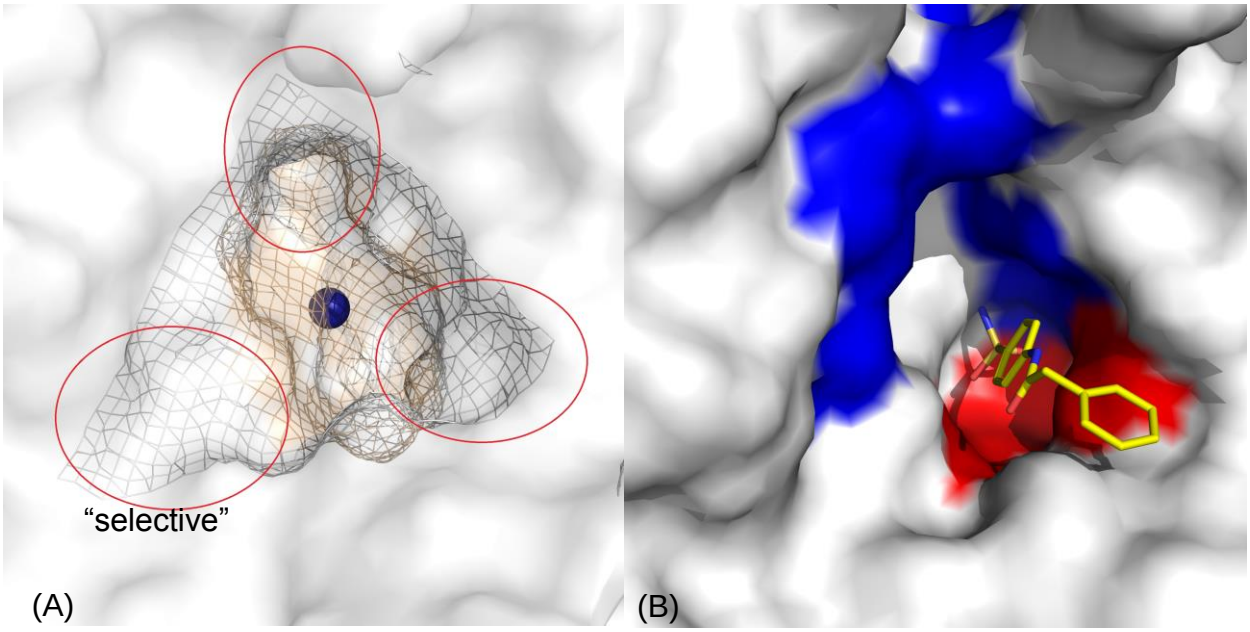

Figure 6-1. (A) Various pockets (encircled mesh) within and around the active site of CA II[29]. (B) An inhibitor, PDB ID: 3OYS[131], extending out of the active site of CA II (white surface), stabilized by hydrophobic (red) and hydrophilic (blue) regions. Active site Zn is shown as a blue sphere.

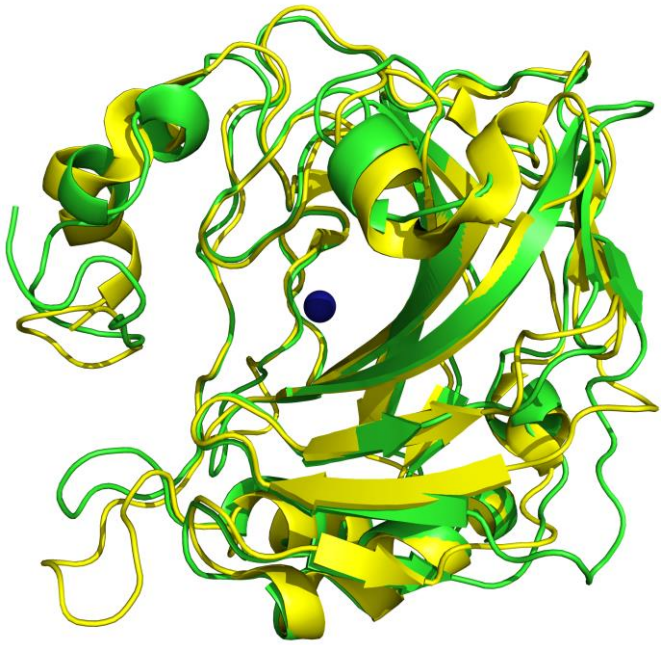

Figure 6-2. Superposition of CA II[29] (yellow) and CA IX[90] (green), showing high conservation in secondary structures.

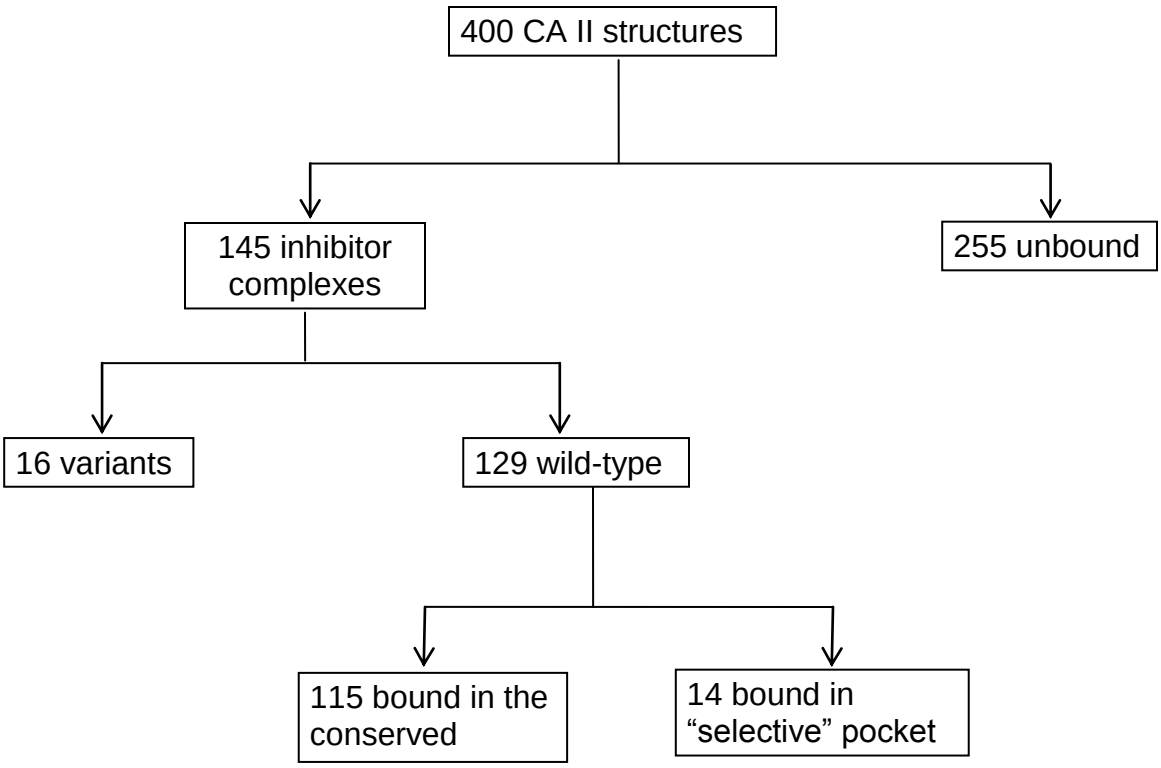

Figure 6-3. Stepwise findings from Protein Data Bank mining.

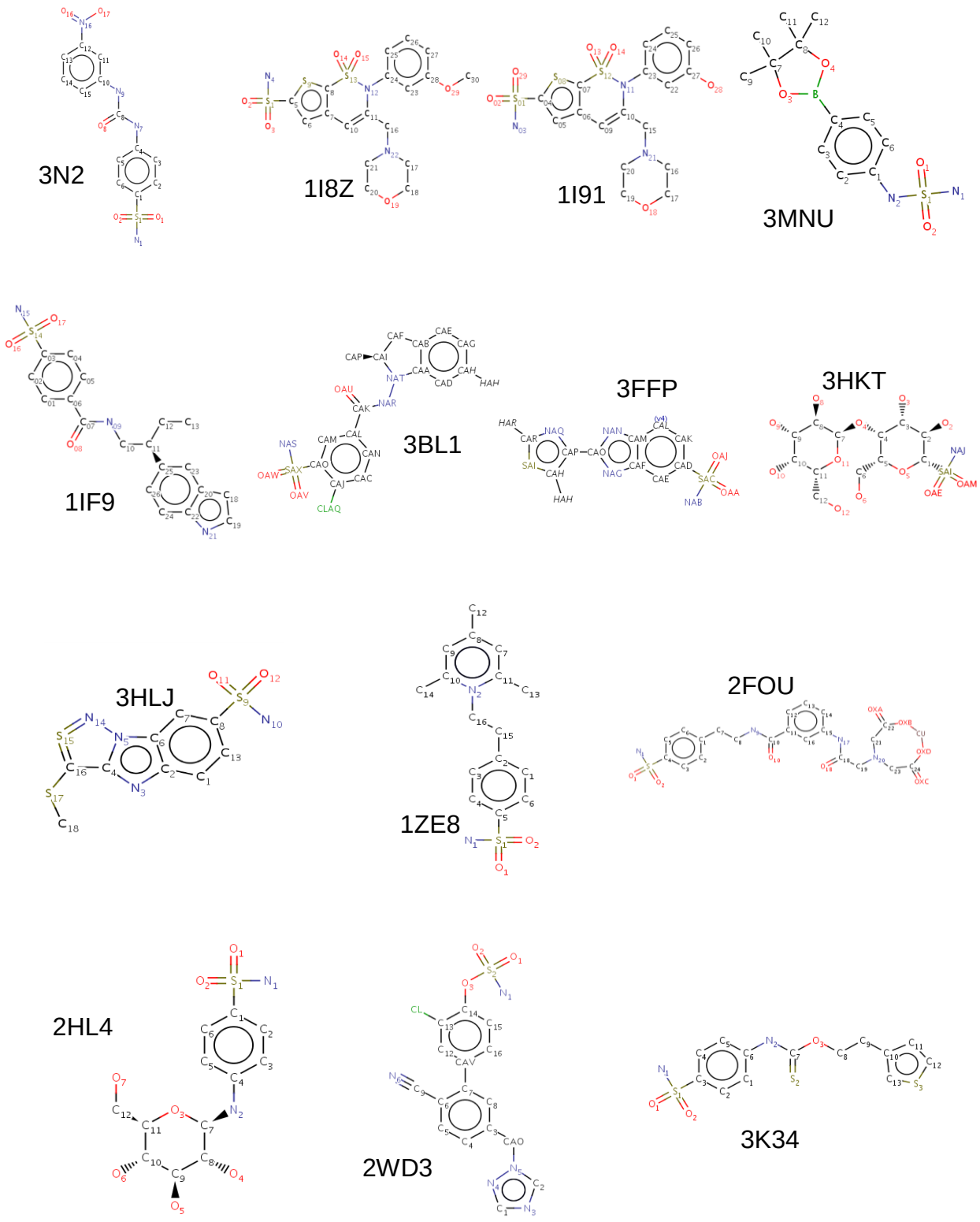

Figure 6-4. Structures of the 14 inhibitors that occupy the "selective" pocket in CA II.

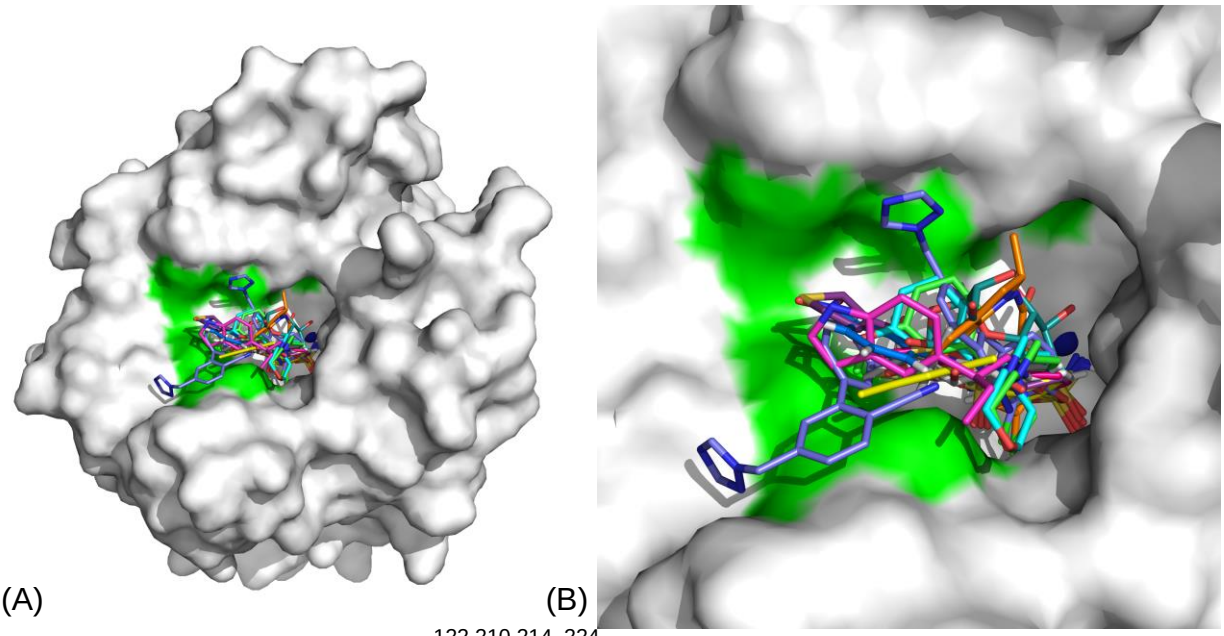

(A) (B)

Figure 6-5. (A) The 14 inhibitors[122,210,214–224] occupying the "selective" pocket in CA II (white surface), where 3 residues differ from CA IX (shown in green). (B) Active site zoomed.

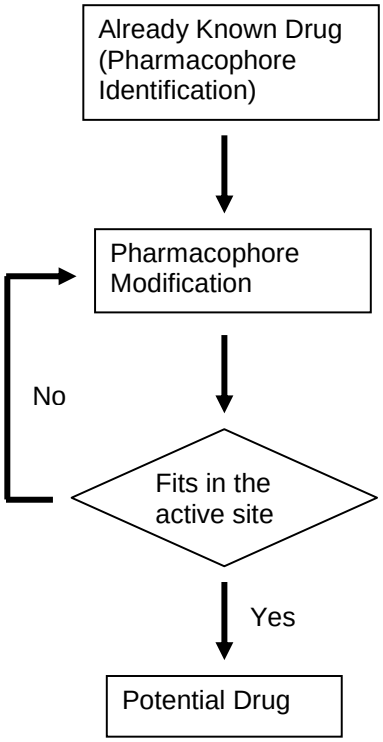

Figure 6-6. Approach to isoform specific drug design and enhancement of inhibition profiles for currently known drugs.

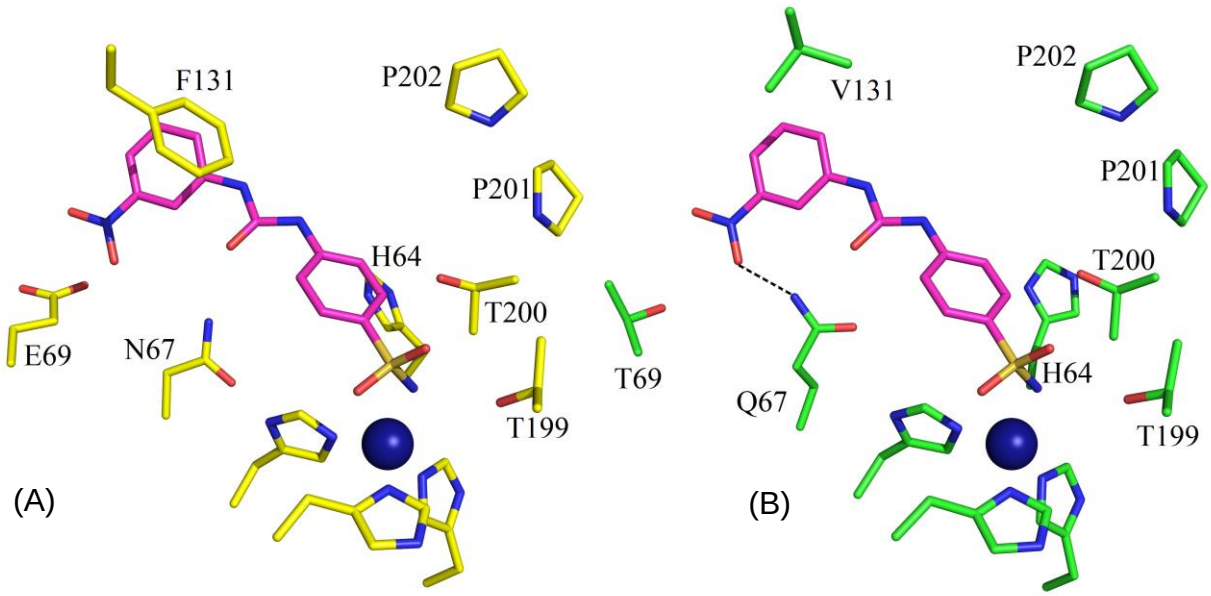

Figure 6-7. Stick representation of (A) PDB ID: 3N2P[122], and (B) the same inhibitor modeled into the active site of CA IX, PDB ID: 3IAI.[90]

CHAPTER 7
FRAGMENT BASED APPROACH − IMIDAZOLE BINDING

Introduction

Structural studies using X-ray crystallography (PDB ID: 3KS3)[29] and MD calulations[30,251] have shown the side chain of His64 to exhibit two conformations in wild-type CA II (wt-CA II) at pH 7.8. The rotation about Cα-Cβ bond of His64 has a $\Delta G \sim 6.0$ kcal/mol (equivalent to $2.45 \times 10^8\ s^{-1}$)[30,252]; hence, its conformational switching can occur faster than catalysis. A possible mechanism for proton transfer (as discussed in Chapter 1) is that His64 accepts a proton in an inward orientation pointing towards the active site, and delivers it to the bulk solution in the outward orientation pointing away from the active site (Figure 7-1). Exactly how protons move in the active site of proteins is not clear but it has been proposed that a Grotthus proton hopping mechanism or the formation of a series of Zundel ($H_5O_2^+$) or Eigen cations ($H_9O_4^+$) may be involved.[30,252,253] It has been postulated that the inward conformation of His64 is poised to accept the excess proton from the water network, while the outward conformation is ready for proton shuttling to the bulk solvent. This observed flexibility of His64 is most likely related to its protonation state.[202] The enzyme displays very strong pH dependence for both k_{cat} and k_{cat}/K_M that are defined by a pK_a of ~7.[28,181,254–256]

When His64 is mutated to Ala (H64A) in carbonic anhydrase II (CA II), it causes a reduction in the enzymatic proton shuttling and thus, decreases the rate of reaction by ~20 fold.[256] This decrease in catalysis has been shown to be rescued in a saturable manner by the addition of exogenous proton acceptors in solution, such as histamine, small imidazoles, pyridines, and their derivatives.[256–260] It has been an intriguing observation that the activity enhancement of H64A CA II by these external proton

donors/acceptors is substantial, with catalysis at saturation levels of certain imidazole and pyridine derivatives approaching that of wt-CA II.[261]

Only two binding sites for such enhancers[260–262] have been successively identified by X-ray crystallography[261] and NMR[253] within and around the active site cavity of H64A CA II, so it is unclear whether or not these sites are indicative of the proton transfer pathway. For example, X-ray diffraction of H64A CA II crystals soaked in 4-methyl imidazole (**4MI**) showed a binding site 12 Å away from the zinc ion making a π-stack with Trp5 in the active site cavity;[261] however, this binding site was not productive in proton transfer in catalysis as demonstrated with subsequent kinetic analysis of a W5A CA II variant,[260] and multi-state empirical valence bond simulations.[30]

The generation and release of a proton during CA catalysis is a key step and contributes to pH regulation in the body. As such CA has long been a well studied model system for understanding the mechanism behind proton transfer in a protein environment. Studying the activity enhancement of H64A CA II by small imidazoles will not only aid in basic science research, but may also help in understanding the functionality of other proteins like bacteriorhodopsin and cytochrome c oxidase that carry out proton transfer.[263,264]

Four small imidazoles: Imidazole (**I**), 1-methyl imidazole (**1MI**), 2-methyl imidazole (**2MI**), and **4MI** have been co-crystallized with H64A CA II to identify binding sites for such compounds and propose a mechanism to explain the activity enhancement. Enzyme kinetics studies to analyze the CA activity enhancement effects of these imidazoles were also performed using an ^{18}O exchange method.[260,261]

Results

Each of the four imidazole compounds; **I**, **1MI**, **2MI**, and **4MI** were co-crystallized with H64A CA II, the structures determined to the highest resolution of at least 1.7 Å (Table 7-1), and the coordinates deposited to the protein data bank with PDB IDs 4HF3 (**I**), 4HEZ (**1MI**), 4HEW (**2MI**), and 4HEY (**4MI**). All the four structures had a main-chain r.m.s.d. < 0.2 Å when compared to wt-CA II (PDB ID: 3KS3)[29], demonstrating no significant structural perturbation of the enzyme. Omit F_o-F_c electron density maps were calculated and the respective imidazoles were located, fitted, and refined. Based on where these compounds were located over the structure, 15 unique sites were characterized (Figure 7-2). Of these 15 sites, three were identified as of significant importance to the rescue of catalysis (sites labeled 1-3 and shown for **4MI** in Figure 7-3), based on their location within the active site. The others were most likely a consequence of surface crystallographic packing arrangements. Sites 1 and 2 are defined as the overlapping regions of the inward and outward conformations, respectively, of His64 in wt-CA II. The binding of imidazoles in Sites 1 and 2 provide a possible proton donor/acceptor group within these locations, thereby restoring the lost proton shuttle capability of the enzyme. Site 3 overlaps with the CO_2 binding site[3], displacing the Zn-OH^-. Thus, binding of any imidazole molecule in this region would suggest enzyme inhibition as the Zn-OH^- is essential for catalysis. The other sites appear mostly on the surface of the enzyme (Sites 5, 7, 9-11, 13-16), and are too distant from the zinc to affect catalysis.

Imidazole (I)

A total of 9 molecules of **I** were located bound to H64A CA II, with an average B-factor of 24.5 $Å^2$ which is comparable to the B-factors of surrounding solvent molecules

and residues (Table 7-2). Absence of a methyl group (as compared with other imidazoles in this study) imparts low hydrophobicity to **I** (log P = -1.0; P = partition coefficient) thereby reducing the possibility of it being involved in hydrophobic interactions. This could explain why **I** is not seen at Sites 1 and 2. However, at concentrations as high as 100 mM in the crystal, **I** was seen to bind to the active site Zn^{2+} (Site 3 in Figure 7-3) forming a very stable coordination bond (ΔG = -12.4 kcal/mol, as calculated by PDBePISA) displacing 4 water molecules including the $Zn\text{-}OH^-$, indicating inhibition. It must be noted that this inhibition is not indicated by kinetics data (Figure 7-4) due to the pH at which those studies were carried out. At pH 6.7, **I** is mostly protonated and the protonated nitrogen can not bind to Zn^{2+}.

1-methyl imidazole (1MI)

1MI is bound at 7 different sites (average B-factor = 26.0 $Å^2$). Although **1MI** and **I** have similar values of pK_a (pK_a ~ 7.1), presence of a methyl group makes **1MI** more hydrophobic in nature, unlike **I**, and possibly therefore 'captured' at Sites 1 and 2 (Table 7-3). There are various other Sites (inside the protein and out on the surface) where **1MI** molecules are located but it is improbable that they affect the catalysis of H64A CA II. Unlike other imidazoles, **1MI** has very few proton donors at this pH; hence it lacks the ability of forming strong H-bonds with Thr200, which could explain its absence at Site 3.

2-methyl imidazole (2MI)

There are the only two molecules of **2MI** (pK_a = 8.2) observed bound to H64A CA II, both with an average B-factor of 19.2 $Å^2$ and in close proximity with each other interacting with the active site residues Val121, Phe131, Leu198, Thr199 and Pro202. The computed higher ΔG values are most likely because of coordination-bond between

imidazole and Zn^{2+} at Site 3 makes this site the most stable. Occupying Sites 3 and 4, **2MI** buries a total surface area of 190 $Å^2$ (Table 7-4).

4-methyl imidazole (4MI)

With an average B-factor of 20.8 $Å^2$, **4MI** shows perhaps the most complete binding profile among all the imidazoles examined, giving structural insights into how an imidazole ring can enhance or inhibit the activity of H64A CA II. Being the most hydrophobic of all the 4 compounds (log P = 0.3) and the presence of 2 donatable protons and a nitrogen that can accept a proton (pK_a = 7.8), makes **4MI** bind at maximum number of sites. It occupies Sites 1 and 2 which offers an explanation on how **4MI** is able to enhance the activity of H64A CA II, by acting as the external proton donor/acceptor for either or both the in and conformation of His64 (Table 7-5). Another molecule of **4MI**, similar to **I** and **2MI**, is seen directly bound to the active site Zn^{2+}, displacing 4 water molecules including Zn-OH^- (Figure 7-3). The displacement of Zn-OH^- by **4MI** clearly suggests the mechanism of inhibition of CA activity by high concentrations of the compound.

Discussion

From kinetic studies, it is clear at low concentrations imidazole and its derivatives enhance the catalytic activity of H64A CA II while at high concentrations (>100 mM), a few of them (**I** and **4MI**) begin to inhibit the enzyme. The mechanism behind this activity enhancement and inhibition has long been discussed. Site 2 is the only site that has previously been found occupied by **4MI**.[261] However, mutation studies on Trp5 (which was initially thought to stabilize the binding of **4MI** by π-stacking) showed that activity enhancement of H64A CA II by **4MI** occurred regardless of the presence of Trp5. Moreover, since the bound **4MI** corresponded to only one (outward) conformation of

His64 (inward conformation is equally important for proton shuttling to be effective), it was not considered enough of a structural proof to be able to conclude the role of **4MI** in activity enhancement.[260]

Presented here is the first structural evidence which may explain the phenomenon. As the data show, there are not one but many regions where these compounds bind. Most of the sites are predominantly composed of hydrophobic amino acids (Sites 3-4, Sites 7-10 and Sites 12-14); however, a methyl group on imidazole (**1MI**, **2MI**, **4MI**) does not seem to affect hydrophobic interactions enough to cause changes in binding orientations, or affinities as suggested by MD simulations (data not shown). It can be suggested that molecules of **1MI** and **4MI** bound at Sites 1 and 2 mimic the inward and outward conformations of His64 (in wt-CA II) and thus enhance the enzyme's activity by aiding in proton shuttling. Similarly, molecules of **I**, **1MI**, **2MI** and **4MI** bound to the active site Zn^{2+} could well be responsible for inhibition. Inhibition of CA by **4MI** binding close to the active Site metal ion has been reported before Elder et al. using NMR in which the catalytic zinc was replaced by catalytic cobalt.[253] However, Site 3 in this study does not completely overlap with the site found by NMR studies.

These crystal structures show some “common binding sites” where at least two small imidazoles bind. It is these common sites which strongly hint towards the binding not being random. It is interesting to note that two bound molecules of **I** share common binding sites (Sites 6 and 7) with **4MI** even though these sites do not appear to offer strong binding interactions (Table 7-2 and Table 7-5). Similarly, bound on the surface near Ile91 at Site 5, both **1MI** and **4MI**, exhibit a dual conformation. Although this site is

outside on the surface and it is unlikely that it can affect catalytic efficiency of the enzyme, presence of both compounds in almost the same orientation with a dual conformer looks interesting (Table 7-3 and Table 7-5).

Most binding sites (on and around the surface of the protein) could be considered unproductive and inconclusive but the three sites (Sites 1-3) within the active site strongly indicate activity enhancement and inhibition. In contrast, a different perspective could also be drawn. The data show that there are so many binding sites for imidazoles that every one of them makes a small contribution, which is why Duda et al did not observe significant effects on activity enhancement when a single binding site (Site 2 in this study) is destroyed by mutagenesis.[261] These studies offer a different approach to isoform-specific CAI design using binding sites which differ among CA isoforms. The imidazoles which bind at these regions act as fragments that can be chemically linked to each other enhancing the overall binding affinity of the resulting compound as suggested by Shuker et al.[265]

Table 7-1. Crystal Structure Details − Imidazoles.

Compound ID	**I**	**1MI**	**2MI**	**4MI**
PDB ID	4HF3	4HEZ	4HEW	4HEY
Data Collection Statistics*				
Temperature (K)	100	100	100	100
Wavelength (Å)	0.9	0.9	1.54	0.9
Space group	$P2_1$	$P2_1$	$P2_1$	$P2_1$
Unit-cell parameters (Å, °): *a, b, c, β*	42.4, 41.5, 71.9, 104.4	42.3, 41.6, 71.9, 104.5	42.3, 41.2, 71.9, 104.4	42.4, 41.3, 71.9, 104.4
Reflections: Theoretical, Measured	86425, 85561	53643, 52034	26628, 26336	43032, 40407
Resolution (Å)	20.0 – 1.1 (1.2 – 1.1)	20.0 – 1.3 (1.4 – 1.3)	20.0 – 1.7 (1.8 – 1.7)	20.0 – 1.4 (1.5 – 1.4)
[a]R_{sym} (%)	8.6 (46.8)	6.3 (37.9)	6.3 (46.2)	7.5 (39.4)
I/σ(I)	13.9 (2.8)	16.0 (3.3)	22.8 (4.2)	13.7 (3.1)
Completeness (%)	99.0 (97.9)	97.0 (96.2)	98.9 (97.2)	93.9 (95.1)
Redundancy	3.6 (3.5)	3.5 (3.5)	6.6 (6.4)	3.3 (3.2)
Final Model Statistics				
[b]R_{cryst} (%)	15.8	15.1	16.5	15.2
[c]R_{free} (%)	17.2	17.0	20.5	18.5
Residue numbers	4 – 261	4 – 261	4 – 261	4 – 261
[d]No. of atoms: *Protein, ligand*[e]*, water*	2385, 45(9), 307	2317, 48(7), 264	2311, 12(2), 146	2323, 54(8), 218
R.M.S.D.: *Bond lengths* (Å), *angles* (°)	0.010, 1.40	0.010, 1.42	0.010, 1.54	0.010, 1.45
Ramachandran statistics (%): *favored, allowed, outliers*	88.4, 11.6, 0.0	87.0, 13.0, 0.0	87.5, 12.5, 0.0	90.3, 9.8, 0.0
Average B-factors (Å^2): *Main chain, side chain, ligand, water*	9.1, 11.7, 24.5, 21.9	12.1, 15.1, 26.0, 24.9	17.1, 20.0, 19.2, 26.2	9.4, 12.0, 20.8, 21.9

*Values in parenthesis represent highest resolution bin. [a]$R_{sym} = \Sigma (|I - \langle I \rangle|) / \Sigma \langle I \rangle$. [b]$R_{cryst} = (\Sigma |Fo| - |Fc| / \Sigma |F_{obs}|) \times 100$. [c]$R_{free}$ is calculated in same manner as R_{cryst}, except that it uses 5% of the reflection data omitted from refinement. [d]Includes alternate conformations. [e]Value in parenthesis represent number of ligands bound in the structure.

Table 7-2. Characterization of binding sites, buried surface area (BSA), hydrogen bonds, and gain in solvation energy (ΔG) for imidazole (**I**).

Binding Sites	Chain ID, B-factor ($Å^2$), Occupancy	BSA ($Å^2$)	H-bonds, ΔG (kcal/mol)
Inside the structure			
Site 3 *(directly to the Zn^{2+})*	C, 12.4, 0.96	160	0, -12.4
Site 6 *(Y7, G12, P13, D243, W245, P247)*	F, 24.6, 0.92	150	2, -0.4
On the surface			
Site 7 *(T55, L57, N71)*	G, 26.3, 0.98	80	0, -0.6
Site 9 *(N130, F131, G132)*	N, 27.5, 0.87	85	1, -0.6
Site 10 *(N180, R182, G183)*	H, 23.2, 0.98	70	0, -0.5
Site 11 *(T37, K39, Q255, I256)*	M, 24.1, 0.87	130	1, 0.0
Site 12 *(F131, V135,L198, P202)*	I, 27.4, 1.00	105	0, -1.1
Site 13 *(L60, N61, N62, G171)*	K, 31.0, 0.60	110	2, -0.3
Site 16 (V49, R182, L185)	E, 24.0, 0.93	80	1, -0.1

Table 7-3. Characterization of binding sites, buried surface area (BSA), hydrogen bonds, and gain in solvation energy (ΔG) for 1-methyl imidazole (**1MI**).

Binding Sites	Chain ID, B-factor ($Å^2$), Occupancy	BSA ($Å^2$)	H-bonds, ΔG (kcal/mol)
Inside the structure			
Site 1 *(H64 "in" conformation)*	F, 26.6, 0.92	125	0, -0.1
Site 2 *(H64 "out" conformation)*	C, 26.7, 1.00	170	0, -0.5
Site 4 *(G92,H94, V121,F131, L198, T199, T200, P201, P202)*	E, 12.2, 0.81	200	1, -0.7
Site 5 *(Q69, F70, D72, I91)*	G, 25.4, dual conformation	110	0, -0.4
On the surface			
Site 9 *(I91, D130, F131, G132)*	J, 31.9, 0.88	105	0, -0.8
Site 14 *(Y51, D52, A54, N178, F179, D180, P181, R182)*	H, 27.8, 0.92	150	0, 0.1
Site 15 *(K112)*	L, 32.0, 0.94	85	0, -0.4

Table 7-4. Characterization of binding sites, buried surface area (BSA), hydrogen bonds, and gain in solvation energy (ΔG) for 2-methyl imidazole (**2MI**).

Binding Sites	Chain ID, B-factor ($Å^2$), Occupancy	BSA ($Å^2$)	H-bonds, ΔG (kcal/mol)
Inside the structure			
Site 3 *(directly bound to Zn^{2+})*	B, 16.3, 1.00	25	4, -14.9
Site 4 *(G92,H94, V121,F131, L198, T199, T200, P201, P202)*	C, 22.1, 1.00	165	1, -0.5

Table 7-5. Characterization of binding sites, buried surface area (BSA), hydrogen bonds, and gain in solvation energy (ΔG) for 4-methyl imidazole (**4MI**).

Binding Sites	Chain ID, B-factor ($Å^2$), Occupancy	BSA ($Å^2$)	H-bonds, ΔG (kcal/mol)
Inside the structure			
Site 1 *(H64 "in" conformation)*	F, 20.6, 0.87	135	0, -0.1
Site 2 *(H64 "out" conformation)*	H, 18.1, 0.95	170	1, 0.2
Site 3 *(directly bound to Zn^{2+})*	E, 9.7, 0.95	150	3, -13.5
Site 4 *(G92,H94, V121,F131, L198, T199, T200, P201, P202)*	G, 29.0, 0.93	150	1, -0.6
Site 5 *(Q69, F70, D72, I91)*	P, 22.9, dual conformation	70	0,-0.2
Site 6 *(Y7, G12, P13, D243, W245, P247)*	C, 24.8, 0.87	165	1, -0.4
On the surface			
Site 7 *(T55, L57, N71)*	K, 25.9, 0.91	90	0, -0.6
Site 8 *(P195, T208)*	J, 11.3, 0.75	140	1, -0.5

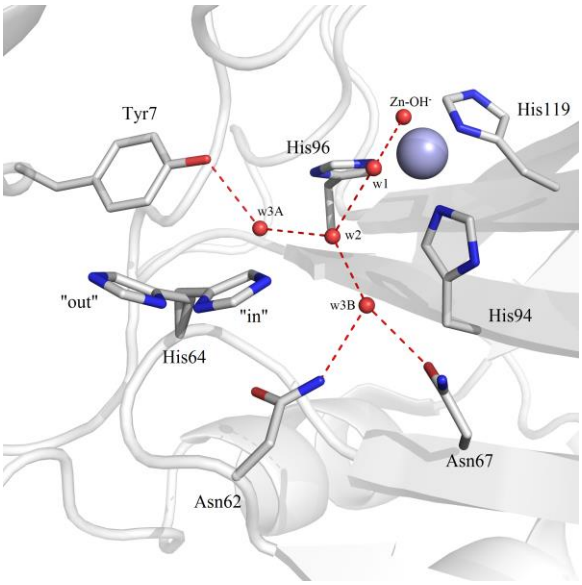

Figure 7-1. Active site of CA II at pH 8.0 (PDB ID: 3KS3)[29] showing the relevant residues and water network required for proton transport.

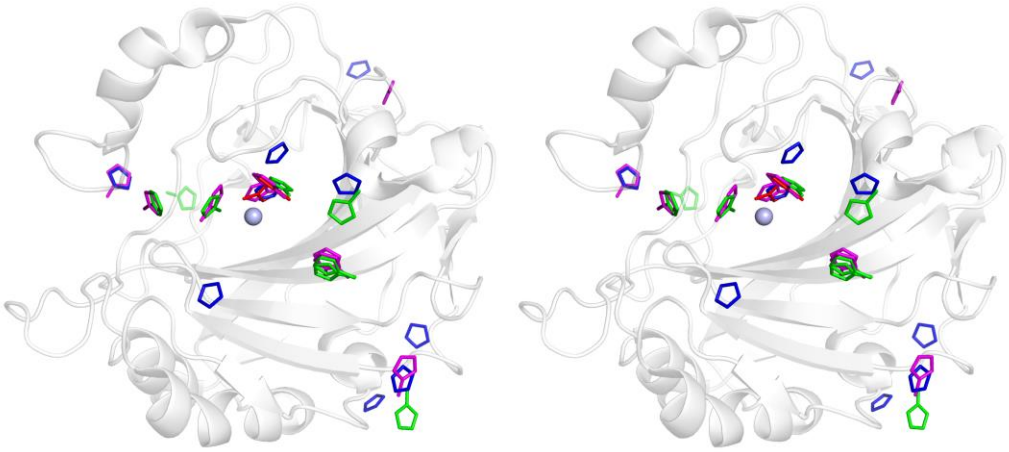

Figure 7-2. Stereo overview of the 15 identified binding sites, **I** (red sticks), **1MI** (green sticks), **2MI** (red sticks), and **4MI** (magenta sticks), in and around H64A CA II. The numbers represent site identification (as given in Tables 2-5).

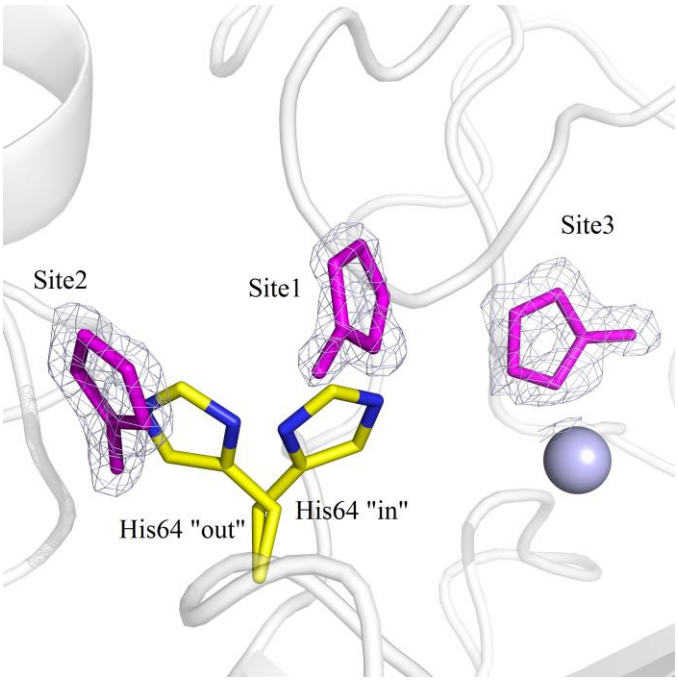

Figure 7-3. Binding sites (Sites 1-3) of **4MI** within and near the active site of H64A CA II. 2FoFc electron density maps are contoured at 1.2 σ. His64 from wt-CA II (PDB ID: 3KS3)[29] is shown as yellow sticks for representation of "in" and "out" conformations.

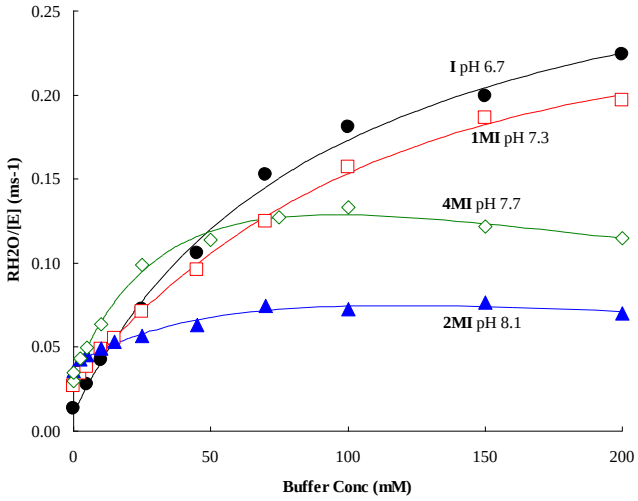

Figure 7-4. Kinetics measurement of H64A CA II in presence of **I** (black) at pH 6.7, **1MI** (red) at pH 7.3, **2MI** (blue) at pH 8.1, and **4MI** (green) at pH 7.7.

CHAPTER 8
FUTURE − FRAGMENT ADDITION TO THE TAIL[266]

Introduction

X-ray Crystallography and Cryoprotectants

Over the last ~20 years, there has been a steady shift from cool/room (277 – 298 K) to cryo (100 K) temperature data collection methods for X-ray protein crystallography to minimize the detrimental effects of radiation damage.[267] The exact nature of the damage is still uncertain, but it is speculated that X-ray radiation produces free radicals, which induces chemical changes on the surface of a protein.[268] This disordering can lead to in the loss of diffraction spots and parts of native structure, which can result in possible erroneous conclusions about the biological mechanism and function.[269] Strategies to control radiation damage are limited, but the use of cryo-protectants and free radical scavengers has been implicated in slowing down the damage.[270] The addition of a cryo-protectant is required prior to flash cooling the crystal in a nitrogen/helium cooled gas stream to minimize the formation of ice while vitrifying the crystal[271], which prevents disruption in the order of the crystal lattice.[272] The cryo-protectant is administrated prior to flash cooling via a co-crystallization or pre-treatment soak of the crystal in a solution consisting of the crystallization reservoir solution and a cryo-protectant, with 20-25% (v/v) glycerol (**GOL**) being the most popular used cryo-protectant. However, some salts and low molecular weight sugars may also be used to fulfill this purpose.

Adapted from: Aggarwal, M.; Boone, C. D.; Kondeti, B.; Tu, C.; Silverman, D. N.; McKenna, R. Effects of cryoprotectants on the structure and thermostability of the human carbonic anhydrase II-acetazolamide complex. *Acta Crystallogr. D Biol. Crystallogr.* 2013, *69*, 860–865.

Another class of cryoprotectants used in flash cooling are oils with low scattering and low optical distortion, including Paratone N, paraffin, and high-density mineral oils.[273] Nevertheless, there use is limited and remains overshadowed by **GOL**. The choice of which cryo-protectant to use is important because it may have deleterious effects on the crystal mosaicity, which may make data reduction and processing more difficult or affect the active site or a loop conformation of the protein, further causing possible misinterpretation of the structure.

Carbonic Anhydrase II and Acetazolamide

Carbonic anhydrase II (CA II) has long been a drug target for the treatment of various diseases such as glaucoma, epilepsy, and altitude sickness.[6,97,274,275] Acetazolamide (**AZM**) is a classical inhibitor of CA II and has been clinically used in the treatment of glaucoma for decades.[96,97,276] It binds and inhibits CA II via the sulfonamide group that directly interacts with the active site zinc, displacing the water that is necessary for catalysis. In addition, a further five water molecules (including the proton transfer water, w1) are displaced, as the **AZM** extends out of the active site and makes hydrophobic and polar interactions with the surrounding amino acid residues of the enzyme (Figure 8-1A and Figure 8-1B).[29,182,187]

Unintentional Binding of Cryoprotectant

Many of the CA II inhibitor complexes including CA II - **AZM** also show an ordered **GOL** bound in the active site, a consequence of using **GOL** as the cryo-protectant during X-ray diffraction data collection. This phenomenon has been observed in more than 40 crystal structures deposited in the PDB. A previously reported high resolution (1.1 Å) CA II - **AZM** crystal complex, showed clearly the **GOL** bound adjacent to the **AZM** ring, displacing a further three water molecules (including the waters, w2

and w3B) compared to the uncomplexed CA II structure, with the **GOL** making seven hydrogen bonds (defined as proton donor/acceptor distance between 2.4 – 3.4 Å) with Asn62, Asn67, Gln92 in the active site and the three remaining water molecules (Figure 7-1C, compared to Figure 7-1A and Figure 7-1B). As mentioned, a **GOL** molecule has been observed in this location in the active site, in several other high-resolution CA II inhibitor complexes[3,153,219]. Hence, this relatively common observation has raised the question whether the **GOL** aids or hinders the inhibitor binding, and/or affects the location and interactions that these inhibitors make in the active site of CA II, thereby affecting the interpretation and subsequence drug design (Figure 7-1).

To address this issue, the catalytic activity, melting temperature (T_m), and inhibition constant (K_I) of **AZM** for CA II were measured: (1) in the presence of **GOL**, (2) in the presence sucrose, and (3) in buffer as control. In addition, crystal structures of CA II - **AZM** complex were determined at (1) room (298 K) and (2) cryo (100 K) temperature using sucrose as a cryo-protectant and compared with previously reported high resolution cryo structures of **AZM** complexed[187] and uncomplexed CA II in the presence of **GOL**.[29] The results suggest **GOL** does not affect either CA II thermostability or the inhibitor binding. However, **GOL** does affect CA II kinetics, presumably as it displaces the solvent in the active site.

Results

Crystal Structure Details

The diffraction data from crystals of CA II in complex with **AZM** obtained at 298 K (RT) and 100 K (using sucrose as cryo-protectant) were solved and refined to a resolution of 1.7 Å and 1.5 Å, respectively (Figure 8-2A and Figure 8-2B). Although the data could have been collected to higher resolution, the in-house system only permitted

a maximal collection resolution of 1.5 Å. In addition, the analysis of R_{sym} for each image indicates no radiation damage to the crystals during RT or cryo-sucrose data collection. Although the cryo-sucrose structure (PDB ID: 3V2M)[266] has a low R_{sym} (19.8%) in the highest resolution bin, the R_{cryst} (41.5%) and R_{free} (45.3%) for that bin are quite high. This is probably due to the presence of some diffused unassigned density (most likely sucrose), causing an under-refinement of the structure. Upon reduction of the data to a resolution of 1.7 Å, the highest resolution bin values of R_{cryst} and R_{free} comply with its R_{sym}.

As reported previously[182,187], the **AZM** was observed to bind in the active site of CA II with its sulfonamide nitrogen directly interacting with the zinc; the pentameric ring is stabilized by hydrophobic interactions with Val121 and Leu198, and polar interactions with Thr199 and Thr200; the molecule also makes hydrogen bonds with two water molecules and the side chain of Gln92 (Figure 8-2). The RT and sucrose structures were superposed with a high resolution structure (PDB ID: 3HS4)[187] of the same complex where **GOL** was used as the cryo-protectant (main chain r.m.s.d. = 0.2 Å). Although there were no significant structural differences between them, there was a small reduction in the unit cell parameters (Δa = 0.6 Å, Δb = 0.4 Å, Δc = 0.8 Å) in the cryo- as compared to RT structure (Table 8-1). This phenomenon of shortening of unit cell edges, as explained by Fraser *et al.*, has been partially attributed to expulsion of water molecules from inside the unit cells because of the addition of cryo-protectants[277]. In addition, a shift (1.2 Å) in the $-CH_3$ group at the tail of **AZM** was seen in the RT structure as compared to the cryo structures (Figure 8-2D), but it does not seem to affect hydrogen bonding pattern or hydrophobic interactions. It is interesting that this

bound **GOL** is absent when CA II crystals are frozen using **GOL**, without the addition of an inhibitor (Figure 8-1A).[29] It can thus be concluded that the binding of **GOL** is stabilized upon binding of a CA inhibitor (CAI) such as **AZM**.

Differential Scanning Calorimetry (DSC)

The thermal stability of CA II and the CA II - **AZM** complex in the presence and absence of cryo-protectants were measured using DSC. A single major unfolding transition (T_m) was observed in the thermograms (Table 8-3). The CA II - **AZM** complex (with no cryo-protectant) had a T_m = 65.3 ºC, which is a ~7 ºC increase in stability compared to uncomplexed CA II (T_m = 58.3 ºC).[71] This can be attributed to the increased enthalpic contributions resulting from the binding energy of **AZM** in the active site of CA II. Addition of **GOL** or sucrose did not have any significant effect on the melting temperature of the CA II - **AZM** complex (ΔT_m = -1.4 and 2.0 ºC, respectively).

Enzyme Kinetics Measurements

^{18}O exchange was used to measure the K_Is of **AZM** for CA II inhibition in the presence of buffer, 20% (v/v) **GOL** and 20% (w/v) sucrose. As shown in Table 8-4, there was a significant 30% reduction in the presence of **GOL**, and a moderate 15% reduction in the presence of sucrose, in enzyme activity. These solution kinetic data suggest there is a weak inhibition effect on the enzyme activity with high concentrations of **GOL** and this could be attributed to displacement of waters w2 and w3B that have previously been shown to be important for the proton transfer during CA catalysis explained in context of Figure 8-1.[254] However, the presence of **GOL** or sucrose did not affect inhibition of CA II by **AZM** (which has a nanomolar affinity for the enzyme).

Discussion

This opportunistic **GOL** binding site provides a possible "fragment" for structure-aided drug design. This opportunistic **GOL** binding site in CA II (lined by Asn62, Asn67 and Gln92) differs by at least one amino acid residue among the other catalytic CAs (Table 8-2). Similarly, in a parallel study (unpublshed) that is currently being carried out, a molecule of sucrose (**SUC**), which presumably came from the cryoprotectant, was seen bound at the opening of the active site of CA IX mimic (CA II with 7 mutations in the active site that makes it mimic the active site of CA IX). On the other hand, presence of **SUC** in a CA II structure has never been seen. Thus, these binding sites hold potential in designing isoform specific CAIs. It is proposed that **GOL** and **SUC** could be chemically incorporated into an inhibitor to impart additional specific hydrogen bonding interactions with the hydrophilic side of the active site (Figure 8-2C) and this approach can be addressed as a combined approach of what was discussed in chapters 6 and 7. As the incorporation of a **GOL**-like substituent onto the ‘tail’ region of **AZM** would presumably be involved in the same hydrogen bond donor/acceptor interactions for **GOL** as those observed in this crystallographic study. As these **GOL**-binding residues vary among the human CA isoforms, this **GOL** binding site could well be considered as a potential therapeutic CA pharmacophore that may impart isoform-specific inhibition.

However, for a CAI that has a tail that binds in the **GOL** binding pocket, the **GOL** in the cryo-protectant could compete for this site. This suggests that a cryo-protectant should be chosen wisely when studying CA-ligand interactions using X-ray crystallography and this phenomenon may be of a general concern to other proteins with hydrophilic active site pockets. Hence, this study also reports a "cautionary tale" when selecting a suitable cryo-protectant for enzyme/ligand crystallography.

Interactions of the cryo-protectant with the protein could have unforeseen effects on ligand binding, ranging from a commensalistic relationship as observed between **GOL** and **AZM** in CA II to a direct competitive inhibition with the ligand as proposed with the aforementioned drug. One is therefore forewarned in the careful consideration of an otherwise prosaic cryo-protectant.

Table 8-1. Crystal Structure Details − CA II-**AZM**

Cryoprotectant	None	Sucrose
PDB ID	3V2J	3V2M
Data-collection statistics		
Temperature (K)	298	100
Wavelength (Å)	1.5418	1.5418
Space group	$P2_1$	$P2_1$
Unit-cell parameters (Å, °): *a, b, c, β*	42.8, 41.7, 72.9, 104.5	42.2, 41.3, 72.1, 104.2
Total theoretical reflections	27697	41243
Unique measured reflections	26188	40468
Resolution (Å)	19.0-1.7 (1.76-1.69)*	19.9-1.5 (1.50-1.47)
[a]R_{sym} (%)	8.9 (43.2)	4.5 (19.8)#
I/σ(I)	12.0 (3.5)	23.4 (6.5)
Completeness (%)	94.6 (91.1)	98.1 (96.2)
Redundancy	4.4 (4.4)	3.9 (3.7)
Final Model Statistics		
[b]R_{cryst} (%)	12.9 (19.0)	16.3 (41.5)#
[c]R_{free} (%)	15.6 (21.5)	18.7 (45.3)#
Residue numbers	4 – 261	4 – 261
[d]No. of atoms: *Protein, inhibitor, water*	2325, 13, 148	2261, 13, 242
R.M.S.D.: *Bond lengths* (Å), *bond angles* (°)	0.01, 1.27	0.01, 1.34
Ramachandran statistics (%): *Most favored, allowed, outliers*	89.4, 10.6, 0.0	89.4, 10.6, 0.0
Average B-factors (Å^2): *Main chain, side chain, inhibitor, solvent*	16.4, 24.0, 15.6, 32.4	13.3, 17.5, 22.3, 25.4

[a]$R_{sym} = \Sigma |I - \langle I \rangle| / \Sigma \langle I \rangle$. [b]$R_{cryst} = (\Sigma ||Fo| - |Fc|| / \Sigma |F_{obs}|) \times 100$. [c]$R_{free}$ is calculated in same manner as R_{cryst}, except that it uses 5% of the reflection data omitted from refinement. [d]Includes alternate conformations. *Values in parenthesis represent highest resolution bin. #Although the cryo-sucrose structure has a low R_{sym} in the highest resolution bin, the R_{cryst} and R_{free} for that bin are high. This is probably due to the presence of some diffused unassigned density (most likely sucrose), causing an under-refinement of the structure.

Table 8-2. Conservation of CA II active site amino acids.

CA Isoform	Position #		
	62	67	92
I	Val	His	Gln
II	Asn	Asn	Gln
III	Asn	Arg	Gln
IV	Asn	Glu	Gln
V (murine)	Thr	Gln	Gln
VI	Asn	Gln	Gln
VII	Asn	Gln	Gln
IX	Asn	Gln	Gln
XII	Asn	Lys	Gln
XIII	Ser	Asn	Gln
XIV	Asn	Gln	Gln

Table 8-3. The major unfolding transition (T_m in °C) of CA II in complex with **AZM**. DSC experiments were carried out in triplicates.

Sample	T_m (°C)
20 μM CA II	58.3 ± 0.1
20 μM CA II + 20% (v/v) **GOL**	59.1 ± 0.1
20 μM CA II + 20% (w/v) sucrose	60.4 ± 0.1
20 μM CA II + **AZM** (40 μM)	65.3 ± 0.1
20 μM CA II + 20% (v/v) **GOL** + **AZM** (40 μM)	63.9 ± 0.7
20 μM CA II + 20% (w/v) sucrose + **AZM** (40 μM)	67.3 ± 0.2

Table 8-4. Inhibition constants (K_Is) of **AZM** for CA II calculated at 10°C, in triplicates.

Buffer	Initial Enzyme Activity (%)	K_I (nM)
50 mM Tris-Cl	100 ± 11	0.48 ± 0.08
50 mM Tris-Cl + 20% (w/v) sucrose	85 ± 8	0.43 ± 0.05
50 mM Tris-Cl + 20% (v/v) **GOL**	69 ± 7	0.56 ± 0.07

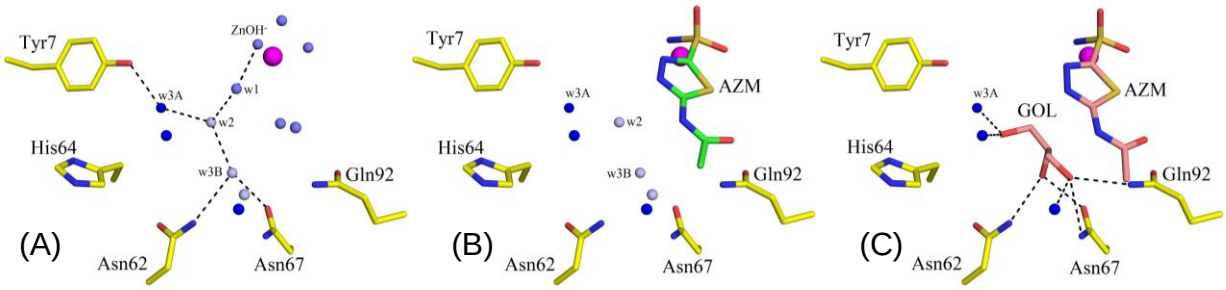

Figure 8-1. Active site of (A) CA II showing ordered waters involved in proton transfer (PDB ID: 3KS3)[29], (B) CA II in complex with **AZM** (PDB ID: 3V2J, this study), and (C) CA II in complex with **AZM** and **GOL** (PDB ID: 3HS4).[187] Waters are colored in gradients of blue: dark (not displaced) - light (**AZM** displaced) - lighter (**GOL** displaced).[266]

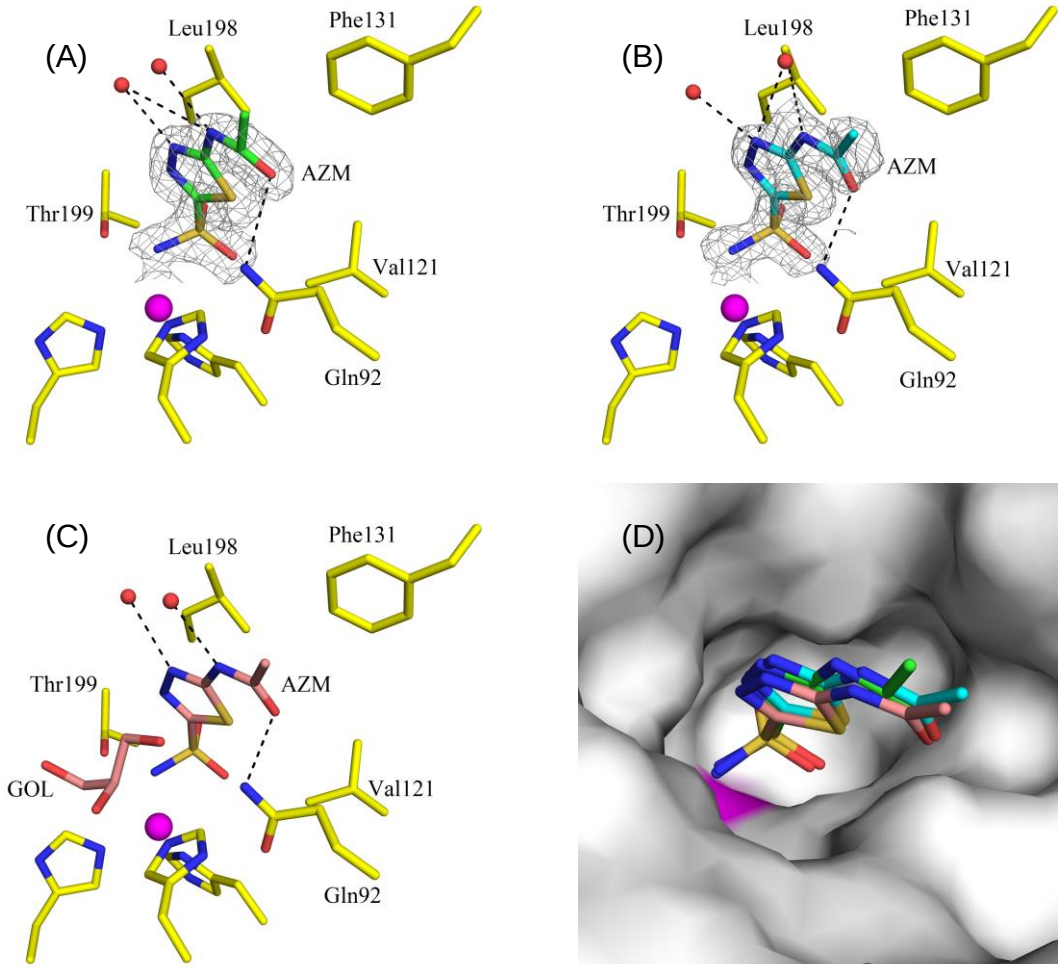

Figure 8-2. Active site of CA II in complex with **AZM** at (A) RT (298 K); (B) cryo (100 K) with sucrose, (C) cryo (100 K) with **GOL** (PDB ID: 3HS4)[187]. (D) Surface representation of the three structures superposed. The |2Fo-Fc| electron density is contoured at 1.0 σ.

LIST OF REFERENCES

(1) Aggarwal, M.; Boone, C. D.; Kondeti, B.; McKenna, R. Structural annotation of human carbonic anhydrases. *J Enzyme Inhib Med Chem* **2013**, *28*, 267–277.

(2) Messerchmidt, A.; Bode, W.; Cygler, M. *Handbook of Metalloproteins*. John Wiley and Sons Ltd., **2004**.

(3) Domsic, J. F.; Avvaru, B. S.; Kim, C. U.; Gruner, S. M.; Agbandje-McKenna, M.; Silverman, D. N.; McKenna, R. Entrapment of Carbon Dioxide in the Active Site of Carbonic Anhydrase II. *J. Biol. Chem.* **2008**, *283*, 30766–30771.

(4) Supuran, C. T. Carbonic anhydrases--an overview. *Curr. Pharm. Des.* **2008**, *14*, 603–614.

(5) Scozzafava, A.; Mastrolorenzo, A.; Supuran, C. T. Carbonic anhydrase inhibitors and activators and their use in therapy. *Expert Opinion on Therapeutic Patents* **2006**, *16*, 1627–1664.

(6) Supuran, C. T.; Scozzafava, A.; Conway, J. *Carbonic anhydrase: its inhibitors and activators*; CRC Press, **2004**.

(7) Pastorekova, S.; Parkkila, S.; Pastorek, J.; Supuran, C. T. Carbonic anhydrases: current state of the art, therapeutic applications and future prospects. *J Enzyme Inhib Med Chem* **2004**, *19*, 199–229.

(8) Chegwidden, W. R.; Carter, N. D. *The carbonic anhydrases: new horizons*; Birkhäuser, **2000**.

(9) Krishnamurthy, V. M.; Kaufman, G. K.; Urbach, A. R.; Gitlin, I.; Gudiksen, K. L.; Weibel, D. B.; Whitesides, G. M. Carbonic anhydrase as a model for biophysical and physical-organic studies of proteins and protein-ligand binding. *Chem. Rev.* **2008**, *108*, 946–1051.

(10) Supuran, C. T.; Scozzafava, A.; Casini, A. Carbonic anhydrase inhibitors. *Med Res Rev* **2003**, *23*, 146–189.

(11) Nishimori, I.; Minakuchi, T.; Onishi, S.; Vullo, D.; Cecchi, A.; Scozzafava, A.; Supuran, C. T. Carbonic anhydrase inhibitors: cloning, characterization, and inhibition studies of the cytosolic isozyme III with sulfonamides. *Bioorg. Med. Chem.* **2007**, *15*, 7229–7236.

(12) Vullo, D.; Franchi, M.; Gallori, E.; Antel, J.; Scozzafava, A.; Supuran, C. T. Carbonic anhydrase inhibitors. Inhibition of mitochondrial isozyme V with aromatic and heterocyclic sulfonamides. *J. Med. Chem.* **2004**, *47*, 1272–1279.

(13) Nishimori, I.; Vullo, D.; Innocenti, A.; Scozzafava, A.; Mastrolorenzo, A.; Supuran, C. T. Carbonic anhydrase inhibitors. The mitochondrial isozyme VB as a new target for sulfonamide and sulfamate inhibitors. *J. Med. Chem.* **2005**, *48*, 7860–7866.

(14) Nishimori, I.; Minakuchi, T.; Onishi, S.; Vullo, D.; Scozzafava, A.; Supuran, C. T. Carbonic anhydrase inhibitors. DNA cloning, characterization, and inhibition studies of the human secretory isoform VI, a new target for sulfonamide and sulfamate inhibitors. *J. Med. Chem.* **2007**, *50*, 381–388.

(15) Vullo, D.; Voipio, J.; Innocenti, A.; Rivera, C.; Ranki, H.; Scozzafava, A.; Kaila, K.; Supuran, C. T. Carbonic anhydrase inhibitors. Inhibition of the human cytosolic isozyme VII with aromatic and heterocyclic sulfonamides. *Bioorg. Med. Chem. Lett.* **2005**, *15*, 971–976.

(16) Vullo, D.; Franchi, M.; Gallori, E.; Pastorek, J.; Scozzafava, A.; Pastorekova, S.; Supuran, C. T. Carbonic anhydrase inhibitors: inhibition of the tumor-associated isozyme IX with aromatic and heterocyclic sulfonamides. *Bioorg. Med. Chem. Lett.* **2003**, *13*, 1005–1009.

(17) Vullo, D.; Innocenti, A.; Nishimori, I.; Pastorek, J.; Scozzafava, A.; Pastoreková, S.; Supuran, C. T. Carbonic anhydrase inhibitors. Inhibition of the transmembrane isozyme XII with sulfonamides-a new target for the design of antitumor and antiglaucoma drugs? *Bioorg. Med. Chem. Lett.* **2005**, *15*, 963–969.

(18) Nishimori, I.; Vullo, D.; Innocenti, A.; Scozzafava, A.; Mastrolorenzo, A.; Supuran, C. T. Carbonic anhydrase inhibitors: inhibition of the transmembrane isozyme XIV with sulfonamides. *Bioorg. Med. Chem. Lett.* **2005**, *15*, 3828–3833.

(19) Lehtonen, J.; Shen, B.; Vihinen, M.; Casini, A.; Scozzafava, A.; Supuran, C. T.; Parkkila, A.-K.; Saarnio, J.; Kivelä, A. J.; Waheed, A.; Sly, W. S.; Parkkila, S. Characterization of CA XIII, a novel member of the carbonic anhydrase isozyme family. *J. Biol. Chem.* **2004**, *279*, 2719–2727.

(20) Supuran, C. T.; Ilies, M. A.; Scozzafava, A. Carbonic anhydrase inhibitors — Part 29 1: Interaction of isozymes I, II and IV with benzolamide-like derivatives. *European Journal of Medicinal Chemistry* **1998**, *33*, 739–751.

(21) Supuran, C. T.; Scozzafava, A.; Ilies, M. A.; Briganti, F. Carbonic anhydrase inhibitors: synthesis of sulfonamides incorporating 2,4,6-trisubstituted-pyridinium-ethylcarboxamido moieties possessing membrane-impermeability and in vivo selectivity for the membrane-bound (CA IV) versus the cytosolic (CA I and CA II) isozymes. *J. Enzym. Inhib.* **2000**, *15*, 381–401.

(22) Scozzafava, A.; Briganti, F.; Ilies, M. A.; Supuran, C. T. Carbonic anhydrase inhibitors: synthesis of membrane-impermeant low molecular weight sulfonamides possessing in vivo selectivity for the membrane-bound versus cytosolic isozymes. *J. Med. Chem.* **2000**, *43*, 292–300.

(23) Winum, J.-Y.; Temperini, C.; El Cheikh, K.; Innocenti, A.; Vullo, D.; Ciattini, S.; Montero, J.-L.; Scozzafava, A.; Supuran, C. T. Carbonic anhydrase inhibitors: clash with Ala65 as a means for designing inhibitors with low affinity for the ubiquitous isozyme II, exemplified by the crystal structure of the topiramate sulfamide analogue. *J. Med. Chem.* **2006**, *49*, 7024–7031.

(24) Saczewski, F.; Sławiński, J.; Kornicka, A.; Brzozowski, Z.; Pomarnacka, E.; Innocenti, A.; Scozzafava, A.; Supuran, C. T. Carbonic anhydrase inhibitors. Inhibition of the cytosolic human isozymes I and II, and the transmembrane, tumor-associated isozymes IX and XII with substituted aromatic sulfonamides activatable in hypoxic tumors. *Bioorg. Med. Chem. Lett.* **2006**, *16*, 4846–4851.

(25) De Simone, G.; Vitale, R. M.; Di Fiore, A.; Pedone, C.; Scozzafava, A.; Montero, J.-L.; Winum, J.-Y.; Supuran, C. T. Carbonic anhydrase inhibitors: Hypoxia-activatable sulfonamides incorporating disulfide bonds that target the tumor-associated isoform IX. *J. Med. Chem.* **2006**, *49*, 5544–5551.

(26) Köhler, K.; Hillebrecht, A.; Schulze Wischeler, J.; Innocenti, A.; Heine, A.; Supuran, C. T.; Klebe, G. Saccharin inhibits carbonic anhydrases: possible explanation for its unpleasant metallic aftertaste. *Angew. Chem. Int. Ed. Engl.* **2007**, *46*, 7697–7699.

(27) Liang, J. Y.; Lipscomb, W. N. Binding of substrate CO2 to the active site of human carbonic anhydrase II: a molecular dynamics study. *Proc. Natl. Acad. Sci. U.S.A.* **1990**, *87*, 3675–3679.

(28) Lindskog, S. Structure and mechanism of carbonic anhydrase. *Pharmacol. Ther.* **1997**, *74*, 1–20.

(29) Avvaru, B. S.; Kim, C. U.; Sippel, K. H.; Gruner, S. M.; Agbandje-McKenna, M.; Silverman, D. N.; McKenna, R. A short, strong hydrogen bond in the active site of human carbonic anhydrase II. *Biochemistry* **2010**, *49*, 249–251.

(30) Maupin, C. M.; Castillo, N.; Taraphder, S.; Tu, C.; McKenna, R.; Silverman, D. N.; Voth, G. A. Chemical rescue of enzymes: proton transfer in mutants of human carbonic anhydrase II. *J. Am. Chem. Soc.* **2011**, *133*, 6223–6234.

(31) Shimahara, H.; Yoshida, T.; Shibata, Y.; Shimizu, M.; Kyogoku, Y.; Sakiyama, F.; Nakazawa, T.; Tate, S.; Ohki, S.; Kato, T.; Moriyama, H.; Kishida, K.; Tano, Y.; Ohkubo, T.; Kobayashi, Y. Tautomerism of histidine 64 associated with proton transfer in catalysis of carbonic anhydrase. *J. Biol. Chem.* **2007**, *282*, 9646–9656.

(32) Fisher, Z.; Hernandez Prada, J. A.; Tu, C.; Duda, D.; Yoshioka, C.; An, H.; Govindasamy, L.; Silverman, D. N.; McKenna, R. Structural and Kinetic Characterization of Active-Site Histidine as a Proton Shuttle in Catalysis by Human Carbonic Anhydrase II†,‡. *Biochemistry* **2005**, *44*, 1097–1105.

(33) Elder, I.; Fisher, Z.; Laipis, P. J.; Tu, C.; McKenna, R.; Silverman, D. N. Structural and kinetic analysis of proton shuttle residues in the active site of human carbonic anhydrase III. *Proteins* **2007**, *68*, 337–343.

(34) Duda, D. M.; Tu, C.; Fisher, S. Z.; An, H.; Yoshioka, C.; Govindasamy, L.; Laipis, P. J.; Agbandje-McKenna, M.; Silverman, D. N.; McKenna, R. Human carbonic anhydrase III: structural and kinetic study of catalysis and proton transfer. *Biochemistry* **2005**, *44*, 10046–10053.

(35) Boriack-Sjodin, P. A.; Heck, R. W.; Laipis, P. J.; Silverman, D. N.; Christianson, D. W. Structure determination of murine mitochondrial carbonic anhydrase V at 2.45-A resolution: implications for catalytic proton transfer and inhibitor design. *Proc. Natl. Acad. Sci. U.S.A.* **1995**, *92*, 10949–10953.

(36) Stridh, M. H.; Alt, M. D.; Wittmann, S.; Heidtmann, H.; Aggarwal, M.; Riederer, B.; Seidler, U.; Wennemuth, G.; McKenna, R.; Deitmer, J. W.; Becker, H. M. Lactate flux in astrocytes is enhanced by a non-catalytic action of carbonic anhydrase II. *J. Physiol. (Lond.)* **2012**, *590*, 2333–2351.

(37) Mitterberger, M. C.; Kim, G.; Rostek, U.; Levine, R. L.; Zwerschke, W. Carbonic anhydrase III regulates peroxisome proliferator-activated receptor-γ2. *Exp. Cell Res.* **2012**, *318*, 877–886.

(38) Imtaiyaz Hassan, M.; Shajee, B.; Waheed, A.; Ahmad, F.; Sly, W. S. Structure, function and applications of carbonic anhydrase isozymes. *Bioorganic & Medicinal Chemistry* **2012**.

(39) Pilka, E. S.; Kochan, G.; Oppermann, U.; Yue, W. W. Crystal structure of the secretory isozyme of mammalian carbonic anhydrases CA VI: implications for biological assembly and inhibitor development. *Biochem. Biophys. Res. Commun.* **2012**, *419*, 485–489.

(40) Di Fiore, A.; Monti, S. M.; Hilvo, M.; Parkkila, S.; Romano, V.; Scaloni, A.; Pedone, C.; Scozzafava, A.; Supuran, C. T.; De Simone, G. Crystal structure of human carbonic anhydrase XIII and its complex with the inhibitor acetazolamide. *Proteins* **2009**, *74*, 164–175.

(41) Cianchi, F.; Vinci, M. C.; Supuran, C. T.; Peruzzi, B.; De Giuli, P.; Fasolis, G.; Perigli, G.; Pastorekova, S.; Papucci, L.; Pini, A.; Masini, E.; Puccetti, L. Selective inhibition of carbonic anhydrase IX decreases cell proliferation and induces ceramide-mediated apoptosis in human cancer cells. *J. Pharmacol. Exp. Ther.* **2010**, *334*, 710–719.

(42) Nagelhus, E. A.; Mathiisen, T. M.; Bateman, A. C.; Haug, F.-M.; Ottersen, O. P.; Grubb, J. H.; Waheed, A.; Sly, W. S. Carbonic anhydrase XIV is enriched in specific membrane domains of retinal pigment epithelium, Muller cells, and astrocytes. *Proc. Natl. Acad. Sci. U.S.A.* **2005**, *102*, 8030–8035.

(43) Bergenhem, N. C.; Hallberg, M.; Wisén, S. Molecular characterization of the human carbonic anhydrase-related protein (HCA-RP VIII). *Biochim. Biophys. Acta* **1998**, *1384*, 294–298.

(44) Tashian, R. E.; Hewett-Emmett, D.; Carter, N.; Bergenhem, N. C. Carbonic anhydrase (CA)-related proteins (CA-RPs), and transmembrane proteins with CA or CA-RP domains. *EXS* **2000**, 105–120.

(45) Picaud, S. S.; Muniz, J. R. C.; Kramm, A.; Pilka, E. S.; Kochan, G.; Oppermann, U.; Yue, W. W. Crystal structure of human carbonic anhydrase-related protein VIII reveals the basis for catalytic silencing. *Proteins* **2009**, *76*, 507–511.

(46) Lakkis, M. M.; Bergenhem, N. C.; O'Shea, K. S.; Tashian, R. E. Expression of the acatalytic carbonic anhydrase VIII gene, Car8, during mouse embryonic development. *Histochem. J.* **1997**, *29*, 135–141.

(47) Hirota, J.; Ando, H.; Hamada, K.; Mikoshiba, K. Carbonic anhydrase-related protein is a novel binding protein for inositol 1,4,5-trisphosphate receptor type 1. *Biochem. J.* **2003**, *372*, 435–441.

(48) Bosanac, I.; Alattia, J.-R.; Mal, T. K.; Chan, J.; Talarico, S.; Tong, F. K.; Tong, K. I.; Yoshikawa, F.; Furuichi, T.; Iwai, M.; Michikawa, T.; Mikoshiba, K.; Ikura, M. Structure of the inositol 1,4,5-trisphosphate receptor binding core in complex with its ligand. *Nature* **2002**, *420*, 696–700.

(49) Jiao, Y.; Yan, J.; Zhao, Y.; Donahue, L. R.; Beamer, W. G.; Li, X.; Roe, B. A.; Ledoux, M. S.; Gu, W. Carbonic anhydrase-related protein VIII deficiency is associated with a distinctive lifelong gait disorder in waddles mice. *Genetics* **2005**, *171*, 1239–1246.

(50) Peles, E.; Schlessinger, J.; Grumet, M. Multi-ligand interactions with receptor-like protein tyrosine phosphatase beta: implications for intercellular signaling. *Trends Biochem. Sci.* **1998**, *23*, 121–124.

(51) Willuda, J.; Honegger, A.; Waibel, R.; Schubiger, P. A.; Stahel, R.; Zangemeister-Wittke, U.; Plückthun, A. High thermal stability is essential for tumor targeting of antibody fragments: engineering of a humanized anti-epithelial glycoprotein-2 (epithelial cell adhesion molecule) single-chain Fv fragment. *Cancer Res.* **1999**, *59*, 5758–5767.

(52) Yao, M.; Bolen, D. W. How valid are denaturant-induced unfolding free energy measurements? Level of conformance to common assumptions over an extended range of ribonuclease A stability. *Biochemistry* **1995**, *34*, 3771–3781.

(53) Samiotakis, A.; Homouz, D.; Cheung, M. S. Multiscale investigation of chemical interference in proteins. *J Chem Phys* **2010**, *132*, 175101.

(54) Wang, Q.; Christiansen, A.; Samiotakis, A.; Wittung-Stafshede, P.; Cheung, M. S. Comparison of chemical and thermal protein denaturation by combination of computational and experimental approaches. II. *J Chem Phys* **2011**, *135*, 175102.

(55) Stadie, W. C.; O'Brien, H. The Catalysis of the Hydration of Carbon Dioxide and Dehydration of Carbonic Acid by an Enzyme Isolated from Red Blood Cells. *J. Biol. Chem.* **1933**, *103*, 521–529.

(56) Jagannadham, M. V.; Balasubramanian, D. The molten globular intermediate form in the folding pathway of human carbonic anhydrase B. *FEBS Lett.* **1985**, *188*, 326–330.

(57) Carlsson, U.; Henderson, L. E.; Lindskog, S. Denaturation and reactivation of human carbonic anhydrases in guanidine hydrochloride and urea. *Biochim. Biophys. Acta* **1973**, *310*, 376–387.

(58) Yazgan, A.; Henkens, R. W. Role of zinc (II) in the refolding of guanidine hydrochloride denatured bovine carbonic anhydrase. *Biochemistry* **1972**, *11*, 1314–1318.

(59) Laurent, G.; Charrel, M.; Garcon, D.; Castay, M.; Marriq, C.; Derrien, Y. On the proteins accompanying human hemoglobin in its preparations. 3 Identification of proteins Y, X1 and X2 with eryhtrocyte carbonic anhydrases and unequal stability of these in an alkaline medium. *Bull. Soc. Chim. Biol.* **1964**, *46*, 603–620.

(60) Riddiford, L. M.; Stellwagen, R. H.; Mehta, S.; Edsall, J. T. Hydrogen ion equilibria of human carbonic anhydrases B and C. *J. Biol. Chem.* **1965**, *240*, 3305–3316.

(61) Svensson, M.; Jonasson, P.; Freskgård, P. O.; Jonsson, B. H.; Lindgren, M.; Mårtensson, L. G.; Gentile, M.; Borén, K.; Carlsson, U. Mapping the folding intermediate of human carbonic anhydrase II. Probing substructure by chemical reactivity and spin and fluorescence labeling of engineered cysteine residues. *Biochemistry* **1995**, *34*, 8606–8620.

(62) Mårtensson, L. G.; Jonsson, B. H.; Andersson, M.; Kihlgren, A.; Bergenhem, N.; Carlsson, U. Role of an evolutionarily invariant serine for the stability of human carbonic anhydrase II. *Biochim. Biophys. Acta* **1992**, *1118*, 179–186.

(63) Mårtensson, L. G.; Jonasson, P.; Freskgård, P. O.; Svensson, M.; Carlsson, U.; Jonsson, B. H. Contribution of individual tryptophan residues to the fluorescence spectrum of native and denatured forms of human carbonic anhydrase II. *Biochemistry* **1995**, *34*, 1011–1021.

(64) Fransson, C.; Freskgård, P. O.; Herbertsson, H.; Johansson, A.; Jonasson, P.; Mårtensson, L. G.; Svensson, M.; Jonsson, B. H.; Carlsson, U. Cis-trans isomerization is rate-determining in the reactivation of denatured human carbonic anhydrase II as evidenced by proline isomerase. *FEBS Lett.* **1992**, *296*, 90–94.

(65) Tweedy, N. B.; Nair, S. K.; Paterno, S. A.; Fierke, C. A.; Christianson, D. W. Structure and energetics of a non-proline cis-peptidyl linkage in a proline-202-->alanine carbonic anhydrase II variant. *Biochemistry* **1993**, *32*, 10944–10949.

(66) Aronsson, G.; Mårtensson, L. G.; Carlsson, U.; Jonsson, B. H. Folding and stability of the N-terminus of human carbonic anhydrase II. *Biochemistry* **1995**, *34*, 2153–2162.

(67) Henkens, R. W.; Kitchell, B. B.; Lottich, S. C.; Stein, P. J.; Williams, T. J. Detection and characterization using circular dichroism and fluorescence spectroscopy of a stable intermediate conformation formed in the denaturation of bovine carbonic anhydrase with guanidinium chloride. *Biochemistry* **1982**, *21*, 5918–5923.

(68) Carlsson, U.; Aasa, R.; Henderson, L. E.; Jonsson, B. H.; Lindskog, S. Paramagnetic and fluorescent probes attached to “buried” sulfhydryl groups in human carbonic anhydrases. Application to inhibitor binding, denaturation and refolding. *Eur. J. Biochem.* **1975**, *52*, 25–36.

(69) Mårtensson, L. G.; Jonsson, B. H.; Freskgård, P. O.; Kihlgren, A.; Svensson, M.; Carlsson, U. Characterization of folding intermediates of human carbonic anhydrase II: probing substructure by chemical labeling of SH groups introduced by site-directed mutagenesis. *Biochemistry* **1993**, *32*, 224–231.

(70) Carlsson, U.; Henderson, L. E.; Nyman, P. O.; Samuelsson, T. Studies on the influence of carboxyl-terminal amino acid residues on the activity and stability of human erythrocyte carbonic anhydrase B. *FEBS Lett.* **1974**, *48*, 167–171.

(71) Avvaru, B. S.; Busby, S. A.; Chalmers, M. J.; Griffin, P. R.; Venkatakrishnan, B.; Agbandje-McKenna, M.; Silverman, D. N.; McKenna, R. Apo-human carbonic anhydrase II revisited: implications of the loss of a metal in protein structure, stability, and solvent network. *Biochemistry* **2009**, *48*, 7365–7372.

(72) Håkansson, K.; Wehnert, A.; Liljas, A. X-ray analysis of metal-substituted human carbonic anhydrase II derivatives. *Acta Crystallogr. D Biol. Crystallogr.* **1994**, *50*, 93–100.

(73) Hunt, J. A.; Ahmed, M.; Fierke, C. A. Metal binding specificity in carbonic anhydrase is influenced by conserved hydrophobic core residues. *Biochemistry* **1999**, *38*, 9054–9062.

(74) Bergenhem, N.; Carlsson, U.; Lind, G.; Astrand, I. M. Denaturation and reactivation of bovine and human cobalt--carbonic anhydrases in guanidine hydrochloride. *Acta Chem. Scand., B, Org. Chem. Biochem.* **1983**, *37*, 244–246.

(75) Borén, K.; Grankvist, H.; Hammarström, P.; Carlsson, U. Reshaping the folding energy landscape by chloride salt: impact on molten-globule formation and aggregation behavior of carbonic anhydrase. *FEBS Lett.* **2004**, *566*, 95–99.

(76) Beychok, S.; Armstrong, J. M.; Lindblow, C.; Edsall, J. T. Optil rotatory dispersion and circular dichroism of human carbonic anhydrases B and C. *J. Biol. Chem.* **1966**, *241*, 5150–5160.

(77) Wong, K. P.; Hamlin, L. M. Acid denaturation of bovine carbonic anhydrase B. *Biochemistry* **1974**, *13*, 2678–2683.

(78) Wong, K. P.; Tanford, C. Denaturation of bovine carbonic anhydrase B by guanidine hydrochloride. A process involving separable sequential conformational transitions. *J. Biol. Chem.* **1973**, *248*, 8518–8523.

(79) Riddiford, L. M. Acid difference spectra of human carbonic anhydrases. *J. Biol. Chem.* **1965**, *240*, 168–172.

(80) Borén, K.; Andersson, P.; Larsson, M.; Carlsson, U. Characterization of a molten globule state of bovine carbonic anhydrase III: loss of asymmetrical environment of the aromatic residues has a profound effect on both the near- and far-UV CD spectrum. *Biochim. Biophys. Acta* **1999**, *1430*, 111–118.

(81) Cabiscol, E.; Levine, R. L. Carbonic anhydrase III. Oxidative modification in vivo and loss of phosphatase activity during aging. *J. Biol. Chem.* **1995**, *270*, 14742–14747.

(82) Di Fiore, A.; Truppo, E.; Supuran, C. T.; Alterio, V.; Dathan, N.; Bootorabi, F.; Parkkila, S.; Monti, S. M.; De Simone, G. Crystal structure of the C183S/C217S mutant of human CA VII in complex with acetazolamide. *Bioorg. Med. Chem. Lett.* **2010**, *20*, 5023–5026.

(83) Baranauskiene, L.; Matulis, D. Intrinsic thermodynamics of ethoxzolamide inhibitor binding to human carbonic anhydrase XIII. *BMC Biophysics* **2012**, *5*, 12.

(84) Matulis, D.; Kranz, J. K.; Salemme, F. R.; Todd, M. J. Thermodynamic stability of carbonic anhydrase: measurements of binding affinity and stoichiometry using ThermoFluor. *Biochemistry* **2005**, *44*, 5258–5266.

(85) Fisher, Z.; Boone, C. D.; Biswas, S. M.; Venkatakrishnan, B.; Aggarwal, M.; Tu, C.; Agbandje-McKenna, M.; Silverman, D.; McKenna, R. Kinetic and structural characterization of thermostabilized mutants of human carbonic anhydrase II. *Protein Eng. Des. Sel.* **2012**, *25*, 347–355.

(86) Stams, T.; Nair, S. K.; Okuyama, T.; Waheed, A.; Sly, W. S.; Christianson, D. W. Crystal structure of the secretory form of membrane-associated human carbonic anhydrase IV at 2.8-A resolution. *Proc. Natl. Acad. Sci. U.S.A.* **1996**, *93*, 13589–13594.

(87) Whitney, P. L.; Briggle, T. V. Membrane-associated carbonic anhydrase purified from bovine lung. *J. Biol. Chem.* **1982**, *257*, 12056–12059.

(88) Waheed, A.; Okuyama, T.; Heyduk, T.; Sly, W. S. Carbonic anhydrase IV: purification of a secretory form of the recombinant human enzyme and identification of the positions and importance of its disulfide bonds. *Arch. Biochem. Biophys.* **1996**, *333*, 432–438.

(89) Mårtensson, L.-G.; Karlsson, M.; Carlsson, U. Dramatic stabilization of the native state of human carbonic anhydrase II by an engineered disulfide bond. *Biochemistry* **2002**, *41*, 15867–15875.

(90) Alterio, V.; Hilvo, M.; Di Fiore, A.; Supuran, C. T.; Pan, P.; Parkkila, S.; Scaloni, A.; Pastorek, J.; Pastorekova, S.; Pedone, C.; Scozzafava, A.; Monti, S. M.; De Simone, G. Crystal structure of the catalytic domain of the tumor-associated human carbonic anhydrase IX. *Proc. Natl. Acad. Sci. U.S.A.* **2009**, *106*, 16233–16238.

(91) Whittington, D. A.; Waheed, A.; Ulmasov, B.; Shah, G. N.; Grubb, J. H.; Sly, W. S.; Christianson, D. W. Crystal structure of the dimeric extracellular domain of human carbonic anhydrase XII, a bitopic membrane protein overexpressed in certain cancer tumor cells. *Proc. Natl. Acad. Sci. U.S.A.* **2001**, *98*, 9545–9550.

(92) Whittington, D. A.; Grubb, J. H.; Waheed, A.; Shah, G. N.; Sly, W. S.; Christianson, D. W. Expression, assay, and structure of the extracellular domain of murine carbonic anhydrase XIV: implications for selective inhibition of membrane-associated isozymes. *J. Biol. Chem.* **2004**, *279*, 7223–7228.

(93) Wykoff, C. C.; Beasley, N. J.; Watson, P. H.; Turner, K. J.; Pastorek, J.; Sibtain, A.; Wilson, G. D.; Turley, H.; Talks, K. L.; Maxwell, P. H.; Pugh, C. W.; Ratcliffe, P. J.; Harris, A. L. Hypoxia-inducible expression of tumor-associated carbonic anhydrases. *Cancer Res.* **2000**, *60*, 7075–7083.

(94) Andersson, D.; Hammarström, P.; Carlsson, U. Cofactor-induced refolding: refolding of molten globule carbonic anhydrase induced by Zn(II) and Co(II). *Biochemistry* **2001**, *40*, 2653–2661.

(95) Kannan, K. K.; Ramanadham, M.; Jones, T. A. Structure, refinement, and function of carbonic anhydrase isozymes: refinement of human carbonic anhydrase I. *Ann. N. Y. Acad. Sci.* **1984**, *429*, 49–60.

(96) Aggarwal, M.; McKenna, R. Update on carbonic anhydrase inhibitors: a patent review (2008 - 2011). *Expert Opin Ther Pat* **2012**, *22*, 903–915.

(97) Supuran, C. T. Carbonic anhydrases: novel therapeutic applications for inhibitors and activators. *Nat Rev Drug Discov* **2008**, *7*, 168–181.

(98) Thiry, A.; Dogné, J.-M.; Masereel, B.; Supuran, C. T. Targeting tumor-associated carbonic anhydrase IX in cancer therapy. *Trends Pharmacol. Sci.* **2006**, *27*, 566–573.

(99) Brahimi-Horn, M. C.; Pouysségur, J. Oxygen, a source of life and stress. *FEBS Lett.* **2007**, *581*, 3582–3591.

(100) Maxwell, P. H.; Wiesener, M. S.; Chang, G. W.; Clifford, S. C.; Vaux, E. C.; Cockman, M. E.; Wykoff, C. C.; Pugh, C. W.; Maher, E. R.; Ratcliffe, P. J. The tumour suppressor protein VHL targets hypoxia-inducible factors for oxygen-dependent proteolysis. *Nature* **1999**, *399*, 271–275.

(101) Semenza, G. L. Hypoxia and cancer. *Cancer Metastasis Rev.* **2007**, *26*, 223–224.

(102) Hon, W.-C.; Wilson, M. I.; Harlos, K.; Claridge, T. D. W.; Schofield, C. J.; Pugh, C. W.; Maxwell, P. H.; Ratcliffe, P. J.; Stuart, D. I.; Jones, E. Y. Structural basis for the recognition of hydroxyproline in HIF-1 alpha by pVHL. *Nature* **2002**, *417*, 975–978.

(103) Neri, D.; Supuran, C. T. Interfering with pH regulation in tumours as a therapeutic strategy. *Nat Rev Drug Discov* **2011**, *10*, 767–777.

(104) Aggarwal, M.; Kondeti, B.; McKenna, R. Insights towards sulfonamide drug specificity in α-carbonic anhydrases. *Bioorg. Med. Chem.* **2013**, *21*, 1526–1533.

(105) Vullo, D.; De Luca, V.; Scozzafava, A.; Carginale, V.; Rossi, M.; Supuran, C. T.; Capasso, C. The first activation study of a bacterial carbonic anhydrase (CA). The thermostable α-CA from Sulfurihydrogenibium yellowstonense YO3AOP1 is highly activated by amino acids and amines. *Bioorg. Med. Chem. Lett.* **2012**, *22*, 6324–6327.

(106) De Luca, V.; Vullo, D.; Scozzafava, A.; Carginale, V.; Rossi, M.; Supuran, C. T.; Capasso, C. Anion inhibition studies of an α-carbonic anhydrase from the thermophilic bacterium Sulfurihydrogenibium yellowstonense YO3AOP1. *Bioorg. Med. Chem. Lett.* **2012**, *22*, 5630–5634.

(107) Fulke, A. B.; Mudliar, S. N.; Yadav, R.; Shekh, A.; Srinivasan, N.; Ramanan, R.; Krishnamurthi, K.; Devi, S. S.; Chakrabarti, T. Bio-mitigation of CO(2), calcite formation and simultaneous biodiesel precursors production using Chlorella sp. *Bioresour. Technol.* **2010**, *101*, 8473–8476.

(108) Ramanan, R.; Kannan, K.; Deshkar, A.; Yadav, R.; Chakrabarti, T. Enhanced algal CO(2) sequestration through calcite deposition by Chlorella sp. and Spirulina platensis in a mini-raceway pond. *Bioresour. Technol.* **2010**, *101*, 2616–2622.

(109) Hunt, J. A.; Lesburg, C. A.; Christianson, D. W.; Thompson, R. B.; Fierke, C. A. Active-site engineering of carbonic anhydrase and its application to biosensors. *EXS* **2000**, 221–240.

(110) Kanbar, B.; Ozdemir, E. Thermal stability of carbonic anhydrase immobilized within polyurethane foam. *Biotechnol. Prog.* **2010**, *26*, 1474–1480.

(111) Vinoba, M.; Lim, K. S.; Lee, S. H.; Jeong, S. K.; Alagar, M. Immobilization of human carbonic anhydrase on gold nanoparticles assembled onto amine/thiol-functionalized mesoporous SBA-15 for biomimetic sequestration of CO2. *Langmuir* **2011**, *27*, 6227–6234.

(112) Pettersen, E. F.; Goddard, T. D.; Huang, C. C.; Couch, G. S.; Greenblatt, D. M.; Meng, E. C.; Ferrin, T. E. UCSF Chimera--a visualization system for exploratory research and analysis. *J Comput Chem* **2004**, *25*, 1605–1612.

(113) Forsman, C.; Behravan, G.; Osterman, A.; Jonsson, B. H. Production of active human carbonic anhydrase II in E. coli. *Acta Chem. Scand., B, Org. Chem. Biochem.* **1988**, *42*, 314–318.

(114) Whitney, P. L. Affinity chromatography of carbonic anhydrase. *Anal. Biochem.* **1974**, *57*, 467–476.

(115) Otwinowski Z.; Minor, W. Processing of x-ray diffraction data collected in oscillation mode. *Methods in Enzymology.* **1997**, *276*, 307-326.

(116) Adams, P. D.; Afonine, P. V.; Bunkóczi, G.; Chen, V. B.; Davis, I. W.; Echols, N.; Headd, J. J.; Hung, L.-W.; Kapral, G. J.; Grosse-Kunstleve, R. W.; McCoy, A. J.; Moriarty, N. W.; Oeffner, R.; Read, R. J.; Richardson, D. C.; Richardson, J. S.; Terwilliger, T. C.; Zwart, P. H. PHENIX: a comprehensive Python-based system for macromolecular structure solution. *Acta Crystallographica Section D Biological Crystallography* **2010**, *66*, 213–221.

(117) Brünger, A. T. Free R value: a novel statistical quantity for assessing the accuracy of crystal structures. *Nature* **1992**, *355*, 472–475.

(118) Emsley, P.; Cowtan, K. Coot: model-building tools for molecular graphics. *Acta Crystallogr. D Biol. Crystallogr.* **2004**, *60*, 2126–2132.

(119) Krissinel, E.; Henrick, K. Inference of macromolecular assemblies from crystalline state. *J. Mol. Biol.* **2007**, *372*, 774–797.

(120) Pastorek, J.; Pastoreková, S.; Callebaut, I.; Mornon, J. P.; Zelník, V.; Opavský, R.; Zaťovicová, M.; Liao, S.; Portetelle, D.; Stanbridge, E. J. Cloning and characterization of MN, a human tumor-associated protein with a domain homologous to carbonic anhydrase and a putative helix-loop-helix DNA binding segment. *Oncogene* **1994**, *9*, 2877–2888.

(121) Alterio, V.; Vitale, R. M.; Monti, S. M.; Pedone, C.; Scozzafava, A.; Cecchi, A.; De Simone, G.; Supuran, C. T. Carbonic anhydrase inhibitors: X-ray and molecular modeling study for the interaction of a fluorescent antitumor sulfonamide with isozyme II and IX. *J. Am. Chem. Soc.* **2006**, *128*, 8329–8335.

(122) Pacchiano, F.; Aggarwal, M.; Avvaru, B. S.; Robbins, A. H.; Scozzafava, A.; McKenna, R.; Supuran, C. T. Selective hydrophobic pocket binding observed within the carbonic anhydrase II active site accommodate different 4-substituted-ureido-benzenesulfonamides and correlate to inhibitor potency. *Chem. Commun. (Camb.)* **2010**, *46*, 8371–8373.

(123) Eriksson, A. E.; Jones, T. A.; Liljas, A. Refined structure of human carbonic anhydrase II at 2.0 A resolution. *Proteins* **1988**, *4*, 274–282.

(124) Temperini, C.; Scozzafava, A.; Supuran, C. T. Carbonic anhydrase inhibitors. X-ray crystal studies of the carbonic anhydrase II-trithiocarbonate adduct--an inhibitor mimicking the sulfonamide and urea binding to the enzyme. *Bioorg. Med. Chem. Lett.* **2010**, *20*, 474–478.

(125) Avvaru, B. S.; Wagner, J. M.; Maresca, A.; Scozzafava, A.; Robbins, A. H.; Supuran, C. T.; McKenna, R. Carbonic anhydrase inhibitors. The X-ray crystal structure of human isoform II in adduct with an adamantyl analogue of acetazolamide resides in a less utilized binding pocket than most hydrophobic inhibitors. *Bioorg. Med. Chem. Lett.* **2010**, *20*, 4376–4381.

(126) Wagner, J.; Avvaru, B. S.; Robbins, A. H.; Scozzafava, A.; Supuran, C. T.; McKenna, R. Coumarinyl-substituted sulfonamides strongly inhibit several human carbonic anhydrase isoforms: solution and crystallographic investigations. *Bioorg. Med. Chem.* **2010**, *18*, 4873–4878.

(127) Biswas, S.; Aggarwal, M.; Güzel, Ö.; Scozzafava, A.; McKenna, R.; Supuran, C. T. Conformational variability of different sulfonamide inhibitors with thienyl-acetamido moieties attributes to differential binding in the active site of cytosolic human carbonic anhydrase isoforms. *Bioorg. Med. Chem.* **2011**, *19*, 3732–3738.

(128) Güzel, O.; Innocenti, A.; Scozzafava, A.; Salman, A.; Supuran, C. T. Carbonic anhydrase inhibitors. Aromatic/heterocyclic sulfonamides incorporating phenacetyl, pyridylacetyl and thienylacetyl tails act as potent inhibitors of human mitochondrial isoforms VA and VB. *Bioorg. Med. Chem.* **2009**, *17*, 4894–4899.

(129) Güzel, O.; Innocenti, A.; Scozzafava, A.; Salman, A.; Supuran, C. T. Carbonic anhydrase inhibitors. Phenacetyl-, pyridylacetyl- and thienylacetyl-substituted aromatic sulfonamides act as potent and selective isoform VII inhibitors. *Bioorg. Med. Chem. Lett.* **2009**, *19*, 3170–3173.

(130) Asiedu, M.; Ossipov, M. H.; Kaila, K.; Price, T. J. Acetazolamide and midazolam act synergistically to inhibit neuropathic pain. *Pain* **2010**, *148*, 302–308.

(131) Hen, N.; Bialer, M.; Yagen, B.; Maresca, A.; Aggarwal, M.; Robbins, A. H.; McKenna, R.; Scozzafava, A.; Supuran, C. T. Anticonvulsant 4-aminobenzenesulfonamide derivatives with branched-alkylamide moieties: X-ray crystallography and inhibition studies of human carbonic anhydrase isoforms I, II, VII, and XIV. *J. Med. Chem.* **2011**, *54*, 3977–3981.

(132) Bialer, M.; Johannessen, S. I.; Levy, R. H.; Perucca, E.; Tomson, T.; White, H. S. Progress report on new antiepileptic drugs: a summary of the Tenth Eilat Conference (EILAT X). *Epilepsy Res.* **2010**, *92*, 89–124.

(133) Stringer, J. L.; Lothman, E. W. During afterdischarges in the young rat in vivo extracellular potassium is not elevated above adult levels. *Brain Res. Dev. Brain Res.* **1996**, *91*, 136–139.

(134) Xiong, Z. Q.; Saggau, P.; Stringer, J. L. Activity-dependent intracellular acidification correlates with the duration of seizure activity. *J. Neurosci.* **2000**, *20*, 1290–1296.

(135) Bonnet, U.; Wiemann, M.; Bingmann, D. CO2/HCO3(-)-withdrawal from the bath medium of hippocampal slices: biphasic effect on intracellular pH and bioelectric activity of CA3-neurons. *Brain Res.* **1998**, *796*, 161–170.

(136) Aribi, A. M.; Stringer, J. L. Effects of antiepileptic drugs on extracellular pH regulation in the hippocampal CA1 region in vivo. *Epilepsy Res.* **2002**, *49*, 143–151.

(137) Halmi, P.; Parkkila, S.; Honkaniemi, J. Expression of carbonic anhydrases II, IV, VII, VIII and XII in rat brain after kainic acid induced status epilepticus. *Neurochem. Int.* **2006**, *48*, 24–30.

(138) Ghandour, M. S.; Langley, O. K.; Zhu, X. L.; Waheed, A.; Sly, W. S. Carbonic anhydrase IV on brain capillary endothelial cells: a marker associated with the blood-brain barrier. *Proc. Natl. Acad. Sci. U.S.A.* **1992**, *89*, 6823–6827.

(139) Ruusuvuori, E.; Li, H.; Huttu, K.; Palva, J. M.; Smirnov, S.; Rivera, C.; Kaila, K.; Voipio, J. Carbonic anhydrase isoform VII acts as a molecular switch in the development of synchronous gamma-frequency firing of hippocampal CA1 pyramidal cells. *J. Neurosci.* **2004**, *24*, 2699–2707.

(140) Masereel, B.; Rolin, S.; Abbate, F.; Scozzafava, A.; Supuran, C. T. Carbonic anhydrase inhibitors: anticonvulsant sulfonamides incorporating valproyl and other lipophilic moieties. *J. Med. Chem.* **2002**, *45*, 312–320.

(141) Chufán, E. E.; Pedregosa, J. C.; Baldini, O. N.; Bruno-Blanch, L. Anticonvulsant activity of analogues of acetazolamide. *Farmaco* **1999**, *54*, 838–841.

(142) De Simone, G.; Scozzafava, A.; Supuran, C. T. Which carbonic anhydrases are targeted by the antiepileptic sulfonamides and sulfamates? *Chem Biol Drug Des* **2009**, *74*, 317–321.

(143) Thiry, A.; Dogné, J.-M.; Supuran, C. T.; Masereel, B. Carbonic anhydrase inhibitors as anticonvulsant agents. *Curr Top Med Chem* **2007**, *7*, 855–864.

(144) Aggarwal, M.; Kondeti, B.; McKenna, R. Anticonvulsant/antiepileptic carbonic anhydrase inhibitors: a patent review. *Expert Opin Ther Pat* **2013**, 23, 717-724.

(145) Hen, N.; Bialer, M.; Wlodarczyk, B.; Finnell, R. H.; Yagen, B. Syntheses and evaluation of anticonvulsant profile and teratogenicity of novel amide derivatives of branched aliphatic carboxylic acids with 4-aminobenzensulfonamide. *J. Med. Chem.* **2010**, *53*, 4177–4186.

(146) Marini, A. M.; Maresca, A.; Aggarwal, M.; Orlandini, E.; Nencetti, S.; Da Settimo, F.; Salerno, S.; Simorini, F.; La Motta, C.; Taliani, S.; Nuti, E.; Scozzafava, A.; McKenna, R.; Rossello, A.; Supuran, C. T. Tricyclic Sulfonamides Incorporating Benzothiopyrano[4,3-c]pyrazole and Pyridothiopyrano[4,3-c]pyrazole Effectively Inhibit α- and β-Carbonic Anhydrase: X-ray Crystallography and Solution Investigations on 15 Isoforms. *J. Med. Chem.* **2012**, *55*, 9619–9629.

(147) Supuran, C. T.; Casini, A.; Mastrolorenzo, A.; Scozzafava, A. COX-2 selective inhibitors, carbonic anhydrase inhibition and anticancer properties of sulfonamides belonging to this class of pharmacological agents. *Mini Rev Med Chem* **2004**, *4*, 625–632.

(148) Dogné, J.-M.; Supuran, C. T.; Pratico, D. Adverse cardiovascular effects of the coxibs. *J. Med. Chem.* **2005**, *48*, 2251–2257.

(149) Dogné, J.-M.; Hanson, J.; Supuran, C.; Pratico, D. Coxibs and cardiovascular side-effects: from light to shadow. *Curr. Pharm. Des.* **2006**, *12*, 971–975.

(150) Dogné, J.-M.; Thiry, A.; Pratico, D.; Masereel, B.; Supuran, C. T. Dual carbonic anhydrase--cyclooxygenase-2 inhibitors. *Curr Top Med Chem* **2007**, *7*, 885–891.

(151) Weber, A.; Casini, A.; Heine, A.; Kuhn, D.; Supuran, C. T.; Scozzafava, A.; Klebe, G. Unexpected nanomolar inhibition of carbonic anhydrase by COX-2-selective celecoxib: new pharmacological opportunities due to related binding site recognition. *J. Med. Chem.* **2004**, *47*, 550–557.

(152) Di Fiore, A.; Pedone, C.; D'Ambrosio, K.; Scozzafava, A.; De Simone, G.; Supuran, C. T. Carbonic anhydrase inhibitors: Valdecoxib binds to a different active site region of the human isoform II as compared to the structurally related cyclooxygenase II "selective" inhibitor celecoxib. *Bioorg. Med. Chem. Lett.* **2006**, *16*, 437–442.

(153) Srivastava, D. K.; Jude, K. M.; Banerjee, A. L.; Haldar, M.; Manokaran, S.; Kooren, J.; Mallik, S.; Christianson, D. W. Structural analysis of charge discrimination in the binding of inhibitors to human carbonic anhydrases I and II. *J. Am. Chem. Soc.* **2007**, *129*, 5528–5537.

(154) Khalifah, R. G. The carbon dioxide hydration activity of carbonic anhydrase. I. Stop-flow kinetic studies on the native human isoenzymes B and C. *J. Biol. Chem.* **1971**, *246*, 2561–2573.

(155) Eriksson, A. E.; Kylsten, P. M.; Jones, T. A.; Liljas, A. Crystallographic studies of inhibitor binding sites in human carbonic anhydrase II: a pentacoordinated binding of the SCN- ion to the zinc at high pH. *Proteins* **1988**, *4*, 283–293.

(156) Carta, F.; Aggarwal, M.; Maresca, A.; Scozzafava, A.; McKenna, R.; Supuran, C. T. Dithiocarbamates: a new class of carbonic anhydrase inhibitors. Crystallographic and kinetic investigations. *Chem. Commun. (Camb.)* **2012**, *48*, 1868–1870.

(157) Carta, F.; Aggarwal, M.; Maresca, A.; Scozzafava, A.; McKenna, R.; Masini, E.; Supuran, C. T. Dithiocarbamates strongly inhibit carbonic anhydrases and show antiglaucoma action in vivo. *J. Med. Chem.* **2012**, *55*, 1721–1730.

(158) Supuran, C. T. Diuretics: from classical carbonic anhydrase inhibitors to novel applications of the sulfonamides. *Curr. Pharm. Des.* **2008**, *14*, 641–648.

(159) De Simone, G.; Di Fiore, A.; Supuran, C. T. Are carbonic anhydrase inhibitors suitable for obtaining antiobesity drugs? *Curr. Pharm. Des.* **2008**, *14*, 655–660.

(160) De Leval, X.; Ilies, M.; Casini, A.; Dogné, J.-M.; Scozzafava, A.; Masini, E.; Mincione, F.; Starnotti, M.; Supuran, C. T. Carbonic anhydrase inhibitors: synthesis and topical intraocular pressure lowering effects of fluorine-containing inhibitors devoid of enhanced reactivity. *J. Med. Chem.* **2004**, *47*, 2796–2804.

(161) Sugrue, M. F. The pharmacology of antiglaucoma drugs. *Pharmacol. Ther.* **1989**, *43*, 91–138.

(162) Carta, F.; Supuran, C. T.; Scozzafava, A. Novel therapies for glaucoma: a patent review 2007 - 2011. *Expert Opin Ther Pat* **2012**, *22*, 79–88.

(163) Mincione, F.; Scozzafava, A.; Supuran, C. T. The development of topically acting carbonic anhydrase inhibitors as anti-glaucoma agents. *Curr Top Med Chem* **2007**, *7*, 849–854.

(164) Steele, R. M.; Benedini, F.; Biondi, S.; Borghi, V.; Carzaniga, L.; Impagnatiello, F.; Miglietta, D.; Chong, W. K. M.; Rajapakse, R.; Cecchi, A.; Temperini, C.; Supuran, C. T. Nitric oxide-donating carbonic anhydrase inhibitors for the treatment of open-angle glaucoma. *Bioorg. Med. Chem. Lett.* **2009**, *19*, 6565–6570.

(165) Mincione, F.; Benedini, F.; Biondi, S.; Cecchi, A.; Temperini, C.; Formicola, G.; Pacileo, I.; Scozzafava, A.; Masini, E.; Supuran, C. T. Synthesis and crystallographic analysis of new sulfonamides incorporating NO-donating moieties with potent antiglaucoma action. *Bioorg. Med. Chem. Lett.* **2011**, *21*, 3216–3221.

(166) Fabrizi, F.; Mincione, F.; Somma, T.; Scozzafava, G.; Galassi, F.; Masini, E.; Impagnatiello, F.; Supuran, C. T. A new approach to antiglaucoma drugs: carbonic anhydrase inhibitors with or without NO donating moieties. Mechanism of action and preliminary pharmacology. *J Enzyme Inhib Med Chem* **2012**, *27*, 138–147.

(167) Liao, S.-Y.; Ivanov, S.; Ivanova, A.; Ghosh, S.; Cote, M. A.; Keefe, K.; Coca-Prados, M.; Stanbridge, E. J.; Lerman, M. I. Expression of cell surface transmembrane carbonic anhydrase genes CA9 and CA12 in the human eye: overexpression of CA12 (CAXII) in glaucoma. *J. Med. Genet.* **2003**, *40*, 257–261.

(168) Innocenti, A.; Scozzafava, A.; Supuran, C. T. Carbonic anhydrase inhibitors. Inhibition of cytosolic isoforms I, II, III, VII and XIII with less investigated inorganic anions. *Bioorg. Med. Chem. Lett.* **2009**, *19*, 1855–1857.

(169) Innocenti, A.; Scozzafava, A.; Supuran, C. T. Carbonic anhydrase inhibitors. Inhibition of transmembrane isoforms IX, XII, and XIV with less investigated anions including trithiocarbonate and dithiocarbamate. *Bioorg. Med. Chem. Lett.* **2010**, *20*, 1548–1550.

(170) Bencini, A.; Failli, P.; Valtancoli, B.; Bani, D. Low molecular weight compounds with transition metals as free radical scavengers and novel therapeutic agents. *Cardiovasc Hematol Agents Med Chem* **2010**, *8*, 128–146.

(171) Szolar, O. H. J. Environmental and pharmaceutical analysis of dithiocarbamates. *Anal. Chim. Acta* **2007**, *582*, 191–200.

(172) Amin, E.; Saboury, A. A.; Mansuri-Torshizi, H.; Moosavi-Movahedi, A. A. Potent inhibitory effects of benzyl and p-xylidine-bis dithiocarbamate sodium salts on activities of mushroom tyrosinase. *J Enzyme Inhib Med Chem* **2010**, *25*, 272–281.

(173) Morpurgo, L.; Desideri, A.; Rigo, A.; Viglino, P.; Rotilio, G. Reaction of N,N-diethyldithiocarbamate and other bidentate ligands with Zn, Co and Cu bovine carbonic anhydrases. Inhibition of the enzyme activity and evidence for stable ternary enzyme-metal-ligand complexes. *Biochim. Biophys. Acta* **1983**, *746*, 168–175.

(174) Stillebroer, A. B.; Mulders, P. F. A.; Boerman, O. C.; Oyen, W. J. G.; Oosterwijk, E. Carbonic anhydrase IX in renal cell carcinoma: implications for prognosis, diagnosis, and therapy. *Eur. Urol.* **2010**, *58*, 75–83.

(175) Siebels, M.; Rohrmann, K.; Oberneder, R.; Stahler, M.; Haseke, N.; Beck, J.; Hofmann, R.; Kindler, M.; Kloepfer, P.; Stief, C. A clinical phase I/II trial with the monoclonal antibody cG250 (RENCAREX®) and interferon-alpha-2a in metastatic renal cell carcinoma patients. *World J Urol* **2011**, *29*, 121–126.

(176) Van Schaijk, F. G.; Oosterwijk, E.; Molkenboer-Kuenen, J. D.; Soede, A. C.; McBride, B. J.; Goldenberg, D. M.; Oyen, W. J. G.; Corstens, F. H. M.; Boerman, O. C. Pretargeting with bispecific anti-renal cell carcinoma x anti-DTPA(In) antibody in 3 RCC models. *J. Nucl. Med.* **2005**, *46*, 495–501.

(177) Pacchiano, F.; Carta, F.; McDonald, P. C.; Lou, Y.; Vullo, D.; Scozzafava, A.; Dedhar, S.; Supuran, C. T. Ureido-substituted benzenesulfonamides potently inhibit carbonic anhydrase IX and show antimetastatic activity in a model of breast cancer metastasis. *J. Med. Chem.* **2011**, *54*, 1896–1902.

(178) Groves, K.; Bao, B.; Zhang, J.; Handy, E.; Kennedy, P.; Cuneo, G.; Supuran, C. T.; Yared, W.; Peterson, J. D.; Rajopadhye, M. Synthesis and evaluation of near-infrared fluorescent sulfonamide derivatives for imaging of hypoxia-induced carbonic anhydrase IX expression in tumors. *Bioorg. Med. Chem. Lett.* **2012**, *22*, 653–657.

(179) Touisni, N.; Maresca, A.; McDonald, P. C.; Lou, Y.; Scozzafava, A.; Dedhar, S.; Winum, J.-Y.; Supuran, C. T. Glycosyl coumarin carbonic anhydrase IX and XII inhibitors strongly attenuate the growth of primary breast tumors. *J. Med. Chem.* **2011**, *54*, 8271–8277.

(180) Casini, A.; Antel, J.; Abbate, F.; Scozzafava, A.; David, S.; Waldeck, H.; Schäfer, S.; Supuran, C. T. Carbonic anhydrase inhibitors: SAR and X-ray crystallographic study for the interaction of sugar sulfamates/sulfamides with isozymes I, II and IV. *Bioorg. Med. Chem. Lett.* **2003**, *13*, 841–845.

(181) Fisher, S. Z.; Maupin, C. M.; Budayova-Spano, M.; Govindasamy, L.; Tu, C.; Agbandje-McKenna, M.; Silverman, D. N.; Voth, G. A.; McKenna, R. Atomic crystal and molecular dynamics simulation structures of human carbonic anhydrase II: insights into the proton transfer mechanism. *Biochemistry* **2007**, *46*, 2930–2937.

(182) Fisher, S. Z.; Aggarwal, M.; Kovalevsky, A. Y.; Silverman, D. N.; McKenna, R. Neutron Diffraction of Acetazolamide-Bound Human Carbonic Anhydrase II Reveals Atomic Details of Drug Binding. *J. Am. Chem. Soc.* **2012**, *134*, 14726–14729.

(183) Di Fiore, A.; Maresca, A.; Alterio, V.; Supuran, C. T.; De Simone, G. Carbonic anhydrase inhibitors: X-ray crystallographic studies for the binding of N-substituted benzenesulfonamides to human isoform II. *Chem. Commun. (Camb.)* **2011**, *47*, 11636–11638.

(184) Alterio, V.; Monti, S. M.; Truppo, E.; Pedone, C.; Supuran, C. T.; De Simone, G. The first example of a significant active site conformational rearrangement in a carbonic anhydrase-inhibitor adduct: the carbonic anhydrase I-topiramate complex. *Org. Biomol. Chem.* **2010**, *8*, 3528–3533.

(185) Coleman, J. E. Chemical reactions of sulfonamides with carbonic anhydrase. *Annu Rev Pharmacol* **1975**, *15*, 221–242.

(186) Supuran, C. T.; Winum, J.-Y.; Wang, B. *Drug Design of Zinc-Enzyme Inhibitors: Functional, Structural, and Disease Applications*; John Wiley & Sons, 2009.

(187) Sippel, K. H.; Robbins, A. H.; Domsic, J.; Genis, C.; Agbandje-McKenna, M.; McKenna, R. High-resolution structure of human carbonic anhydrase II complexed with acetazolamide reveals insights into inhibitor drug design. *Acta Crystallogr. Sect. F Struct. Biol. Cryst. Commun.* **2009**, *65*, 992–995.

(188) Kanamori, K.; Roberts, J. D. Nitrogen-15 nuclear magnetic resonance study of benzenesulfonamide and cyanate binding to carbonic anhydrase. *Biochemistry* **1983**, *22*, 2658–2664.

(189) Bennett, B.; Langan, P.; Coates, L.; Mustyakimov, M.; Schoenborn, B.; Howell, E. E.; Dealwis, C. Neutron diffraction studies of Escherichia coli dihydrofolate reductase complexed with methotrexate. *Proc. Natl. Acad. Sci. U.S.A.* **2006**, *103*, 18493–18498.

(190) Adachi, M.; Ohhara, T.; Kurihara, K.; Tamada, T.; Honjo, E.; Okazaki, N.; Arai, S.; Shoyama, Y.; Kimura, K.; Matsumura, H.; Sugiyama, S.; Adachi, H.; Takano, K.; Mori, Y.; Hidaka, K.; Kimura, T.; Hayashi, Y.; Kiso, Y.; Kuroki, R. Structure of HIV-1 protease in complex with potent inhibitor KNI-272 determined by high-resolution X-ray and neutron crystallography. *Proc. Natl. Acad. Sci. U.S.A.* **2009**, *106*, 4641–4646.

(191) Gardberg, A. S.; Del Castillo, A. R.; Weiss, K. L.; Meilleur, F.; Blakeley, M. P.; Myles, D. A. A. Unambiguous determination of H-atom positions: comparing results from neutron and high-resolution X-ray crystallography. *Acta Crystallogr. D Biol. Crystallogr.* **2010**, *66*, 558–567.

(192) Bennett, B. C.; Gardberg, A. S.; Blair, M. D.; Dealwis, C. G. On the determinants of amide backbone exchange in proteins: a neutron crystallographic comparative study. *Acta Crystallogr. D Biol. Crystallogr.* **2008**, *D64*, 764–783.

(193) Minor, W.; Cymborowski, M.; Otwinowski, Z.; Chruszcz, M. HKL-3000: the integration of data reduction and structure solution--from diffraction images to an initial model in minutes. *Acta Crystallogr. D Biol. Crystallogr.* **2006**, *62*, 859–866.

(194) Pflugrath, J. W. The finer things in X-ray diffraction data collection. *Acta Crystallogr. D Biol. Crystallogr.* **1999**, *55*, 1718–1725.

(195) Schoenborn, B. P.; Langan, P. Protein crystallography with spallation neutrons. *J Synchrotron Radiat* **2004**, *11*, 80–82.

(196) Helliwell, J. R.; Habash, J.; Cruickshank, D. W. J.; Harding, M. M.; Greenhough, T. J.; Campbell, J. W.; Clifton, I. J.; Elder, M.; Machin, P. A.; Papiz, M. Z.; Zurek, S. The recording and analysis of synchrotron X-radiation Laue diffraction photographs. *Journal of Applied Crystallography* **1989**, *22*, 483–497.

(197) Evans, P. Scaling and assessment of data quality. *Acta Crystallogr. D Biol. Crystallogr.* **2006**, *62*, 72–82.

(198) Diederichs, K.; Karplus, P. A. Improved R-factors for diffraction data analysis in macromolecular crystallography. *Nat. Struct. Biol.* **1997**, *4*, 269–275.

(199) Weiss, M. S.; Hilgenfeld, R. On the use of the merging R factor as a quality indicator for X-ray data. *Journal of Applied Crystallography* **1997**, *30*, 203–205.

(200) Collaborative Computational Project, Number 4 The CCP4 suite: programs for protein crystallography. *Acta Crystallographica Section D Biological Crystallography* **1994**, *50*, 760–763.

(201) Adams, P. D.; Mustyakimov, M.; Afonine, P. V.; Langan, P. Generalized X-ray and neutron crystallographic analysis: more accurate and complete structures for biological macromolecules. *Acta Crystallogr. D Biol. Crystallogr.* **2009**, *65*, 567–573.

(202) Fisher, Z.; Kovalevsky, A. Y.; Mustyakimov, M.; Silverman, D. N.; McKenna, R.; Langan, P. Neutron structure of human carbonic anhydrase II: a hydrogen-bonded water network “switch” is observed between pH 7.8 and 10.0. *Biochemistry* **2011**, *50*, 9421–9423.

(203) Kovalevsky, A. Y.; Hanson, B. L.; Mason, S. A.; Yoshida, T.; Fisher, S. Z.; Mustyakimov, M.; Forsyth, V. T.; Blakeley, M. P.; Keen, D. A.; Langan, P. Identification of the elusive hydronium ion exchanging roles with a proton in an enzyme at lower pH values. *Angew. Chem. Int. Ed. Engl.* **2011**, *50*, 7520–7523.

(204) Lesburg, C. A.; Huang, C.; Christianson, D. W.; Fierke, C. A. Histidine --> carboxamide ligand substitutions in the zinc binding site of carbonic anhydrase II alter metal coordination geometry but retain catalytic activity. *Biochemistry* **1997**, *36*, 15780–15791.

(205) Opavský, R.; Pastoreková, S.; Zelník, V.; Gibadulinová, A.; Stanbridge, E. J.; Závada, J.; Kettmann, R.; Pastorek, J. Human MN/CA9 gene, a novel member of the carbonic anhydrase family: structure and exon to protein domain relationships. *Genomics* **1996**, *33*, 480–487.

(206) Hilvo, M.; Baranauskiene, L.; Salzano, A. M.; Scaloni, A.; Matulis, D.; Innocenti, A.; Scozzafava, A.; Monti, S. M.; Di Fiore, A.; De Simone, G.; Lindfors, M.; Jänis, J.; Valjakka, J.; Pastoreková, S.; Pastorek, J.; Kulomaa, M. S.; Nordlund, H. R.; Supuran, C. T.; Parkkila, S. Biochemical characterization of CA IX, one of the most active carbonic anhydrase isozymes. *J. Biol. Chem.* **2008**, *283*, 27799–27809.

(207) Abbate, F.; Coetzee, A.; Casini, A.; Ciattini, S.; Scozzafava, A.; Supuran, C. T. Carbonic anhydrase inhibitors: X-ray crystallographic structure of the adduct of human isozyme II with the antipsychotic drug sulpiride. *Bioorg. Med. Chem. Lett.* **2004**, *14*, 337–341.

(208) Svastová, E.; Hulíková, A.; Rafajová, M.; Zat'ovicová, M.; Gibadulinová, A.; Casini, A.; Cecchi, A.; Scozzafava, A.; Supuran, C. T.; Pastorek, J.; Pastoreková, S. Hypoxia activates the capacity of tumor-associated carbonic anhydrase IX to acidify extracellular pH. *FEBS Lett.* **2004**, *577*, 439–445.

(209) Cecchi, A.; Hulikova, A.; Pastorek, J.; Pastoreková, S.; Scozzafava, A.; Winum, J.-Y.; Montero, J.-L.; Supuran, C. T. Carbonic anhydrase inhibitors. Design of fluorescent sulfonamides as probes of tumor-associated carbonic anhydrase IX that inhibit isozyme IX-mediated acidification of hypoxic tumors. *J. Med. Chem.* **2005**, *48*, 4834–4841.

(210) Menchise, V.; De Simone, G.; Alterio, V.; Di Fiore, A.; Pedone, C.; Scozzafava, A.; Supuran, C. T. Carbonic anhydrase inhibitors: stacking with Phe131 determines active site binding region of inhibitors as exemplified by the X-ray crystal structure of a membrane-impermeant antitumor sulfonamide complexed with isozyme II. *J. Med. Chem.* **2005**, *48*, 5721–5727.

(211) Abbate, F.; Winum, J.-Y.; Potter, B. V. L.; Casini, A.; Montero, J.-L.; Scozzafava, A.; Supuran, C. T. Carbonic anhydrase inhibitors: X-ray crystallographic structure of the adduct of human isozyme II with EMATE, a dual inhibitor of carbonic anhydrases and steroid sulfatase. *Bioorg. Med. Chem. Lett.* **2004**, *14*, 231–234.

(212) Winum, J.-Y.; Vullo, D.; Casini, A.; Montero, J.-L.; Scozzafava, A.; Supuran, C. T. Carbonic anhydrase inhibitors. Inhibition of cytosolic isozymes I and II and transmembrane, tumor-associated isozyme IX with sulfamates including EMATE also acting as steroid sulfatase inhibitors. *J. Med. Chem.* **2003**, *46*, 2197–2204.

(213) Winum, J.-Y.; Vullo, D.; Casini, A.; Montero, J.-L.; Scozzafava, A.; Supuran, C. T. Carbonic anhydrase inhibitors: inhibition of transmembrane, tumor-associated isozyme IX, and cytosolic isozymes I and II with aliphatic sulfamates. *J. Med. Chem.* **2003**, *46*, 5471–5477.

(214) Kim, C.-Y.; Whittington, D. A.; Chang, J. S.; Liao, J.; May, J. A.; Christianson, D. W. Structural aspects of isozyme selectivity in the binding of inhibitors to carbonic anhydrases II and IV. *J. Med. Chem.* **2002**, *45*, 888–893.

(215) Grzybowski, B. A.; Ishchenko, A. V.; Kim, C.-Y.; Topalov, G.; Chapman, R.; Christianson, D. W.; Whitesides, G. M.; Shakhnovich, E. I. Combinatorial computational method gives new picomolar ligands for a known enzyme. *Proc. Natl. Acad. Sci. U.S.A.* **2002**, *99*, 1270–1273.

(216) Temperini, C.; Cecchi, A.; Scozzafava, A.; Supuran, C. T. Carbonic anhydrase inhibitors. Interaction of indapamide and related diuretics with 12 mammalian isozymes and X-ray crystallographic studies for the indapamide-isozyme II adduct. *Bioorg. Med. Chem. Lett.* **2008**, *18*, 2567–2573.

(217) Crocetti, L.; Maresca, A.; Temperini, C.; Hall, R. A.; Scozzafava, A.; Mühlschlegel, F. A.; Supuran, C. T. A thiabendazole sulfonamide shows potent inhibitory activity against mammalian and nematode alpha-carbonic anhydrases. *Bioorg. Med. Chem. Lett.* **2009**, *19*, 1371–1375.

(218) Baranauskienė, L.; Hilvo, M.; Matulienė, J.; Golovenko, D.; Manakova, E.; Dudutienė, V.; Michailovienė, V.; Torresan, J.; Jachno, J.; Parkkila, S.; Maresca, A.; Supuran, C. T.; Gražulis, S.; Matulis, D. Inhibition and binding studies of carbonic anhydrase isozymes I, II and IX with benzimidazo[1,2-c][1,2,3]thiadiazole-7-sulphonamides. *J Enzyme Inhib Med Chem* **2010**, *25*, 863–870.

(219) Jude, K. M.; Banerjee, A. L.; Haldar, M. K.; Manokaran, S.; Roy, B.; Mallik, S.; Srivastava, D. K.; Christianson, D. W. Ultrahigh resolution crystal structures of human carbonic anhydrases I and II complexed with “two-prong” inhibitors reveal the molecular basis of high affinity. *J. Am. Chem. Soc.* **2006**, *128*, 3011–3018.

(220) Di Fiore, A.; Scozzafava, A.; Winum, J.-Y.; Montero, J.-L.; Pedone, C.; Supuran, C. T.; De Simone, G. Carbonic anhydrase inhibitors: binding of an antiglaucoma glycosyl-sulfanilamide derivative to human isoform II and its consequences for the drug design of enzyme inhibitors incorporating sugar moieties. *Bioorg. Med. Chem. Lett.* **2007**, *17*, 1726–1731.

(221) Woo, L. W. L.; Jackson, T.; Putey, A.; Cozier, G.; Leonard, P.; Acharya, K. R.; Chander, S. K.; Purohit, A.; Reed, M. J.; Potter, B. V. L. Highly potent first examples of dual aromatase-steroid sulfatase inhibitors based on a biphenyl template. *J. Med. Chem.* **2010**, *53*, 2155–2170.

(222) Behnke, C. A.; Le Trong, I.; Godden, J. W.; Merritt, E. A.; Teller, D. C.; Bajorath, J.; Stenkamp, R. E. Atomic resolution studies of carbonic anhydrase II. *Acta Crystallogr. D Biol. Crystallogr.* **2010**, *66*, 616–627.

(223) Di Fiore, A.; Monti, S. M.; Innocenti, A.; Winum, J.-Y.; De Simone, G.; Supuran, C. T. Carbonic anhydrase inhibitors: crystallographic and solution binding studies for the interaction of a boron-containing aromatic sulfamide with mammalian isoforms I-XV. *Bioorg. Med. Chem. Lett.* **2010**, *20*, 3601–3605.

(224) Lopez, M.; Paul, B.; Hofmann, A.; Morizzi, J.; Wu, Q. K.; Charman, S. A.; Innocenti, A.; Vullo, D.; Supuran, C. T.; Poulsen, S.-A. S-glycosyl primary sulfonamides--a new structural class for selective inhibition of cancer-associated carbonic anhydrases. *J. Med. Chem.* **2009**, *52*, 6421–6432.

(225) Dundas, J.; Ouyang, Z.; Tseng, J.; Binkowski, A.; Turpaz, Y.; Liang, J. CASTp: computed atlas of surface topography of proteins with structural and topographical mapping of functionally annotated residues. *Nucleic Acids Res.* **2006**, *34*, W116–118.

(226) Siegel, R.; Naishadham, D.; Jemal, A. Cancer statistics, 2012. *CA: A Cancer Journal for Clinicians* **2012**, *62*, 10–29.

(227) Jaakkola, P.; Mole, D. R.; Tian, Y. M.; Wilson, M. I.; Gielbert, J.; Gaskell, S. J.; Kriegsheim Av; Hebestreit, H. F.; Mukherji, M.; Schofield, C. J.; Maxwell, P. H.; Pugh, C. W.; Ratcliffe, P. J. Targeting of HIF-alpha to the von Hippel-Lindau ubiquitylation complex by O2-regulated prolyl hydroxylation. *Science* **2001**, *292*, 468–472.

(228) Dorai, T.; Sawczuk, I.; Pastorek, J.; Wiernik, P. H.; Dutcher, J. P. Role of carbonic anhydrases in the progression of renal cell carcinoma subtypes: proposal of a unified hypothesis. *Cancer Invest.* **2006**, *24*, 754–779.

(229) Ord, J. J.; Agrawal, S.; Thamboo, T. P.; Roberts, I.; Campo, L.; Turley, H.; Han, C.; Fawcett, D. W.; Kulkarni, R. P.; Cranston, D.; Harris, A. L. An investigation into the prognostic significance of necrosis and hypoxia in high grade and invasive bladder cancer. *J. Urol.* **2007**, *178*, 677–682.

(230) Swietach, P.; Vaughan-Jones, R. D.; Harris, A. L. Regulation of tumor pH and the role of carbonic anhydrase 9. *Cancer Metastasis Rev.* **2007**, *26*, 299–310.

(231) Hutchison, G. J.; Valentine, H. R.; Loncaster, J. A.; Davidson, S. E.; Hunter, R. D.; Roberts, S. A.; Harris, A. L.; Stratford, I. J.; Price, P. M.; West, C. M. L. Hypoxia-inducible factor 1alpha expression as an intrinsic marker of hypoxia: correlation with tumor oxygen, pimonidazole measurements, and outcome in locally advanced carcinoma of the cervix. *Clin. Cancer Res.* **2004**, *10*, 8405–8412.

(232) Sung, F. L.; Hui, E. P.; Tao, Q.; Li, H.; Tsui, N. B. Y.; Dennis Lo, Y. M.; Ma, B. B. Y.; To, K. F.; Harris, A. L.; Chan, A. T. C. Genome-wide expression analysis using microarray identified complex signaling pathways modulated by hypoxia in nasopharyngeal carcinoma. *Cancer Lett.* **2007**, *253*, 74–88.

(233) Koukourakis, M. I.; Giatromanolaki, A.; Sivridis, E.; Pastorek, J.; Karapantzos, I.; Gatter, K. C.; Harris, A. L. Hypoxia-activated tumor pathways of angiogenesis and pH regulation independent of anemia in head-and-neck cancer. *Int. J. Radiat. Oncol. Biol. Phys.* **2004**, *59*, 67–71.

(234) Potter, C. P. S.; Harris, A. L. Diagnostic, prognostic and therapeutic implications of carbonic anhydrases in cancer. *Br. J. Cancer* **2003**, *89*, 2–7.

(235) Hussain, S. A.; Ganesan, R.; Reynolds, G.; Gross, L.; Stevens, A.; Pastorek, J.; Murray, P. G.; Perunovic, B.; Anwar, M. S.; Billingham, L.; James, N. D.; Spooner, D.; Poole, C. J.; Rea, D. W.; Palmer, D. H. Hypoxia-regulated carbonic anhydrase IX expression is associated with poor survival in patients with invasive breast cancer. *Br. J. Cancer* **2007**, *96*, 104–109.

(236) Trastour, C.; Benizri, E.; Ettore, F.; Ramaioli, A.; Chamorey, E.; Pouysségur, J.; Berra, E. HIF-1alpha and CA IX staining in invasive breast carcinomas: prognosis and treatment outcome. *Int. J. Cancer* **2007**, *120*, 1451–1458.

(237) Swinson, D. E. B.; Jones, J. L.; Richardson, D.; Wykoff, C.; Turley, H.; Pastorek, J.; Taub, N.; Harris, A. L.; O'Byrne, K. J. Carbonic anhydrase IX expression, a novel surrogate marker of tumor hypoxia, is associated with a poor prognosis in non-small-cell lung cancer. *J. Clin. Oncol.* **2003**, *21*, 473–482.

(238) Gieling, R. G.; Babur, M.; Mamnani, L.; Burrows, N.; Telfer, B. A.; Carta, F.; Winum, J.-Y.; Scozzafava, A.; Supuran, C. T.; Williams, K. J. Antimetastatic Effect of Sulfamate Carbonic Anhydrase IX Inhibitors in Breast Carcinoma Xenografts. *J. Med. Chem.* **2012**, *55*, 5591–5600.

(239) McDonald, P. C.; Winum, J.-Y.; Supuran, C. T.; Dedhar, S. Recent developments in targeting carbonic anhydrase IX for cancer therapeutics. *Oncotarget* **2012**, *3*, 84–97.

(240) Dubois, L.; Peeters, S.; Lieuwes, N. G.; Geusens, N.; Thiry, A.; Wigfield, S.; Carta, F.; McIntyre, A.; Scozzafava, A.; Dogné, J.-M.; Supuran, C. T.; Harris, A. L.; Masereel, B.; Lambin, P. Specific inhibition of carbonic anhydrase IX activity enhances the in vivo therapeutic effect of tumor irradiation. *Radiother Oncol* **2011**, *99*, 424–431.

(241) Oprea, T. I.; Davis, A. M.; Teague, S. J.; Leeson, P. D. Is there a difference between leads and drugs? A historical perspective. *J Chem Inf Comput Sci* **2001**, *41*, 1308–1315.

(242) Ghose, A. K.; Viswanadhan, V. N.; Wendoloski, J. J. A knowledge-based approach in designing combinatorial or medicinal chemistry libraries for drug discovery. 1. A qualitative and quantitative characterization of known drug databases. *J Comb Chem* **1999**, *1*, 55–68.

(243) Ghosh, A. K.; Thompson, W. J.; Fitzgerald, P. M.; Culberson, J. C.; Axel, M. G.; McKee, S. P.; Huff, J. R.; Anderson, P. S. Structure-based design of HIV-1 protease inhibitors: replacement of two amides and a 10 pi-aromatic system by a fused bis-tetrahydrofuran. *J. Med. Chem.* **1994**, *37*, 2506–2508.

(244) Amari, S.; Aizawa, M.; Zhang, J.; Fukuzawa, K.; Mochizuki, Y.; Iwasawa, Y.; Nakata, K.; Chuman, H.; Nakano, T. VISCANA: visualized cluster analysis of protein-ligand interaction based on the ab initio fragment molecular orbital method for virtual ligand screening. *J Chem Inf Model* **2006**, *46*, 221–230.

(245) Greer, J.; Erickson, J. W.; Baldwin, J. J.; Varney, M. D. Application of the three-dimensional structures of protein target molecules in structure-based drug design. *J. Med. Chem.* **1994**, *37*, 1035–1054.

(246) Craig, J. C.; Duncan, I. B.; Hockley, D.; Grief, C.; Roberts, N. A.; Mills, J. S. Antiviral properties of Ro 31-8959, an inhibitor of human immunodeficiency virus (HIV) proteinase. *Antiviral Res.* **1991**, *16*, 295–305.

(247) Feher, M.; Schmidt, J. M. Property distributions: differences between drugs, natural products, and molecules from combinatorial chemistry. *J Chem Inf Comput Sci* **2003**, *43*, 218–227.

(248) Li, Y.; Wang, H.; Oosterwijk, E.; Tu, C.; Shiverick, K. T.; Silverman, D. N.; Frost, S. C. Expression and activity of carbonic anhydrase IX is associated with metabolic dysfunction in MDA-MB-231 breast cancer cells. *Cancer Invest.* **2009**, *27*, 613–623.

(249) Wermuth, C.G. *The Practice of Medicinal Chemistry*. Elsevier, **2008**.

(250) Wendler, K.; Thar, J.; Zahn, S.; Kirchner, B. Estimating the hydrogen bond energy. *J Phys Chem A* **2010**, *114*, 9529–9536.

(251) Maupin, C. M.; Voth, G. A. Preferred orientations of His64 in human carbonic anhydrase II. *Biochemistry* **2007**, *46*, 2938–2947.

(252) Maupin, C. M.; McKenna, R.; Silverman, D. N.; Voth, G. A. Elucidation of the proton transport mechanism in human carbonic anhydrase II. *J. Am. Chem. Soc.* **2009**, *131*, 7598–7608.

(253) Elder, I.; Tu, C.; Ming, L.-J.; McKenna, R.; Silverman, D. N. Proton transfer from exogenous donors in catalysis by human carbonic anhydrase II. *Arch. Biochem. Biophys.* **2005**, *437*, 106–114.

(254) Silverman, D. N.; McKenna, R. Solvent-mediated proton transfer in catalysis by carbonic anhydrase. *Acc. Chem. Res.* **2007**, *40*, 669–675.

(255) Roy, A.; Taraphder, S. Identification of proton-transfer pathways in human carbonic anhydrase II. *J Phys Chem B* **2007**, *111*, 10563–10576.

(256) Tu, C. K.; Silverman, D. N.; Forsman, C.; Jonsson, B. H.; Lindskog, S. Role of histidine 64 in the catalytic mechanism of human carbonic anhydrase II studied with a site-specific mutant. *Biochemistry* **1989**, *28*, 7913–7918.

(257) Dave, K.; Scozzafava, A.; Vullo, D.; Supuran, C. T.; Ilies, M. A. Pyridinium derivatives of histamine are potent activators of cytosolic carbonic anhydrase isoforms I, II and VII. *Org. Biomol. Chem.* **2011**, *9*, 2790–2800.

(258) Saada, M.-C.; Vullo, D.; Montero, J.-L.; Scozzafava, A.; Winum, J.-Y.; Supuran, C. T. Carbonic anhydrase I and II activation with mono- and dihalogenated histamine derivatives. *Bioorg. Med. Chem. Lett.* **2011**, *21*, 4884–4887.

(259) Saada, M.-C.; Montero, J.-L.; Vullo, D.; Scozzafava, A.; Winum, J.-Y.; Supuran, C. T. Carbonic anhydrase activators: gold nanoparticles coated with derivatized histamine, histidine, and carnosine show enhanced activatory effects on several mammalian isoforms. *J. Med. Chem.* **2011**, *54*, 1170–1177.

(260) An, H.; Tu, C.; Duda, D.; Montanez-Clemente, I.; Math, K.; Laipis, P. J.; McKenna, R.; Silverman, D. N. Chemical rescue in catalysis by human carbonic anhydrases II and III. *Biochemistry* **2002**, *41*, 3235–3242.

(261) Duda, D.; Tu, C.; Qian, M.; Laipis, P.; Agbandje-McKenna, M.; Silverman, D. N.; McKenna, R. Structural and Kinetic Analysis of the Chemical Rescue of the Proton Transfer Function of Carbonic Anhydrase II†. *Biochemistry* **2001**, *40*, 1741–1748.

(262) Briganti, F.; Mangani, S.; Orioli, P.; Scozzafava, A.; Vernaglione, G.; Supuran, C. T. Carbonic anhydrase activators: X-ray crystallographic and spectroscopic investigations for the interaction of isozymes I and II with histamine. *Biochemistry* **1997**, *36*, 10384–10392.

(263) Silverman D.N. Marcus rate theory applied to enzymatic proton transfer. *Biochimica et Biophysica Acta (BBA)/Bioenergetics* **2000**, *1458*, 88–103.

(264) Kresge, A. J.; Silverman, D. N. Application of Marcus rate theory to proton transfer in enzyme-catalyzed reactions. *Meth. Enzymol.* **1999**, *308*, 276–297.

(265) Shuker, S. B.; Hajduk, P. J.; Meadows, R. P.; Fesik, S. W. Discovering high-affinity ligands for proteins: SAR by NMR. *Science* **1996**, *274*, 1531–1534.

(266) Aggarwal, M.; Boone, C. D.; Kondeti, B.; Tu, C.; Silverman, D. N.; McKenna, R. Effects of cryoprotectants on the structure and thermostability of the human carbonic anhydrase II-acetazolamide complex. *Acta Crystallogr. D Biol. Crystallogr.* **2013**, *69*, 860–865.

(267) Garman, E. “Cool” crystals: macromolecular cryocrystallography and radiation damage. *Curr. Opin. Struct. Biol.* **2003**, *13*, 545–551.

(268) Garman, E. F.; Owen, R. L. Cryocooling and radiation damage in macromolecular crystallography. *Acta Crystallogr. D Biol. Crystallogr.* **2006**, *62*, 32–47.

(269) Holton, J. M. A beginner’s guide to radiation damage. *J Synchrotron Radiat* **2009**, *16*, 133–142.

(270) Kmetko, J.; Warkentin, M.; Englich, U.; Thorne, R. E. Can radiation damage to protein crystals be reduced using small-molecule compounds? *Acta Crystallogr. D Biol. Crystallogr.* **2011**, *67*, 881–893.

(271) Ravelli, R. B. G.; Garman, E. F. Radiation damage in macromolecular cryocrystallography. *Curr. Opin. Struct. Biol.* **2006**, *16*, 624–629.

(272) Chapman, M. S.; Somasundaram, T. De-icing: recovery of diffraction intensities in the presence of ice rings. *Acta Crystallogr. D Biol. Crystallogr.* **2010**, *66*, 741–744.

(273) Garman, E. F.; Doublié, S. Cryocooling of macromolecular crystals: optimization methods. *Meth. Enzymol.* **2003**, *368*, 188–216.

(274) Forwand, S. A.; Landowne, M.; Follansbee, J. N.; Hansen, J. E. Effect of acetazolamide on acute mountain sickness. *N. Engl. J. Med.* **1968**, *279*, 839–845.

(275) Katritzky, A. R.; Caster, K. C.; Maren, T. H.; Conroy, C. W.; Bar-Ilan, A. Synthesis and physicochemical properties of thiadiazolo[3,2-a]pyrimidinesulfonamides and thiadiazolo[3,2-a]triazinesulfonamides as candidates for topically effective carbonic anhydrase inhibitors. *J. Med. Chem.* **1987**, *30*, 2058–2062.

(276) Maren, T. H. Carbonic anhydrase: chemistry, physiology, and inhibition. *Physiol. Rev.* **1967**, *47*, 595–781.

(277) Fraser, J. S.; van den Bedem, H.; Samelson, A. J.; Lang, P. T.; Holton, J. M.; Echols, N.; Alber, T. Accessing protein conformational ensembles using room-temperature X-ray crystallography. *Proc. Natl. Acad. Sci. U.S.A.* **2011**, *108*, 16247–16252.

BIOGRAPHICAL SKETCH

Mayank was born and brought up in Delhi, India. After having completed an engineering degree in biotechnology from India, he moved to the United States for higher studies. He received an M.S. Biotechnology (2009) from Claflin University (Orangeburg, SC), under the guidance of Dr. Nicholas Panasik Jr. identifying the factors responsible for imparting thermostability to enzymes where he used various bioinformatics tools and wrote codes in *Python* to describe the detailed distribution patterns of factors that are commonly attributed as the molecular basis for thermostability – glycines and prolines, ion pairs, buried and solvent accessible surface area, and lengths of loops. In addition, he worked at the SC Center for Biotechnology Research on the use of microRNAs in vaccines against HIV, during which he co-authored 2 research articles.

In August 2013, Mayank graduated from the University of Florida (Gainesville, FL) with a Ph.D. in Biomedical Sciences under the mentorship of Dr. Robert McKenna in the Department of Biochemistry and Molecular Biology at the College of Medicine. In pursuit of developing isoform-specific inhibitors for CA, he expanded his studies learning various techniques from expression/purification of a protein to its crystallization and structure determination. He also carried out computational modeling for collaborators, on proteins such as APE1, MCT1, TorsinA, HIV-gp120, APE1, HLA II and CD147 to identify putative regions of binding with other proteins. His main research focus however, was studying structure activity relationships in metalloenzymes. In addition, he had also assisted 6 Ph.D. students and 3 undergraduate students in the McKenna lab. So far, Mayank has authored/co-authored a total of 17 peer-reviewed articles/reviews and 4 more manuscripts are in preparation.